



The Adhesion of Protective Coatings to Novel REACH
Compliant Packaging Steel Substrates

Matthew James Dodd

Submitted to Swansea University in Fulfilment for the Degree
of Doctor of Engineering

Swansea University

2023

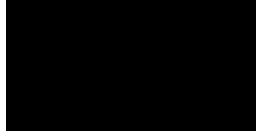
Copyright: The Author, Matthew J. Dodd, 2023.



Declarations

This work has not previously been accepted in substance for any degree and is not being concurrently submitted in candidature for any degree.

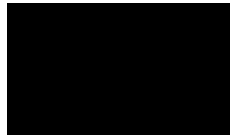
Signed:



Date: 03/06/2023

This thesis is the result of my own investigations, except where otherwise stated. Other sources acknowledged by footnotes giving explicit references. A bibliography is appended.

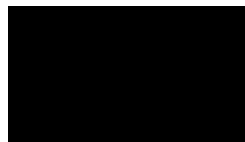
Signed:



Date: 03/06/2023

I hereby give consent for my thesis, if accepted, to be available for photocopying and for inter-library loan, and for the title and summary to be made available to outside organisations.

Signed:



Date: 03/06/2023

Acknowledgements

I would like to express my gratitude and give acknowledgments to several individuals who have provided invaluable help and support during my engineering doctorate journey.

Firstly, to my academic supervisor Dr. Eifion Jewell, without whom I feel completing this would not have been possible. Your continuous support and ability to educate and motivate has meant that I've always stayed on-track heading in the right direction. Diolch Eif! Also, a massive thank you to my industrial supervisor, Dr. Arnoud de-Vooy. Although our time together on this project was cut short, your insights, advice and attention to detail always ensured I was asking the right questions and producing industrially relevant research.

There are a number of people in the University who I was also like to express my thanks to. In particular Dr. Natalie Wint, your patience, thoroughness and care over my work has ensured I have never been left wanting for feedback. Thank you for always steering in the right direction with your expertise. Dr. Christian Griffiths, your continuous help on this project with everything from experimental insights to academic interpretation, including during my postdoctoral studies, has got me to this point. I'm incredibly grateful mate! To the whole group at PMRC Baglan, especially Leighton Medway (Uncle Leights) for indulging all of my engineering ideas and providing some life advice along the way. Soon to be Dr. Jamie Williams, who would have thought we would have got to this point! It's been a pleasure to sap the mood alongside you, especially while representing the mighty Whites, upwards and onwards my boy!

Finally, to all of my friends and family, in particular my parents Karen and Nick, my sister Beck with her brilliant family and my wonderful girlfriend Dr. Jess Lewis M.D (the real doctor in the family as my Gran always reminds me). Your support has got me to where I am today, academically, professionally and personally. Thank you all.

Summary

Chromium coated packaging steel substrates are used in applications which require a lacquer coating which insulates the can and cans contents from each other. Legislative pressures in Europe defined by REACH (Registration, Evaluation, Authorisation and Restriction of Chemicals) have dictated the removal of Cr (VI) from the electrocoating process of these packaging steel substrates, as well as restricting the use of bisphenol-A (BPA) used in protective lacquers. Both chemicals have been shown to pose significant safety risks due to their inherent toxicity to humans and the environment.

Cr (III) electrocoating's have since been investigated as a replacement but are, as yet, in their commercial infancy. One such material is TCCT (Trivalent Chromium Coated Technology) which is produced by TATA Steel Europe. In addition, lacquers have been developed to which bisphenol-A has not intentionally been added (BPANI) satisfying both REACH legislation and a consumer dictated move away from BPA. The combination of these two novel technologies enables conformity to legislative pressures.

The work presented in this thesis reports an investigation into the physical and chemical characteristics of TCCT packaging steel substrates, specifically looking at the effect of chromium oxide coating weight. An established methodology is used to investigate the adhesive performance of both epoxy based and BPANI lacquers to TCCT before and after a retort process, which is used to simulate industrial pressure cooking conditions. Comparisons are made to commercially mature substrate materials. The TCCT manufacturing process is replicated on a laboratory scale with view to validating a self-sufficient process of sample creation. The effect of various electroplating parameters such as applied current density, electrolysis time, pulsing, temperature and pH are investigated. These samples are characterised using a consistent methodology. This consists of surface topographical analysis, visual analysis using electron microscopy and a copper sulphate dip test. These techniques showed the similar visual characteristics of industrially made and laboratory made TCCT samples but highlighted a more inconsistent coating deposited on the laboratory made samples.

Contents

Table of Nomenclature.....	15
1 Introduction.....	17
1.1 Project Motivation and Stimuli	18
1.2 Aims and Objectives	18
1.3 Political Landscape.....	19
2 Literature Review	21
2.1 Introduction	21
2.2 Packaging Steel Materials	21
2.2.1 Blackplate.....	22
2.2.2 Chromium Coatings Used for Packaging Steel.....	22
2.3 Can Manufacture	30
2.3.1 Two Piece Can Manufacturing.....	30
2.3.2 Three Piece Can Manufacture	30
2.3.3 Can End Manufacture	30
2.3.4 Packaging Steel Lifecycle.....	32
2.4 Packaging Steel Protective Coatings.....	32
2.4.1 Protective Coating Chemistry	33
2.5 The Corrosion of Packaging Steel.....	35
2.5.1 Corrosion Fundamentals	35
2.5.2 Corrosion Mechanisms	37
2.6 The Adhesion of Lacquers to Packaging Steel.....	42
2.6.1 Mechanisms of Adhesion.....	43
2.6.2 Adhesion Testing	47
2.7 Literature Review Conclusions	50
3 Materials and Methods.....	53
3.1 Materials	53
3.1.1 Substrate Materials.....	53
3.1.2 Organic Coatings.....	54
3.2 Sample Preparation and Processing.....	54
3.2.1 Coating and Curing	54
3.2.2 Retort Process	56
3.3 Analysis Methods	58
3.3.1 White Light Interferometry	58
3.3.2 Atomic Force Microscopy.....	58
3.3.3 Surface Tension and Wetting Angle	60

3.3.4	Spherical Spectrophotometry	61
3.3.5	Gloss Measurement	63
3.3.6	Scanning Electron Microscopy	65
3.3.7	Differential Scanning Calorimetry and Thermogravimetric Analysis	65
3.3.8	Fourier Transform Infra-Red Spectroscopy	66
3.3.9	X-Ray Fluorescence	66
3.3.10	X-Ray Photoelectron Spectroscopy	67
3.3.11	Glow Discharge Optical Emission Spectroscopy	68
3.3.12	Cyclic Voltammetry	69
3.3.13	Scanning Vibrating Electrode Technique (SVET).....	69
3.3.14	Scratch Testing Adhesion	74
3.4	Conclusion.....	75
4	Characterisation of TCCT Packaging Steel Substrates: The Effect of Chromium Oxide Coating Weight.....	77
4.1	Introduction	77
4.2	Materials and Methodology.....	78
4.3	Physical Characterisation	78
4.3.1	The Effect of Surface Topography.....	79
4.3.2	The Effect of the Adhesive Interface – Surface Tension and Contact Angle	83
4.3.3	Metallic Coating Morphology.....	90
4.3.4	Characterising Thin Chromium Oxide Films Aesthetically - Substrate Colour and Reflectance Analysis	91
4.4	Chemical Characterisation	95
4.4.1	XPS Surface Scans	95
4.4.2	GDOES Depth Profiles	98
4.5	Conclusions	101
5	The Adhesive Performance of Protective Coatings on Novel TCCT substrates with Varying Chromium Oxide Coating Weights	104
5.1	Introduction	104
5.2	Materials and Methodology.....	105
5.3	Adhesion Performance	105
5.3.1	Dry Adhesion – Failure Characteristics Pre-Retort	105
5.4	Failure Characteristics Post Retort in Simulant Solutions.....	107
5.4.1	Simulant Solution: De-Ionised Water	107
5.4.2	Simulant Solution: NaCl	108
5.4.3	Simulant Solution: Citric Acid + NaCl	109
5.5	Failure Mechanisms and Post-Retort Visualisation	110

5.5.1	Water Uptake assessment of Polyester Based (BPANI) Lacquer	112
5.5.2	Copper Sulphate Study Identifying Surface Iron	116
5.5.3	Corrosion Resistance of the Substrate	123
5.6	Conclusions	131
6	Laboratory Electroplating of TCCT Substrate Materials: Chromium Metal and Chromium Oxide Deposition	134
6.1	Introduction	134
6.2	Strategy Employed	135
6.3	Electrolyte Chemistry	135
6.3.1	Electroplating Process and Equipment Set Up.....	136
6.3.2	Sulphite Removal Process.....	138
6.3.3	Cyclic Voltammetry	139
6.4	Validation of the Electroplating Process	140
6.4.1	Calibration of the XRF.....	141
6.4.2	Chromium Metal Depositing Electrolyte.....	142
6.4.3	Chromium Oxide Depositing Electrolyte.....	150
6.5	The Two-step Electroplating Process.....	156
6.6	Chromium Oxide Homogeneity - CuSO ₄ Test	157
6.7	Rate Limiting Step of Chromium Metal and Chromium Oxide Deposition 158	
6.8	Additional Work to Assess the Impact of Hydrogen Evolution on the Electroplating Process.....	161
6.9	Conclusions	163
7	Conclusions.....	165
8	Recommendations for Future Work	169
9	Appendix I – SVET Repeats.....	171
10	Appendix II – List of Publications.....	173
11	Bibliography	174

Table of Figures

Figure 2.1 - Schematic showing the structure of ECCS (9).....	22
Figure 2.2 - Chromium total plotted against current density illustrating the regimes of deposition for Cr III based electrolyte (29).....	26
Figure 2.3 - The impact of simulant on measured wet adhesion for an exposure of 1.5 h at 121 °C. Pre-retort adhesion failure of each system is represented by the horizontal lines (39).....	29
Figure 2.4 - Main measured parameters in a double seam (42).....	31
Figure 2.5 - Typical round section food and drink cans (42).....	31
Figure 2.6 - Reaction formation of an epoxyphenolic lacquer.....	34
Figure 2.7 - Anodic and cathodic reactions that occur on substrate materials represented as an Evans droplet (53).	37
Figure 2.8 - Pitting corrosion schematic.	38
Figure 2.9 - Filiform corrosion filament on a steel substrate (59)	41
Figure 2.10 - Diagram of a coating mechanically interlocking with a surface.....	44
Figure 2.11 - Illustration of good and poor wettability and its effect on adhesion (81).	45
Figure 2.12 - The electric double layer effect of a polymeric material on metal substrate (67).....	47
Figure 3.1 - Meyer bar coating method used to coat the substrate materials with lacquers.	55
Figure 3.2 - Erichsen depth borer method for measuring coating thickness.....	55
Figure 3.3 - Labelled image of the Certoclav Multicontrol 2 used for pressure cooking steel samples.....	56
Figure 3.4 - Internal schematic of the CertoClav autoclave.....	57
Figure 3.5 - Data logger information for the Certoclav Multicoltrrol 2.....	57
Figure 3.6 - Image detailing the AFM process used.	59
Figure 3.7 - A contact angle measurement of DI water on a metallic surface.	60
Figure 3.8 - Spherical spectrophotometer - influence of SPEX and SPIN (108).....	62
Figure 3.9 - CIELAB colour chart (110).....	63
Figure 3.10 - Gloss meter geometry ($\theta=20^\circ, 60^\circ, 85^\circ$) and the specular and diffuse components of surface reflection (103).....	64

Figure 3.11 - Visualisation of the XPS method of excitation; the photoelectric effect.	68
Figure 3.12 - A schematic showing the lines of current flux and equipotential through an electrolyte in which a metal is corroding.	70
Figure 3.13 - Schematic showing limitations of the SVET with respect to spatial resolution i.) anode-cathode distance is greater than scan height and localised corrosion can be resolved and ii.) anode-cathode distance is smaller than scan height and localised corrosion cannot be resolved (73).	73
Figure 3.14 - The Sheen Instruments scratch tester used for adhesion investigations.	74
Figure 3.15 - Schematic of a scratch testing process.	75
Figure 4.1 - White light interferometry 2D and 3D plots of (a) blackplate, TCCT substrates coated with (b) low CrOx (3mg/m^2), (c) medium CrOx (13mg/m^2) and (d) high CrOx (23mg/m^2) and (e) ECCS (9mg/m^2).	80
Figure 4.2 - Surface roughness data as measured by white light interferometry for 15 TCCT samples and ECCS at x5, x10 and x20 magnifications.	81
Figure 4.3 - AFM plots illustrating the 3D topographies of (a) blackplate, TCCT substrates coated with (b) low CrOx (3mg/m^2), (c) medium CrOx (13mg/m^2) and (d) high CrOx (23mg/m^2) and (e) ECCS (9mg/m^2).	82
Figure 4.4 - Image showing the pendant drop method of measuring surface tension (a) and graphical depiction of the surface tensions of DI water, epoxyphenolic and BPANI lacquers.	85
Figure 4.5 - Relationship between chromium oxide coating weight of TCCT substrates and contact angle of DI water.	86
Figure 4.6 - DSC data for the (a) epoxyphenolic and (b) BPANI lacquers.	89
Figure 4.7 - SEM imagery showing the surfaces of TCCT substrates coated with (a) low CrOx (3mg/m^2), (b) medium CrOx (13mg/m^2), (c) high CrOx (23mg/m^2) and (d) ECCS (9mg/m^2).	90
Figure 4.8 - SEM imagery showing the surfaces of TCCT samples coated with (a) low CrOx (3mg/m^2), and (b) high CrOx (23mg/m^2) at magnifications of 10000x.	91
Figure 4.9 - Spherical spectrophotometry data for TCCT sample set: L^* values, measured with specular light excluded.	93
Figure 4.10 - Gloss measurements of TCCT sample set and ECCS taken at a 20 degree angle of reflectance.	94

Figure 4.11 - XPS wide scans of TCCT substrates coated with low CrOx (3mg/m ²), medium CrOx (13 mg/m ²), high CrOx (23 mg/m ²) and ECCS (9 mg/m ²).....	96
Figure 4.12 - Peak fitting components of (a) Fe 2p and (b) Cr 2p used for XPS analysis.	98
Figure 4.13 - GDOES depth profiles of TCCT substrates coated with (a) low CrOx (3mg/m ²), (b) medium CrOx (13 mg/m ²), (c) high CrOx (23 mg/m ²) and (d) ECCS (9 mg/m ²).....	100
Figure 5.1 - Dry adhesion measurements of TCCT substrates and ECCS coated with both epoxyphenolic and BPANI lacquers.	106
Figure 5.2 - Adhesion measurements of TCCT substrates and ECCS coated with both epoxyphenolic and BPANI lacquers after a retort in DI water simulant solution. ..	108
Figure 5.3 - Adhesion measurements of TCCT substrates and ECCS coated with both epoxyphenolic and BPANI lacquers after a retort in 1 % w/v NaCl simulant solution.	109
Figure 5.4 - Adhesion measurements of TCCT substrates and ECCS coated with both epoxyphenolic and BPANI lacquers after a retort in citric acid + NaCl (0.25 % + 0.25 % w/v) simulant solution.	110
Figure 5.5 - TCCT substrate with chromium oxide coating weight low (3 mg/m ²) post-retort in (a) DI water, (b) NaCl and (c) Citric and NaCl solutions visualising lacquer failure mechanisms.....	111
Figure 5.6 - FTIR graphs representing TCCT samples coated with (a) high CrOx (23 mg/m ²), (b) medium CrOx (13 mg/m ²), (c) low CrOx (3 mg/m ²) and (d) ECCS (9 mg/m ²) pre retort and post retort in DI water, 0.5% NaCl and 1% NaCl.	113
Figure 5.7 - Quantification of water uptake of BPANI coated TCCT samples coated with low CrOx (3 mg/m ²), medium CrOx (13 mg/m ²) and high CrOx (23 mg/m ²) and ECCS (9 mg/m ²) post retort in DI water, 0.5% NaCl and 1% NaCl illustrating a percentage of the coatings in.....	115
Figure 5.8 - SEM and optical imagery of a TCCT substrate with low CrOx coating weight (3 mg/m ²) showing copper on its surface after a CuSO ₄ dip.	118
Figure 5.9 - XRF data for the TCCT substrates coated with low CrOx (3mg/m ²), medium CrOx (9 and 13 mg/m ²) and high CrOx (23 mg/m ²) after dipping in CuSO ₄ with ECCS (9 mg/m ²) used as a control. Data is represented in PPM of copper. ...	119

Figure 5.10 - EDX map and corresponding images of the iron and copper plot for a TCCT sample with chromium oxide coating of 3 mg/m ² , highlighting copper on the substrates surface.	120
Figure 5.11 - Light microscope images (a-c) showing the quantification of copper area on substrate materials with differing light and contrast settings.....	121
Figure 5.12 - Area ratio of copper on the surface of TCCT and ECCCS substrate materials plotted with their respective site densities.....	122
Figure 5.13 - SVET colour charts representing TCCT coated with 3 mg/m ² of chromium oxide and image of sample post-process.	124
Figure 5.14 - SVET colour charts representing TCCT coated with 13 mg/m ² of chromium oxide and image of sample post-process.	125
Figure 5.15 - SVET colour charts representing TCCT coated with 23 mg/m ² of chromium oxide and image of sample post-process.	126
Figure 5.16 - SVET colour charts representing ECCS coated with 9 mg/m ² of chromium oxide and image of sample post-process.	127
Figure 5.17 - SVET anodic data for TCCT substrates coated with low CrOx (3 mg/m ²), medium CrOx (13 mg/m ²), high CrOx (23 mg/m ²) and ECCS (9 mg/m ²).....	128
Figure 5.18 - SVET cathodic data for TCCT substrates coated with low CrOx (3 mg/m ²), medium CrOx (13 mg/m ²), high CrOx (23 mg/m ²) and ECCS (9 mg/m ²).	128
Figure 5.19 - SVET mass loss data for TCCT substrates coated with low CrOx (3 mg/m ²), medium CrOx (13 mg/m ²), high CrOx (23 mg/m ²) and ECCS (9 mg/m ²).	130
Figure 6.1 – Images of the laboratory scale electroplating set up used in Swansea University detailing (a) the alkaline cleaning station and (b) the rinse, pickle and electroplating cell.....	137
Figure 6.2 - Simplified schematic detailing the TCCT electroplating set up highlighting the electrical connections and equipment used.....	138
Figure 6.3 - Cyclic voltammograms of fresh and pre-plated electrolyte used for chromium metal deposition illustrating the characteristic CO ₂ surface explosion peak of formic acid oxidation indicating that the electrolyte is sufficiently uncontaminated from sulphate ions.	140
Figure 6.4 - XRF calibration: Conversion from PPM to mg/m ²	141

Figure 6.5 - (a) Relationship between applied current density, electrolysis time and quantity of chromium metal deposit and (b) regimes of TCCT layer deposition as proposed by TATA Steel Europe.....	143
Figure 6.6 - Image showing cathodic hydrogen evolution in the TCCT manufacturing process.....	144
Figure 6.7 - The effect of the length of current pulse on the quantity of chromium metal deposit at a 30 A/dm ² current density.	145
Figure 6.8 - The effect on the quantity of chromium metal deposition when pulsing the current for 0.8 s.	146
Figure 6.9 - The effect of electrolyte temperature changes on the quantity of chromium metal deposition at various current densities.	147
Figure 6.10 - The effect of electrolyte (a) at pH 2.3 and (b) at pH 2.8 on quantity of chromium metal deposition at varying electrolyte temperatures.	149
Figure 6.11 - Relationship between applied current density, electrolysis time and quantity of chromium oxide deposit.	150
Figure 6.12 - The effect of the length of current pulse on the quantity of chromium metal deposit at a 30 A/dm ² current density.....	152
Figure 6.13 - The effect of pulsing current for 0.8 s on the quantity of chromium oxide deposit.	153
Figure 6.14 - The effect of electrolyte temperature changes on the quantity of chromium oxide deposition at various current densities.....	154
Figure 6.15 - The effect of electrolyte pH changes on the quantity of chromium oxide deposition at various current densities.	155
Figure 6.16 - GDOES profiles of (a) industrially made TCCT with 3 mg/m ² of chromium oxide and (b) TCCT made in Swansea University attempting to replicate industrial quantities of 60 mg/m ² chromium metal and 2-5 mg/m ² of chromium oxide.	156
Figure 6.17 - Area ratio of copper on the surface of industrially made TCCT samples compared with lab made TCCT samples.	158
Figure 6.18 - The efficiency of the chromium oxide deposition process plotted against varying current densities, highlighting the effect of the hydrogen evolution cathodic reaction as a rate limiting step.....	160

Figure 6.19 - Rendered CAD image of the initial design of a rotating cylinder electrode set-up to investigate the effect of hydrogen evolution on the deposition of chromium metal and oxide coatings.....	161
Figure 6.20 - Top view of CAD drawing of the rotating cylinder electrode design.	162
Figure 9.1 - SVET colour charts representing a repeat scan of TCCT coated with 3 mg/m ² of chromium oxide and image of sample post-process.	171
Figure 9.2 - SVET colour charts representing a repeat scan of TCCT coated with 23 mg/m ² of chromium oxide.	172
Figure 9.3 - SVET colour charts representing a repeat scan of ECCS coated with 9 mg/m ² of chromium oxide.	172

Table of Tables

Table 2.1 - List of Adhesion Mechanisms (79).....	43
Table 3.1 - 2019 TCCT electroplating parameter information and chromium metal and oxide chemistries for samples acquired for project.....	53
Table 3.2 - Details of the lacquers used.	54
Table 3.3 - Simulant solutions compositions and associated foodstuffs.....	56
Table 3.4 - Gloss measurement selection criteria.	64
Table 4.1 – Surface topographical data Ra, Rt and Rz values for blackplate, TCCT substrates coated with low CrOx – 3mg/m ² , medium CrOx – 13 mg/m ² and high CrOx - (23 mg/m ²) and (e) ECCS.....	79
Table 4.2 - AFM surface roughness's (Ra) of blackplate, TCCT substrates coated with low CrOx (3mg/m ²), medium CrOx (13 mg/m ²) and high CrOx (23 mg/m ²) and ECCS (9 mg/m ²).	82
Table 4.3 - Contact angle measurements of TCCT substrates coated with low CrOx (3mg/m ²), medium CrOx (13 mg/m ²), high CrOx (23 mg/m ²) and ECCS (9 mg/m ²).	87
Table 4.4 – Glass transition temperatures (T _g) for the epoxyphenolic and BPANI lacquers.	88

Table 4.5 - Numerical spherical spectrophotometry data for TCCT substrates coated with low CrOx (3 mg/m ²), medium CrOx (13 mg/m ²), high CrOx (23 mg/m ²) and ECCS (9 mg/m ²).	92
Table 4.6 - XPS chemical constituents of low (3mg/m ²), medium (13 mg/m ²) and high (23 mg/m ²) chromium oxide coated TCCT samples and ECCS.....	97
Table 5.1 – Numerical quantification of water uptake from FTIR data shown in section 5.5.1 as a percentage of the coatings initial O-H stretching quantity for TCCT samples coated with low CrOx (3mg/m ²), medium CrOx (13 mg/m ²), high CrOx (23 mg/m ²) and ECCS (9 mg/m ²).....	115
Table 5.2 - Composition of copper sulphate solution used to visualise defects in chromium oxide layer on chromium oxide coated substrate materials.....	117
Table 5.3 - Area ration of copper on the surface of TCCT and ECCCS substrate materials highlighting differences in site density and therefore chromium oxide layer homogeneity.....	122
Table 6.1 - Electrolyte chemistries used to electroplate the chromium metal and oxide TCCT layers.....	136
Table 6.2 - Pre-treatment steps for substrate material prior to electroplating processes.	137
Table 6.3 - Area ration of copper on the surface of TCCT and ECCCS substrate materials highlighting differences in site density and therefore chromium oxide layer homogeneity.....	157

Table of Nomenclature

Abbreviations	Description
AFM	Atomic Force Microscopy
BPA	Bisphenol-A
BPANI	Bisphenol-A Non-Intent
Cr (III)	Trivalent Chromium
Cr (VI)	Hexavalent Chromium
DRD	Drawn and Re-drawn
DWI	Drawn Wall Iron
EP	Epoxyphenolic
ECCS	Electrolytic Chromium Coated Steel
FTIR	Fourier Transform Infra-Red Spectroscopy
GDOES	Glow Discharge Optical Emission Spectroscopy
HCD	High Current Density
PCL	Pilot Coating Line
REACH	Registration, Evaluation, Authorisation and Restriction of Chemicals
SEM	Scanning Electron Microscopy
TCCT	Trivalent Chromium Coating Technology
XPS	X-ray Photoelectron Spectroscopy
XRF	X-ray Fluorescence
WLI	White Light Interferometry

Chapter 1 - Introduction

1 Introduction

Metal packaging has a diverse range of uses, including but not limited too; beverage containers, aerosols, paint cans and bakeware, being particularly prevalent in the food packaging industry where goods are hermetically sealed and, if necessary, pressure cooked to ensure the contents are preserved. Subsequent refrigeration of the goods is not necessary as microbiological deterioration of the food is restricted. This particular market is moving from strength to strength, especially in the wake of the COVID-19 pandemic where the world's population has re-discovered value in the ability to store products for extended periods of time. Coupled with this there is growing consumer awareness of the various health benefits of storing organic produce in metal-based packaging products (1,2). This market is anticipated to be driven by a number of additional factors, including significant R&D efforts (e.g., increase in the usage of aerosol cans in the pharmaceutical industry) and the rising urbanisation of the world (3).

Historically tinned steel was used as the main metallic food packaging material. However, in more recent decades, in part as a result of fluctuating tin prices, chromium plated substrate materials, such as electro-chromium coated steel (ECCS) were developed as an alternative to tinplate. ECCS consists of a steel substrate with an extremely thin (10-30 nm) layer of chromium metal / chromium (hydr)oxide which offers corrosion protection with a comparably improved aesthetic and provides a surface onto which protective lacquers can adhere. It is for these reasons that ECCS has been used globally in the manufacture of packaging steel since its inception.

Cans can either be made from two or three pieces. Two piece cans consist of a body and an end whereas three piece cans consist of a body and two ends. The substrates are lacquered and then drawn or punched into the desired geometries, hence the coating applied must be able to withstand the mechanical forces exerted during this production step.

The global metal packaging market was valued at 108.8 billion USD in 2020 and is expected to grow to 147.4 billion USD by 2030 at a compound annual growth rate of 3.1% with established products and whole supply chains (4,5).

For a material as ubiquitous as steel, innovation and development can be astonishingly rapid – especially when motivated by the need to conform to legislation, reduce carbon emissions and improve resource efficiency, cost, and productivity.

1.1 Project Motivation and Stimuli

In October 2003, the European commission proposed new chemical legislation known as REACH (Registration, Evaluation, Authorisation and restriction of Chemicals). These regulations became necessary to adequately measure and track, through a volume-triggered system, the use of harmful and hazardous chemicals (6). The list of chemicals to be monitored under REACH is comprehensive and includes the key constituent of ECCS, Cr (VI), which is the most toxic form of chromium (7). It is a known carcinogen and is classified as a substance of very high concern (SVHC) due to its toxicity and sensitising qualities. For this reason, it is included in the REACH regulations and will ideally be phased out completely by 2024. Additionally, in some European countries, legislation has dictated that bisphenol-A (a key monomer in epoxyphenolic coatings) must be removed from food contact applications, i.e., from the protective lacquers applied to cans due to associated health risks.

This project is driven by the need of the packaging steel industry to conform to legislation defined by REACH. This is required in order to access European and global markets while satisfying a consumer driven need to remove chemicals that are harmful to human and environmental health from manufacturing processes.

Therefore, TATA Steel has interest in producing and further developing TCCT, a novel substrate to which different lacquers can be applied, so as to conform to legislative pressures. This material is still in development and its characterisation and lacquer adhesion performance pre and post-processing poses interesting avenues for research which are addressed in this work.

1.2 Aims and Objectives

The aim of this research is to understand how the adhesion interface between a novel substrate and applied organic coatings react to the processing environment in the context of a food packaging can. Novel substrate materials coated with two different lacquers are investigated and comparisons are made to commercially mature products.

The objective of this work was to first characterise the substrate materials physically and chemically, along with the lacquers separately, and investigate their interaction both before and after a retort process. The combination of elevated temperature and pressure simulate industrial processes, after which the adhesion of protective coatings is evaluated. Objectively, adhesive failure mechanisms and

quantitative adhesive performance data of epoxy based and BPANI (bisphenol-A non-intent) lacquers on TCCT substrates were to be established. This will lend insight into the potential of their commercial use and highlight areas for improvement.

The effect of the substrate is to be further investigated by replicating the TCCT electroplating process in the laboratory and attempting to recreate samples independently. The objective is to understand the effect of a range of electroplating parameters and to optimise the deposition process so as to create samples which could be proven to be chemically comparable thus enabling manufacturing process recommendations to industry. A list of publications produced from this work can be found in Appendix II: List of publications.

1.3 Political Landscape

This project began in late 2018 within a relatively stable economic and political landscape. On 31st January 2020 the UK officially left the European Union which had many knock-on effects for the steel industry, such as potential export tariffs of up to 25%. For TATA Steel, efficiencies were found through splitting the European arm of the business from the UK, effectively creating two different companies.

In the context of this project, this influenced the strategy due to a change in industrial supervision and therefore a restriction on sample access by June 2020. This motivated research into the production process of novel packaging steel substrates as opposed to solely their characterisation and performance.

Chapter 2 - Literature Review

2 Literature Review

2.1 Introduction

This review examines many subject areas pertaining to packaging steel including the lifecycle of steel substrates used in can making, from the unprocessed substrate material through to its storage and eventual use. Crucial points in this cycle are further examined; the electroplating of chromium metal and oxide (surface chemistry analysis), lacquering (adhesion mechanisms and measurements) and the retort process. Further information is presented regarding the adhesion of protective lacquers to substrates and their subsequent performance in various environmental conditions. This evaluation proves crucial in understanding the complexities of the interaction between established and developmental substrate technologies and lacquer coatings.

2.2 Packaging Steel Materials

Steel has been used as a packaging material since 1812 when Hall and Dankin began to produce dip coated commercially ‘tinned’ products (8). This was, historically, the choice of materials for food packaging cans due to favourable strength and corrosion properties coupled with the low cost price of the steel substrate onto which the tin was coated. In recent times the cost of tin has increased significantly, while it has also become evident that cans required more protection from their relatively ‘aggressive’ chemical contents. This substrate is not the focus of this work and will therefore not be mentioned further.

Tin free steel (TFS) or electro chromium coated steel (ECCS) was developed as an alternative to tinplate in lacquered applications. This material requires a much thinner metallic coating while still serving to extend the life of food products by offering protection from physical and chemical damage. Large scale commercialisation of technology has resulted in optimisation of materials where-by substrates have become thinner, stronger, and more formable.

Typically, metallic coatings are overcoated with an organic lacquer which is cured prior to the formation and filling of a food packaging can. Two such lacquers include epoxyphenolic and bisphenol-A non-intent (BPANI). Such organic lacquers provide a protective layer during handling, can forming, filling and cooking processes, each of which induces stress on the lacquer / substrate interface.

2.2.1 Blackplate

Blackplate is a light gauge base steel substrate which is the product of a single or dual step cold milling process. This substrate is characterised by its low carbon content ensuring both malleability and ductility as well as being cost-effective (9). This steel is prone to corrosion and is visually unappealing so is metallicity coated when used for packaging applications.

2.2.2 Chromium Coatings Used for Packaging Steel

2.2.2.1 Electrolytic Chromium Coated Steel (ECCS)

The industry standard for many years has been electrolytic chromium coated steel (ECCS). This substrate is characterised by a duplex coating of chromium metal (50-150 mg/m²) and chromium oxide / hydroxide (7-35 mg/m²) totalling between 10 and 30 nm in thickness. The specification of this deposition is standardised as part of EN 10202:2001 (10).

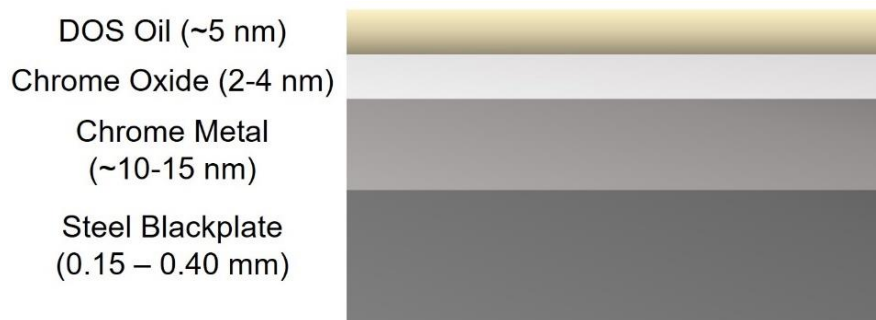


Figure 2.1 - Schematic showing the structure of ECCS (9).

As seen in Figure 2.1, the total chromium layer thickness is approximately 20 nm having an additional coating of lubrication (dioctyl sebacate (DOS oil)) applied serving to further protect the substrate before inspection, coiling and packaging. This metallic coating is significantly thinner than that of the lowest grade of tinplate (8).

Prior to the electroplating processes, the strip is alkaline cleaned at a low current density to ‘scrub’ the surface of any impurities, grease or inorganic oxides. The surface is then activated in a pickling bath containing sulphuric acid which involves the removal of any oxidic scale from the surface before being thoroughly rinsed.

The chromium is cathodically reduced onto both surfaces of the base substrate by an electrolytic process where the strip passes at high speed through one or more plating cells, typically within a matter of seconds. This electrodeposition of chromium is achieved through use of one of three processes which are established globally: "one step vertical process" (V-1), "two step vertical process" (V-2), and the "one step horizontal high current density process" (HCD) and three processes utilise Cr (VI) electrolytes (11). The chromium oxide thickness is best controlled in the two-step vertical process ($\sim 15 \text{ mg/m}^2$) with the one step vertical and HCD deposition of chromium oxide being less controllable offering coating weights of 10 and 2-8 mg/m^2 respectively (12).

Sulphate (SO_4^{2-}) and fluoride (F) are both present in the chromium oxide layers of all three electroplating techniques as a consequence of the composition of the electrolytes. Sulphuric acid is always used in the V-1 and HCD processes due to the single electrolyte nature of the deposition method (12). The two step (V-2) process does not use sulphuric acid in the chromium oxide electrolyte, but this is always used in the chromium metal electrolyte as it is necessary for the efficiency of the process (10)

Post electroplating, the substrate is passivated using chromic acid, further aiding in the corrosion protection of the substrate. Metal oxides are developed on the surface to create this barrier and in the case of Cr (VI) also exhibit some additional positive characteristics such as abrasion resistance and enhanced aesthetics. Passivation treatment also helps prevent sulphide staining in packaging steel and improves lacquer / laminate adhesion (13). This sulphide staining is characterised by the appearance of blue-black or brown marks on the interior of tinplate or ECCS cans. This occurs during processing when sulphur compounds from the product's proteins react with iron in the presence of residual oxygen, usually at cut edges or other points where iron exposure is increased. The deposit formed is a combination of iron sulphides, oxides and hydroxides. This can happen with products that contain protein, such as peas, sweet corn, fish, or meat, and is most visible in the headspace. While it is considered a cosmetic issue, it does not pose any harm and does not lead to further corrosion (14).

The production process of a can encompasses inherent deformation of the substrate. This deformation and straining of the ECCS substrate has been shown to cause cracking which exposes iron on the surface (15). This is problematic due to

chromium's corrosion potential being more positive than that of iron hence iron will corrode preferentially. For this reason, ECCS is commonly coated with a lacquer or laminate to stabilise this barrier and to prevent contamination and degradation of the substrate and foodstuff.

While ECCS does not have any Cr (VI) present in its final product state, the manufacturing process does utilise these harmful chemistries. One replacement for Cr (VI) based manufacturing process utilises Cr (III) and is the subject of this research(16,17).

2.2.2.2 Trivalent Chromium Coated Technology (TCCT)

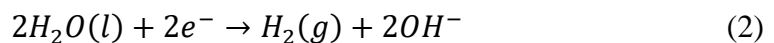
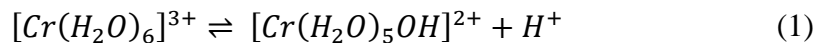
Research in the past decades have focussed on the development of Cr (III) electrolytes for decorative purposes with thicknesses up to and exceeding 100 μm (18,19). There has also been research into the use of Cr (III) in phosphate coatings. Phosphating processes involving chrome are used to apply a protective coating on metal surfaces. In this process, the metal substrate is immersed in a phosphating solution containing chromium ions and phosphate salts. The chemical reactions during this treatment form a thin, protective layer of chromium phosphate on the surface. This layer serves as a base for subsequent coating applications like paint and enhances corrosion resistance and adhesion properties. It's a critical process in industries such as automotive and appliance manufacturing for ensuring the longevity and durability of metal components (20).

More recent studies, however, focus on the technologies application in the packaging steel industry (21). Trivalent Chromium Coated Technology (TCCT) has been developed by Tata Steel and represents the next generation of REACH compliant packaging steel. Similarly to ECCS, these chromium layers are cathodically deposited onto a steel strip using Cr (III) based electrolytes.

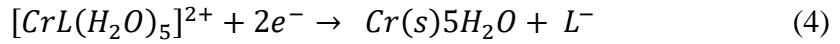
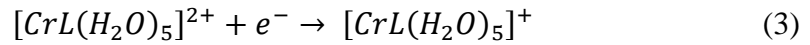
The chemistry of TCCT is controlled by the constituents of the electrolyte. The Cr (III) sources previously investigated include chromium chloride (CrCl_3), chromium acetate ($\text{Cr}(\text{CH}_3\text{COO})_3$) and chromium sulphate ($\text{Cr}_2(\text{SO}_4)_2$) (22). Current density, temperature, bath composition and mass transfer are key parameters in determining both the quantity and nature of chromium deposits from Cr (III) based electrolytes (23) and optimisation of both manufacturing process and electrolyte composition the subject of ongoing work.

2.2.2.2.1 Electrodeposition Mechanisms

At low pH, many metal ions exist in aqueous solution as aquo coordination complexes, often with the formula $[M(H_2O)_6]^{3+}$ (24). In the case of the trivalent chromium electrolytes used in the manufacture of TCCT, this complex is $[Cr(H_2O)_6]^{3+}$ which has low thermodynamic stability and high kinetic inertness. For this reason, complexing agents such as formate, acetate or glycine are used in these electrolytes to destabilise this very stable $[Cr(H_2O)_6]^{3+}$ complex ensuring metallic deposition without which the metal ions would form polymeric oxides, *Equation 1* (25). *Equation 2* takes place at the cathode, leading to a substantial increase in pH near the surface of the electrode. When the pH exceeds 4.5, the $[Cr(H_2O)_6]^{3+}$ complex undergoes hydrolysis, initiating reactions which ultimately yield high molecular weight polymers. These polymers are structured with Cr^{3+} ions connected through hydroxyl bridges; a process known as olation (22,26). As these polymers grow in molecular weight during the olation process, they eventually precipitate near the cathode surface. This precipitation restricts the accessibility of the Cr^{3+} ions for the intended reduction reaction.



Previous studies have investigated the influence of bath composition, mass transfer and applied potential of chromium deposition from a trivalent source containing formate using a rotating disk electrode, Song et.al (26). Key findings indicated that two consecutive reduction steps are required for chromium deposition: the reduction of a trivalent-Cr complex ion to a divalent-Cr complex ion and the reduction of the divalent chromium complex ion to metallic Cr. These steps are represented by *Equations 3 and 4* where L^- represents the formate complexing ligand. This reaction is summarised in *Equation 5*. The reduction of Cr^{3+} to Cr^0 is inherently difficult due to the reduction potential of the Cr^{3+} ion being more electro-negative than that of the reduction potential of H_2 , this inherently restricts the deposition process (27). The speed of these reactions is dictated by the transport of the chromium complex to the cathodes surface through the double layer.



These reactions have been studied by Wijenberg et.al who investigated the effect of electroplating parameters such as current density and electroplating time on the composition and structure of chromium metal-carbide-oxide coatings from a trivalent chromium-formate electrolyte without a buffering agent with chromium originating from a sulphate source (28). A deposition mechanism was proposed based on the deprotonation of water ligands due to an increase in pH caused by the hydrogen evolution reaction; three regimes were proposed, Figure 2.2.

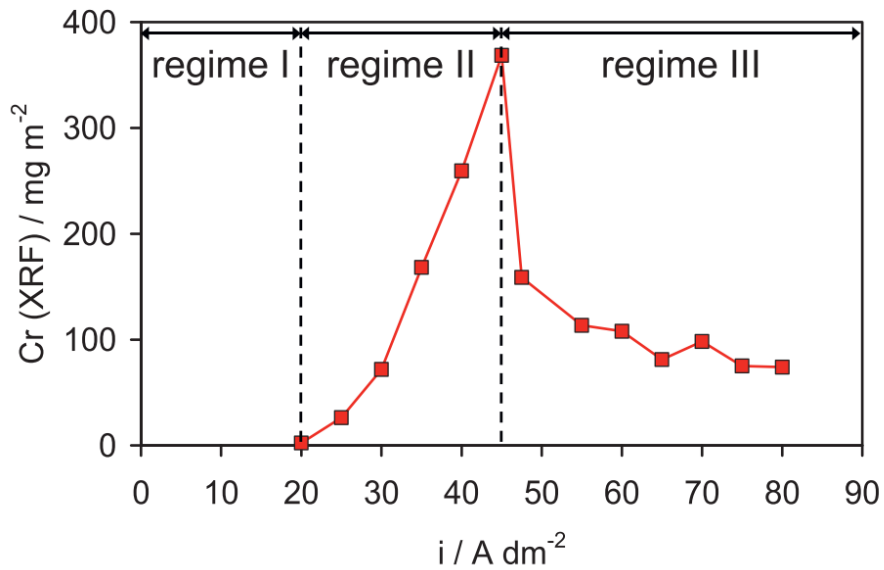


Figure 2.2 - Chromium total plotted against current density illustrating the regimes of deposition for Cr III based electrolyte (28).

At low current densities no deposit is formed on the electrode due to soluble $[Cr(HCOO)(OH)(H_2O)_4]^+$ being formed; this defines regime 1. Above a certain threshold of current density, $Cr(HCOO)(OH)_2(H_2O)_3$ is deposited on the electrode, this is regime 2. Part of the deposit is reduced to chromium metal and formate is broken

down leading to the formation of chromium carbide. The amount and composition of this deposit is dependent on the current density, mass flux and electrolysis time. Further increasing the current density lead to the deposition of $[\text{Cr}(\text{HCOO})(\text{OH})_3(\text{H}_2\text{O})_2]^-$ resulting in a deposit on the electrode which is mainly comprised of chromium oxide; this is regime 3 (28). In contrast to regime 2, the amount and composition of the deposit in regime 3 are almost invariant of the applied current density, mass flux and electrolysis time. These coatings were produced via a one-step electroplating process, depositing a mixed chromium metal-carbide-oxide coating layer. This electrolyte was evolved to contain only sodium-based salts (as opposed to potassium and sodium salts) allowing for increased solubility, electrolyte conductivity and kinematic viscosity which in turn meant that lower current densities were used and therefore lower rectifier voltages made the process more efficient. Due to the energy requirements necessary to obtain a consistent and substantial chromium oxide layer in regime 3, along with the chemistry of the metal-oxide-carbide layer formed, this coating procedure evolved to become a dual electrolyte process. The benefit of this is that the thickness of the coating can be tightly controlled with the optimisation of electroplating parameters, specifically the applied current density (29).

For trivalent chromium baths originating from sulphate sources (similar to those used in the production of TCCT), Protsenko et.al found that the optimal temperature for electrodeposition of metallic coatings was 35°C due to a decrease in temperature and increase in current density leading to increasing current efficiencies (30). This low temperature has been noted to affect the aesthetic quality of the deposit. Sulphites have since been discovered in basic chromium sulphate and have been shown to inhibit the chromium deposit onto the cathode through inhibiting the oxidation of formic acid (providing formate is used as the complexing agent) (31). Cyclic voltammetry measurements are required to check for the presence of sulphite and if found, applying a long reductive current will solve this issue.

Further work by *Haque et al.* has investigated current density, electrolysis time, temperature and pH on the trivalent chromium deposits used for decorative purposes, formed with CrCl_3 (23). The deposition process was affected by all factors, but a current density of 20 A/dm^2 , temperature of 40 °C and pH of 3 gave optimal current efficiencies.

In Cr (III) based electroplating processes, there is potential of breakdown of useful electrolyte components at the anode, this may form hazardous products such as Cr (VI). The oxidation reactions of Cr (III) based electrolytes with formate additions have been studied using both platinum mixed metal oxide (MMO) coated anodes comprising of iridium oxide (IrO_2) and tantalum oxide (Ta_2O_5) (32). It was concluded that the MMO electrodes allow safe usage of the electrolyte for industrial applications, platinum electrodes do not.

2.2.2.2.2 Characterisation and Performance of Historic TCCT

Melvin et.al provided physical and chemical characterisation of early iteration TCCT substrates manufactured using a single electrolyte, comparing them to ECCS and tinplate. Focus was placed on heat the treatment of materials up to temperatures of 200 °C (33). This heating of the substrate before coating was found to improve the adhesion of an organic lacquer by 5-15 % through forming additional oxide rich sites to which the lacquer could bond. It was concluded that increased chromium oxide levels improve the dry adhesion of protective coatings, and that heat treatment can be a key factor in influencing the adhesion of lacquers. A marked reduction in $\text{Cr}(\text{OH})_3$ hydroxide groups was measured at the surface after the heat treatment of 200 °C. Chromium carbide was found to be included in the surface layers of the TCCT, not being present on ECCS. In addition, iron was found in the chromium metal layer (5-10 nm) post heat treatment which was postulated to be a product of iron diffusion. This study concluded that the changes in physical characteristics of TCCT were insignificant post heat treatment.

Wint et.al studied the corrosion characteristics of one TCCT variation and compared it to the performance of ECCS (34). It was shown that filiform corrosion and cathodic disbondment were prevalent on the TCCT substrate and it was proposed that this was due to the porosity of the metallic coating. Within the localised corrosion cell, anodic metal dissolution located in the vicinity of a defect is coupled to the cathodic delamination form by a thin gel-like electrolyte, which ingresses beneath the coating. The thread-like anodic dissolution (filiform corrosion) involves anodic undercutting at the 'active head', driven by differential aeration arising from O_2 diffusion in the filament tail; this consists of dry corrosion product (35–37).

Allman et al. (16) (38) investigated the adhesion of BPANI lacquers to TCCT substrates. This work was focussed on assessing the adhesive performance in

simulated industrial conditions. Lacquer adhesion was characterised through scratch testing and surface chemistry was investigated through use of XPS. TCCT samples 61 and 63 respectively were first generation (single electrolyte) samples with 8.9 and 1.4% Cr metal and 25.0 and 27.1% Cr oxide respectively. In all cases ECCS outperformed the TCCT samples in lacquer failure force after coating with epoxyphenolic and BPANI lacquer apart from BPANI coated ECCS after retort in a citric acid and salt solution. A retort solution of 1% NaCl gave the lowest adhesion values of 2-6 N for TCCT and 8-12 N for ECCS. This was closely followed by lactic acid (3-4 N), acetic acid (4-5 N) and citric acid (7-10 N).

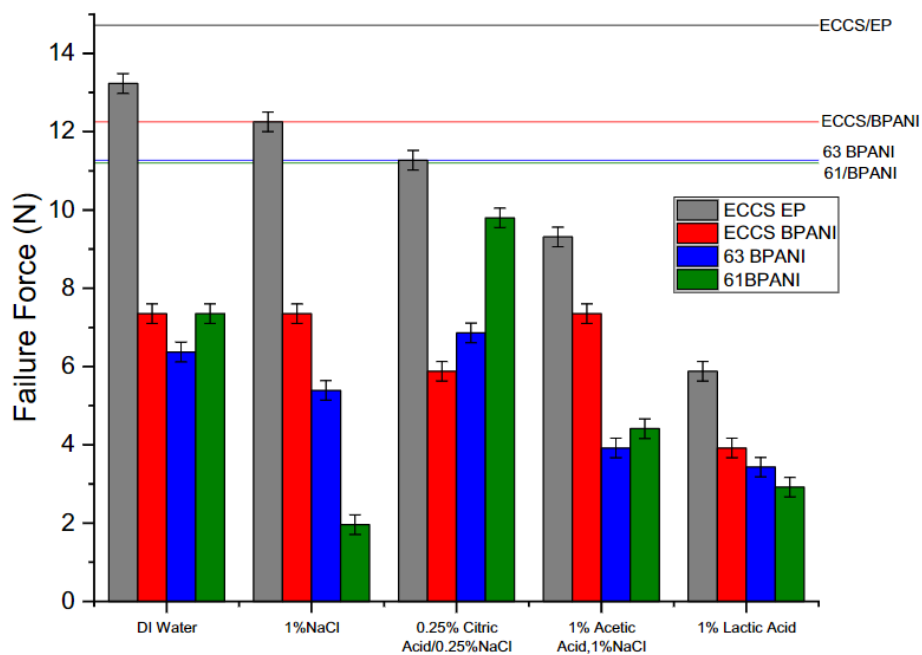


Figure 2.3 - The impact of simulant on measured wet adhesion for an exposure of 1.5 h at 121 °C. Pre-retort adhesion failure of each system is represented by the horizontal lines (38)

The findings from these studies indicate that a complete, homogenous chromium oxide layer is imperative in attaining desired adhesion characteristics in both dry and wet conditions. It highlights the superior performance of ECCS even when coated with BPANI lacquer, apart from in a solution of 0.25% citric acid / 0.25% NaCl. This retort solution may warrant further investigation.

More recently, *Prabhakar et al.* have studied the characterisation and delamination behaviour of TCCT materials using a similar methodology to *Wint et al.* assessing cathodic delamination (39). It was concluded that chromium oxide coating weight is crucial in limiting the delamination of a PVB coating using the SKP

technique; a chromium oxide thickness of 6 nm was found to perform similarly to that of traditional ECCS when a range of coating thicknesses 1.5 – 12 nm were tested.

2.3 Can Manufacture

2.3.1 Two Piece Can Manufacturing

Two-piece cans are constructed from a disc of metal which is reformed into a cylinder creating a seamless container. An end piece is then fashioned from a separate piece of substrate and seamed onto the can post filling. This production step is carried out through either the Draw and Wall-Iron (DWI) or the Draw and Redraw (DRD) process. DWI cans are drawn from an initial blank into a cup and then redrawn to the desired radii specification. Wall-ironing dictates the desired height of the can. The DWI process is economical for manufacturing large quantities of cans where the height is greater than the diameter of the can. DRD cans are drawn from a blank in two stages, firstly into a shallow cup, and then again to produce a can of the desired specification.

2.3.2 Three Piece Can Manufacture

Three-piece cans are made from a rolled piece of flat substrate onto which a seam is added, usually by welding. Ends are then added to the can separately. Three piece cans are subject to less metal deformation through the manufacturing process due to the separate end pieces. One of the ends is typically attached by the manufacturer and the other by the can filler (40). Three-piece cans are extremely versatile in their application due to their ability to be formed into any practical combination of height and diameter (14).

2.3.3 Can End Manufacture

The can end should be strong enough to withstand both the internal and external pressure applied to it. It serves to protect the product and act as a means of opening the can through either conventional methods or in the form of an 'Easy-Open' end. The ends are manufactured from sheet substrate into a circular blank where a press then contours the geometries required. This blank may be lacquered, in which case lubricant is required before end formation to ensure the integrity of the lacquered layer. The final step in can end manufacture is the thinning of the outer circumference allowing for it to be broken easily for opening. Once filled, a seaming process will

hermetically seal the can and is one of the most critical control points and is illustrated in Figure 2.4, ring pull may also be fastened. Figure 2.5 illustrates the various food and drink cans and their various shapes and manufacturing methods (14)The shaping is completed via a two-step roller process, the specification of which is provided by the can maker.

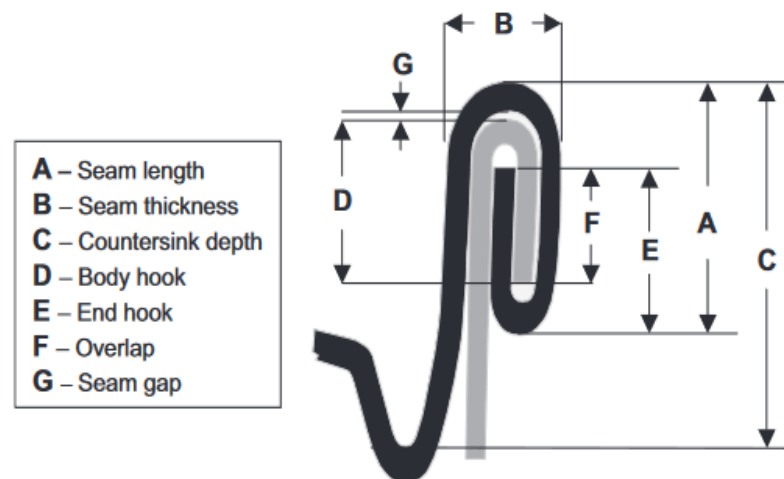


Figure 2.4 - Main measured parameters in a double seam (41).

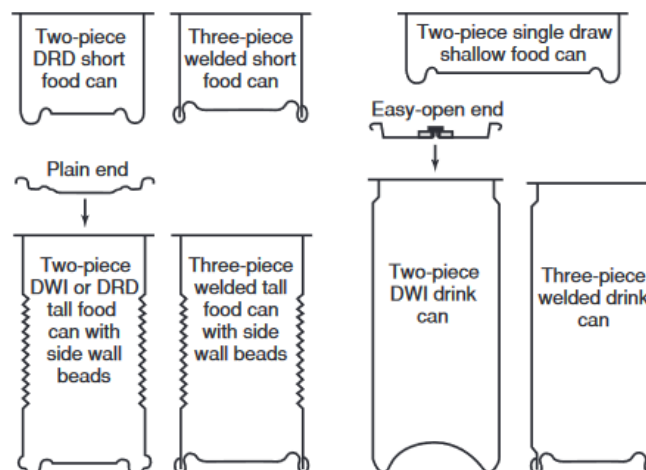


Figure 2.5 - Typical round section food and drink cans (41).

2.3.4 Packaging Steel Lifecycle

Once filled and seamed, a can containing food products may be sterilised before storing until use. It is imperative that the lacquer / substrate boundary's integrity is maintained throughout these two processes.

Filling for carbonated beverages usually occurs under vacuum while filling for food usually occurs under ambient pressure and while the foodstuff is hot or yet to be cooked. In the case of food, the cans are subjected to a retort process which further cooks the food and ensures the microbiological safety of the product (42). The high heat and pressure environment (typically 121-140 °C), coupled with the varying food stuff chemistries, leads to a range of interactions that occur between the lacquer and the substrate. This is commonly accepted as the harshest environment which canned goods will experience in their lifetime (43).

It is of utmost important that the lacquer / substrate boundary remains intact when subjected to heat, pressure and varying chemical mixtures over the whole lifecycle of the product.

2.4 Packaging Steel Protective Coatings

Organic coatings (lacquers and laminates) are widely used in the manufacture of metallically coated food cans. They are typically applied as single or multiple coats to the interior and exterior of the can, with film thicknesses ranging from 1.5 to 15 µm (44,45). The interior coating must protect the metal from corrosion while also avoiding or limiting metal-food contact. The outer coating is typically a polyester lacquer over which the label is printed, and it serves to decorate and protect the can's exterior. The barrier that the lacquers provide increase the longevity of the product and is key in ensuring the packaged contents are always of the highest quality, whenever consumed. It is worth noting that not all substrates require a protective coating. For example, in the case of tin cans which hold lightly coloured mildly acidic liquids, interactions are mitigated by the tin oxidising more readily than the foodstuff and the fact that there is limited oxygen available to drive this process in a hermetically sealed can.

Lacquers are deposited using an anilox roller coating and are therefore in liquid form. The composition of these coatings can be up to 80% solvent in order to ensure ideal wetting conditions (46). The main function of the solvent is to regulate properties such as viscosity and surface tension, aiding in the formation of a thin lacquer layer.

These coatings are cured at high temperatures which induce a cross-linking reaction in the polymer therefore ‘setting’ it. During this process not only does the lacquer become cured, but it also adheres to the substrate. This bonding needs to be able to withstand the forming of the can to come and the retort process in which the can is sterilised. These bonding theories are explored further in section 0.

The interaction between packaging steel and its protective lacquer has traditional been investigated through the analysis of the substrate, However, using infrared techniques, the lacquer may be investigated in detail. Manfredi et. al used FTIR (Fourier transform infrared spectroscopy), DSC (Differential scanning calorimetry) and TGA (Thermo-gravimetric analysis) to obtain helpful information about the degree of curing and composition of epoxyphenolic lacquers (47).

2.4.1 Protective Coating Chemistry

Due to the variety of substrates and foodstuffs there are a range of lacquers and lacquer chemistries used to optimise the coating, curing, adhesion and performance properties. Legislation is ever changing and dictates the lacquer chemistries to some extent. Volatile Organic Compound (VOC’s) emissions are currently being targeted for reduction in this particular industry. Hydrocarbons, ketones, alcohols and esters are examples of these compounds.

2.4.1.1 Phenolic

These resins are most commonly composed of phenols and aldehydes which have been shown to be highly corrosion resistant and protect cans from sulphide staining. Due to their low flexibility and poor adhesive characteristics, they are not used in the food packaging industry in their unblended form but are commonly used as crosslinkers (48).

2.4.1.2 Epoxyphenolic Coatings

Epoxyphenolic lacquers are traditionally the mainstay of the food packaging industry due to their high degree of flexibility, adhesion and thermal stability coupled with their chemical resistance (49). The most common epoxy coatings are synthesised from bisphenol A (BPA) and epichlorohydrin to form bisphenol A-diglycidyl ether epoxy resins, Figure 2.6. Phenolic resins are often added to lacquer chemistries due to their ability to increase cross-linking and therefore the corrosion resistance and ability to

resist sulphide staining (50). These epoxyphenolic resins are produced through the reaction of an epoxy and phenol formaldehyde resins (46).

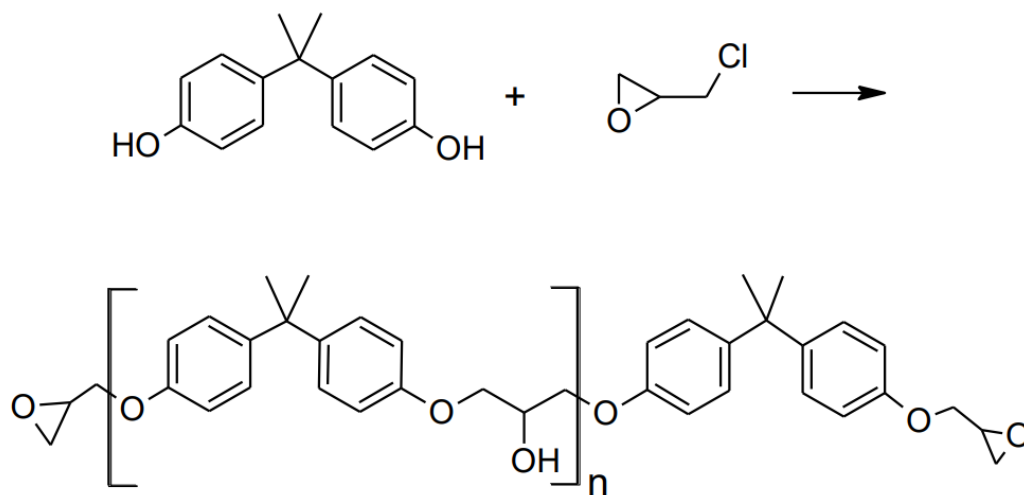


Figure 2.6 - Reaction formation of an epoxyphenolic lacquer.

2.4.1.3 Polyester Coatings

Polyesters are formed through a condensation reaction between an alcohol and a carboxylic acid and are increasingly used due to legislative pressure dictating the removal of BPA from food contact materials (51). A common use for these coatings includes polyethylene terephthalate (PET) films which are often laminated onto substrate materials. They have been shown to be unstable in acidic conditions and have poor corrosion resistance (52).

2.4.1.4 Oleoresin

These coatings are made from mixtures of oil and plants and were the first to be used in the packaging steel industry (53). Their use largely stopped with the development of epoxy coatings, however, have been rediscovered as BPA-free alternatives. Although rather flexible, these resins have been reported to change the organoleptic properties of food as well as exhibiting poor adhesion and corrosion characteristics when in contact with metal surfaces (54). For these reasons their use is restricted to mild foods such as various types of beans.

2.4.1.5 Acrylic

The most common monomer used to synthesise acrylic coatings is Ethylacrylate. Like phenolic coatings, acrylic layers show good corrosion resistance and sulphide stain resistance, however, they have been shown to be brittle which poses issues when used for canning applications. They are absent of BPA and so are under investigation as replacement coatings to epoxyphenolic and are most used to coat the exterior of cans (55).

2.4.1.6 Vinyl

Vinyl coatings are synthesised using vinyl chloride and vinyl acetate monomers. Due to their poor adhesive characteristics, they are used as a ‘topcoat’ (56). Stabilisers and plasticisers such as vinyl organosols are necessary to ensure thermal stability. A common use for this material is the coating of soft drink cans.

2.4.1.7 Polyolefins

Polyolefin coatings are a relatively new product and exhibit good corrosion protection, adhesion and flexibility without impacting the flavour of food. A polyolefin is formed by the addition reaction of two individual monomer olefins, resulting in fibres that are then dispersed in an aqueous solution. These are used in beverage applications.

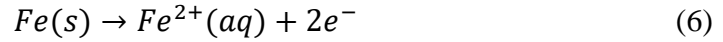
2.5 The Corrosion of Packaging Steel

The prevention and study of corrosion is of significant economic impact with its associated impact costing approximately 3.4 % of global GDP or USD \$2.5 trillion (57). Corrosion is the main mechanism by which delamination, flaking or defects may occur in a lacquer or laminate coating. The substrate passivation layer can significantly affect the corrosion characteristics of substrates and therefore the deterioration of the metal (58). The inhibition of this process is imperative for the consistency and longevity of packaging steel and therefore must be observed for all packaging substrates.

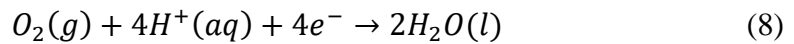
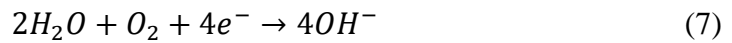
2.5.1 Corrosion Fundamentals

When in contact with air, a metal surface will often form a passive oxide layer on its surface. Corrosion does not initiate until an electrolyte is present allowing for ionic conductivity and therefore the dissolution of metal. This process is defined as an

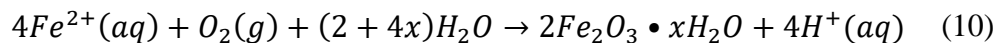
electrochemical redox reaction involving the transfer of electrons between two different species in electrical contact. Metal oxidation occurs when electrons are lost from the metal anode to a cathodic species, which accepts these electrons and is reduced. The anodic oxidation reaction is given in *Equation 6*.



The electrons liberated during the anodic reaction allow coupling to the cathode at which the reduction reactions take place. These reactions are given in *Equations 7, 8 and 9*.



At higher, alkaline pH conditions, hydroxyl compounds form (*Equation 7*). Oxygen reduction reaction (*Equation 8*) is favoured in neutral to high pH solutions with hydrogen evolution reaction (*Equation 9*) being favoured at lower pH's. The Fe^{2+} ions produced in the initial anodic reaction (*Equation 6*) are then oxidised by oxygen present in the system to produce the insoluble hydrated oxide containing Fe^{3+} , as represented by *Equation 10*. The reactions described are simplified in Figure 2.7.



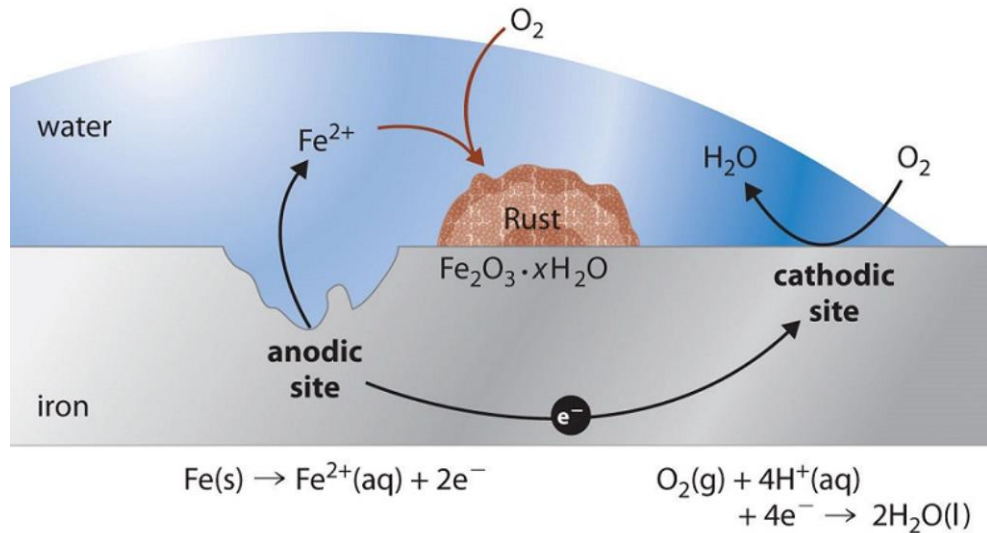


Figure 2.7 - Anodic and cathodic reactions that occur on substrate materials represented as an Evans droplet (53).

2.5.2 Corrosion Mechanisms

Many mechanisms of corrosion may present within the context of packaging steel and their protective coatings. Pitting and cathodic disbondment mechanisms are detailed within this section as they have been identified as the most relevant within the scope of this study (59).

2.5.2.1 Pitting Corrosion

Pitting corrosion is a localised form of corrosion that results in the formation of small holes or pits on a metal surface. The process of pitting corrosion can be divided into two main stages: initiation and propagation (60,61).

The initiation of pitting corrosion occurs when a localised area on the metal surface becomes deprived of oxygen or protective layers, which allows it to be exposed to the surrounding environment. The process of initiation can be triggered by several factors. Presence of aggressive ions: Certain ions such as chloride, bromide, and fluoride are known to be highly aggressive and can trigger the initiation of pitting corrosion by breaking down the protective layer on the metal surface. High-temperature exposure: High temperatures can cause the breakdown of the protective oxide layer on the metal surface, leading to the initiation of pitting corrosion (62). Mechanical damage: Mechanical damage such as scratches, dents, and cracks can also break down the protective layer, leading to the initiation of pitting corrosion.

Once the initiation phase has occurred, the corrosion process progresses to the propagation phase. During this phase, the metal surface undergoes anodic and cathodic reactions that result in the formation of a pit. The mechanism of propagation can be described in terms of the following steps. Anodic dissolution: At the bottom of the pit, the metal undergoes anodic dissolution, where metal ions are released into the solution. This is due to the fact that the metal surface becomes anodic (positive) relative to the surrounding cathodic (negative) surface. Cathodic reaction: The surrounding cathodic surface provides electrons to the metal ions released from the anodic dissolution, resulting in the formation of corrosion products. Transport of metal ions: The metal ions released from the anodic dissolution are transported away from the pit by diffusion and convection. This results in the formation of a pit with a cone-like shape, with the tip of the cone being the site of the anodic dissolution and the walls of the pit being the site of the cathodic reaction. Re-passivation: The propagation of pitting corrosion is often self-limiting, as the corrosion products generated during the cathodic reaction can help to re-form a protective oxide layer on the metal surface (63). This can slow down or stop the progression of the pit. Pits that survive the nucleation process are known as metastable pits since their continued survival is dependent on their maintaining the oxide layer. If the pit cover ruptures, the pit will die (64). It is only when pits become stable that the corrosive attack becomes potentially damaging. Pitting corrosion is visualised in Figure 2.8.

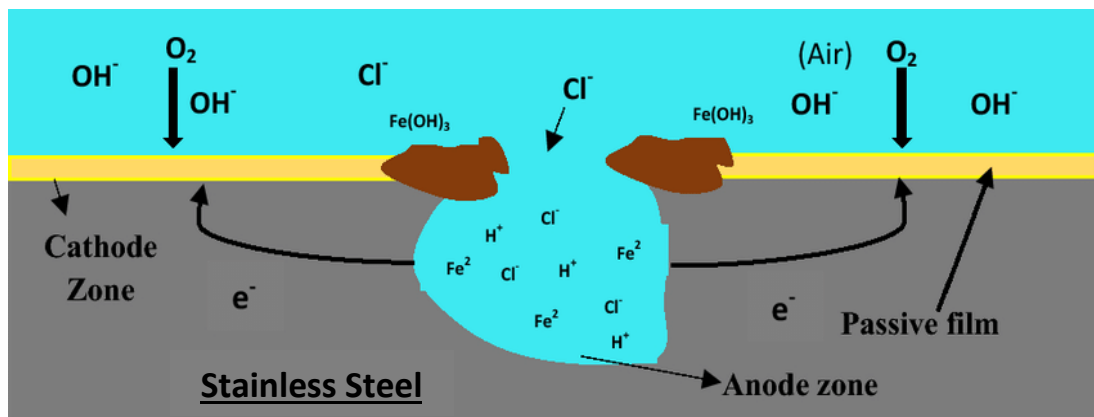


Figure 2.8 - Pitting corrosion schematic.

2.5.2.2 Cathodic Disbondment

Cathodic disbondment is also a key corrosion mechanism by which the adhesion of organic coatings on substrate materials is damaged. Cathodic disbondment of a coating can occur in the presence of a coating defect when the metal substrate is exposed (65,66). This involves the loss of adhesion between a coating and substrate due to the products of a cathodic reduction reaction that takes place in the interfacial region of coatings. In this case, the diffusion rate of oxygen through the electrolyte layer limits the corrosion rate (67). At an intact (defect-free) metal/polymer interface the kinetics for electrochemical reactions are very low. The metal oxidation is completely inhibited and no electrons are available for oxygen reduction. This results in a positively charged interface. When these two interfaces are brought into contact, via a defect in the coating, electrons flow through the metal from the defect to the intact interface. Here they are available for oxygen reduction, provided there is ionic conduction along the interface to close the circuit. Intermediate products of the oxygen reduction are hydroxyl radicals (*Equation 7*). The hydroxyls are aggressive and reactive molecules that cause the destruction of the adhesion between polymer coating and steel substrates. At such high pH at the delaminating interface, iron is passive; even though the bond between polymer and metal is gradually destroyed, there is little or no corrosion of iron. The anodic reaction occurs only at the defect site itself (59).

Boelen et al. investigated the mechanisms of defect growth in packaging cans with a polymer protective coating. One of the key findings in this study was that oxygen reduction is the rate-determining step in the cathodic disbondment of the PET coating as proved by witnessing no disbondment in cans to which ascorbic acid had been added to eliminate the dissolved oxygen in solution. In addition, chromium metal and oxide levels were found to be crucial in the adhesion of this coating serving to prevent iron exposure from the underlying substrate and inhibit the propagation of corrosion respectively.

This is further evidenced by the findings of Doherty et.al who state that cathodic blistering started when corrosion first began under a lacquered coating on ECCS. It is suggested that this blistering is caused by an osmotic transfer of water through the coating and that initiation of defects may be from inconsistencies in the substrates pre-treatment or defects caused by the DRD process (68).

Understanding D values or diffusivity values is crucial when discussing the osmotic transfer of water through a protective coating. Essentially, D values can help in quantifying the rate at which water molecules permeate through the coating. Higher D values signify a rapid transfer rate, potentially leading to increased corrosion (69).

The diffusivity values for many polymers (including epoxy resins) in relation to water vapor tend to be in the range of 10^{-10} to 10^{-12} m²/s. Epoxy lacquers, being relatively impermeable, would likely be at the lower end of this range, showcasing their effectiveness in preventing the transmission of water molecules and hence their utility in corrosion protection (70). Polyester lacquers, while still offering a reasonable level of protection, might exhibit D values at the higher end of the afore mentioned range due to their molecular structure and the types of bonds present (71).

2.5.2.3 Filiform Corrosion

Filiform corrosion, a type of localized corrosion, manifests itself through worm-like filaments primarily under organic coatings such as paint on metal substrates, including chrome-plated steel. The mechanism is facilitated through a series of microcell formations. The anodic sites, where metal dissolution occurs, are located at the head of the filaments, while the cathodic sites are towards the tail, encouraging the propagation of filaments beneath the coating. Filiform corrosion leverages the inherent heterogeneities in the chrome-plated surface, including defects from manufacturing processes such as microscopic inclusions or imperfections in the coating. To prevent filiform corrosion on chrome-plated steel effectively, various approaches may be used. This might include refining the initial treatment processes to reduce imperfections in the substrate, upgrading the chrome plating process to create a more consistent and less porous surface, and adding protective layers after plating that can better resist water and oxygen.

This mechanism has been investigated on TCCT (34), however, is out of scope for this project and will not be mentioned further.

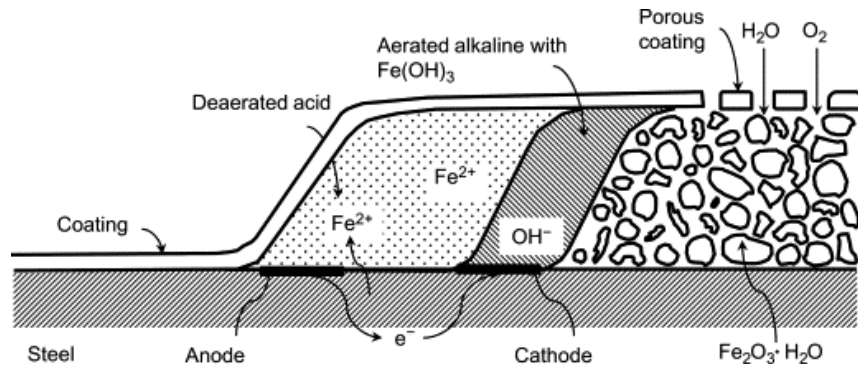


Figure 2.9 - Filiform corrosion filament on a steel substrate (58)

2.5.2.4 Corrosion of TCCT

The corrosion of chrome plated packaging steel has been researched in some detail. Notably, *Wint et.al* investigated the atmospheric corrosion of TCCT using a scanning kelvin probe (72). It was found that differences between the Cr^{3+} and Cr^{6+} based coatings in terms of resistance to atmospheric corrosion, such as cathodic delamination and FFC occur, firstly due to pores in the Cr^{3+} coating which exist because of the deposition mechanism, and secondly due to the chemical composition of the coating. XPS depth profiles indicate that layers containing Cr^{3+} have a greater presence of surface metallic iron and fewer outer OH^- groups, potentially leading to accelerated rates of delamination caused by corrosion. It was suggested that future work concentrates on the quantitative measurement of the adhesion of organic coatings and lacquers to chromium-based coatings, and consequently the correlation between adhesion and corrosion properties.

In a continuation of this work, *Edy et al.* examined the corrosion resistance of TCCT by examining the metallic coating formation (59). It is shown in this work that the thickness, composition, and quality of the chromium metal coating is important. Substrates containing similar amounts of Cr_2O_3 compared to that of ECCS performed comparably in resistance to corrosion delamination of an organic coating. It is plausible that the Cr_2O_3 negated the detrimental effect of the pores as highlighted by *Wint et al.* and hindered the interfacial electron transfer process at the delamination front which in turn limits the oxygen reduction reaction. This finding is important in understanding the adhesion behaviour of the substrate.

The use of citric acid as a pretreatment for TCCT substrates was investigated by *Allman et.al* through use of the SVET (Scanning vibrating electrode technique) (73)

It was found that it was possible to increase the adhesion performance of the substrate. The operating window of treatment was a function of solution temperature and time, with the best performance being achieved in 5 mins at 95°C. Overexposure to citric acid had a detrimental effect on substrate/lacquer adhesion. The primary mechanisms of citric acid treatment were identified as iron dissolution and chrome oxidation, which enhanced the number of substrate surface bonding sites.

2.6 The Adhesion of Lacquers to Packaging Steel

Adhesion refers to the process whereby two distinct surfaces stick to each other, often involving physical, chemical, or mechanical bonds facilitated through various intermolecular and surface forces (in the case of this research these surfaces are chromium plated steel substrates and an organic lacquer) (74). The adhesion properties associated with these lacquers are key in determining the success of a canned food product.

It is imperative that both the dry and wet adhesion properties of the lacquer are adequate. Dry adhesion represents the polymer binding force in the absence of an aqueous solution whereas wet adhesion is a measure of the capacity of the coating to block the formation of a metal-solution interface. The lacquer must remain strong through the mechanical processing of the substrate and provide an adequate barrier between the can contents and the substrate without delaminating or flaking (46).

Failure of adhesion is the separation of or near the interface of the materials, usually occurring under mechanical tension or due to chemical interactions such as corrosion. Adhesion resistance is an irreversible macroscopic property which can be tested in numerous ways including tape testing, scratch testing and T-peel testing (75). When measuring adhesion, it is important to identify the location of failure as this determines whether adhesion or cohesion is being measured. In this case cohesion is defined as the intra-coating molecular adhesion force (76).

The adhesion performance of lacquers to substrate materials is dependent on the surface chemistry of the substrates and the chemistry and curing of the coating (77). This will dictate the nature of the bonding which may take place. It is commonly accepted that there is no single theory to explain adhesion, but it is commonly divided into physical and chemical mechanisms.

2.6.1 Mechanisms of Adhesion

Adhesion is a complex phenomenon and can be dependent on many factors. In the case of adhesion of coatings to steel packaging substrates these could be, but are not limited to, temperature, surface topology, interacting chemistries and environment. There are many different theories relating to the mechanisms of adhesion, but it is widely accepted that no theory acts singularly in a given situation, Table 2.1 (78). A combination of theories will likely explain adhesion more accurately. The theories of mechanical interlocking, adsorption, chemisorption / chemical bonding, diffusion bonding and electrostatic bonding are discussed.

Table 2.1 - List of Adhesion Mechanisms (78).

Number	Adhesion Theory	Scale of Action
1	Mechanical Interlocking	Macroscopic
2	Adsorption	Molecular
3	Chemisorption / Chemical Bonding	Molecular
4	Diffusion	Molecular
5	Electrostatic	Macroscopic

2.6.1.1 Mechanical Interlocking Theory

Mechanical adhesion is concerned with the interlocking of the surface topology of a substrate with a polymer. The factors that influence this mechanism are the surface roughness (and therefore the surface area), porosity and wettability of the polymer. This is visualised in Figure 2.10 where good wetting gives rise to mechanical interlocking.

Van der Waals forces play a crucial role in mechanical adhesion. These forces act over an extremely small distance, in the range of approximately a nanometre, and are responsible for holding polymer chains together. They can be ruptured by extreme deformation of a metal substrate after coating due to their brittle nature. However, Osouli-Bostanabad et.al proved that polished surfaces have shown some of the highest adhesion strengths among steel surfaces with varying roughness levels, contradicting this theory and proving that this model is not always accurate (79).

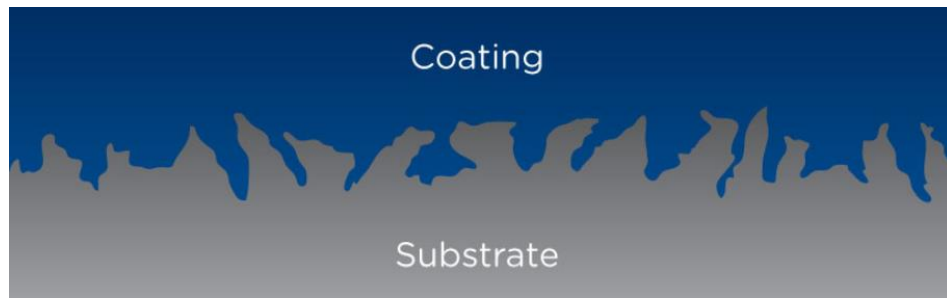


Figure 2.10 - Diagram of a coating mechanically interlocking with a surface.

2.6.1.2 Adsorption Theory

Adsorption theory considers the surface energy, wettability and weak boundary layer interactions. The adhesive, or polymer in this case, must have lower surface energy than the substrate in order to wet. As shown in Figure 2.11, poor wetting of the polymer on the substrate may result in defects or air bubbles at the interface causing a non-homogenous contact area exacerbated by the contact angle and therefore the surface tension (78). Good wettability ensures that maximal surface area between the polymer and substrate is realised.

If the interface between the polymer coating and substrate is disturbed by air bubbles, inclusions or interactions between components of the coating / substrate and the inclusions, adhesion will be negatively impacted. Poor wettability is an example of a mechanism of forming a weak boundary layer. Air entrapment or inclusions will inhibit the formation of chemical bonds and therefore reduce the adhesive potential. It is therefore clear that the coating should spread on the substrate to achieve good adhesion. Spreading the coating will make it easier for it to penetrate surface structures and introduce new binding sites. Contact angle is often used to evaluate bonding issues as it is a measure of wettability.

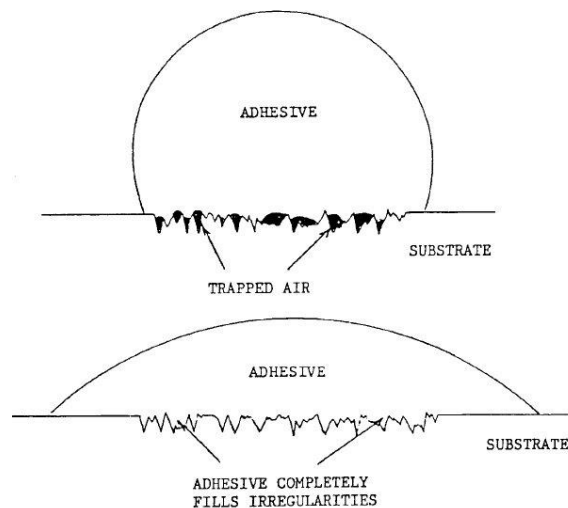


Figure 2.11 - Illustration of good and poor wettability and its effect on adhesion (80).

2.6.1.3 Chemisorption / Chemical Bonding Theory

Chemical interactions at the lacquer / substrate interface can prove crucial in dictating the desired adhesion properties. Chemisorption theory of adhesion (otherwise known as the interaction theory or thermodynamic theory) is the most commonly accepted mechanism of adhesion with bonding occurring due to Van der Waals forces or bonding between substrate and lacquer (81).

Chemical bonding has the potential to be extremely strong as electrons are shared or swapped between atoms forming covalent or ionic bonds. Hydrogen bonding is a slightly weaker classification of chemical bond but still effects the adhesion characteristics positively along with other intermolecular forces. These intermolecular forces may be defined as any of the following (16):

- Dipole
- Dipole-dipole forces
- London dispersion forces
- Polarisability

In the case of chromium plated substrates, the chemical interactions between the lacquer and the passive oxide rich surface is critical for good adhesion performance. This bond is dependent upon the formation of chelates of the polymer's oxygen atoms with the metal atoms (82). A mixture of mechanical and chemical

adhesion is the strongest form due to the atoms / molecules of the two joining materials becoming interlinked and establishing bonds that can be ionic or covalent in nature.

2.6.1.4 Diffusion Theory

The interdiffusion of substrate to adhesive will give rise to good adhesion characteristics. This mechanism is likely to occur at high temperatures where a high degree of polymer chain mobility is observed such as during the lamination of polymers onto polymer substrates. Such a mechanism therefore is not pertinent to the application in discussion and is therefore only briefly mentioned in this review.

2.6.1.5 Electrostatic Theory

This theory outlines the adhesion of a polymer to a dissimilar surface, taking place due to an interaction between unlike electronic band structures. Specifically, it draws upon the electric double layer effect illustrated in Figure 2.12, explaining how the surfaces electrically attract each other when one surface has a net positive charge and the other a net negative charge.

The composition of the electric double layer has consequences for the overall adhesion properties for the polymer. On the bottom surface of the polymer is a homogenous layer of charged ions. However, a second layer of ions are attracted to the first via the Coulomb force electrically screening the first layer from the bulk material. This diffuse layer is loosely associated with the surface layer due to its motion being influenced by both thermal and electric effects. This is countered by the addition of an adhesion promoter within the polymers structure such as organosilanes. This treatment in particular has been proven to greatly improve the adhesion between the interfacial layer of the polymer and substrate through it containing two reactive groups which form strong bonds between both the polymer and the substrate. This chemical link is characterised by its high bond strength, corrosion resistance and moisture barrier properties promoting both wet and dry adhesion and improved bulk physical properties (83). *Randow et al.* investigated this and has shown that this theory is applicable to polymeric films. It was shown that the adhesion depended on the physical absorption and the static electrification of the plasticised PVS, LDPE or plasticised PVC (16)(84).

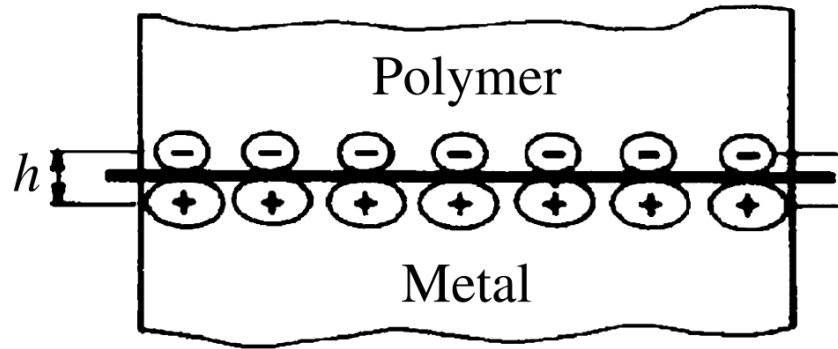


Figure 2.12 - The electric double layer effect of a polymeric material on metal substrate (67).

2.6.2 Adhesion Testing

Many methods have been used historically to assess the adhesion properties, strength and quality of coatings to substrates. The methods are split broadly into two categories: subjective assessments based on visual representations of adhesion, and quantitative analysis which provides numerical classifications of adhesion.

In 1975, Mittal provided a review of thin film (<1 μm thick) adhesion measurements splitting the techniques into three categories: nucleation methods, mechanical methods and miscellaneous techniques. The review focussed mainly on the quantitative methods of measurement but states the 'ideal test', incorporating all requirements and process variables such as weathering, does not exist and therefore a diversity of testing is always advised (85).

The relevant adhesion tests that may be used on a macro scale either in industry or as a standard in order to understand the quality or strength of adhesive bonds are noted. It is imperative that the testing methods are both reliable and repeatable. The method of testing must not interfere with the samples surface chemistry in any way, as well as being suited to a range of chemical environments itself. The methods employed must characterise a large enough surface area as to draw conclusions about the substrate / coating as a whole and be suited to measuring a range of coating and substrate thicknesses. The testing method used will be dependent on the in use application.

2.6.2.1 Scratch Testing

Pioneered in the 1950s, scratch testing is perhaps the most accepted method used to quantitatively measure the adhesion strength of a protective coating (86). This method is used in industry as well as academic settings and is known for its simplicity.

This test involves dragging a sharp, weighted tip across the surface of a coated substrate. This tip will eventually cause the disbondment of the coating and hence a quantitative value of failure force is achieved. This coating failure will (in the case of metallic packaging steel) cause an electrical contact between the tip and the substrate and it is at this point at which the failure weight is recorded. This is then translated into a failure force as opposed to adhesion force due to the result being a measured combination of the cohesive bonding of the coating and the adhesive force between the coating and the substrate. This testing method is operated in accordance with ISO 1518:2011 (87).

Allman et al. have used this testing method to examine the adhesion of lacquers to ECCS and TCCT substrates (38). This study proved the superior properties of both epoxyphenolic and BPANI lacquers to ECCS substrates. The measured adhesion performance of the BPANI lacquer on both the ECCS and the TCCT is considerably less when compared to the epoxyphenolic lacquer. This adhesion is further negatively affected by mild saline and acidic conditions. These findings are attributed to the sensitivity of the BPANI lacquers to vapour absorption and therefore aid in the corrosion of the substrate through this inherent porosity which is at further detriment to the adhesion properties. It was noted that when DI water was used as a simulant solution for the BPANI lacquer, the adhesion was completely recoverable under ambient conditions. This is due to the polyester readily absorbing H₂O into the bulk and has been proven elsewhere (88,89).

2.6.2.2 Tape and Cross Hatch Testing

The adhesive strength of a coating can be measured through a tape test, and by extension a cross hatch test. The premise of a tape test is that tape is adhered to the coating and peeled off at 90° to the substrate. The coating is then examined for defects and inconsistencies. The speed at which this tape is removed is crucial (90). The cross hatch test employs the same experimental procedure, however, a cross hatch is manually cut into the coating through use of either a machine or handheld instrument.

The inherent problem with these methods is the subjective method of assessment and therefore the technique is limited as far as quantifiable information is concerned. It is also widely accepted that these techniques are mostly suitable for hard yet flexible coatings (91). In the case of the handheld cross hatch test, it is difficult to be consistent in both the angle of the instrument and force applied and therefore leads to further questioning of this technique's validity.

2.6.2.3 Dome Testing

This is yet another extension of a tape test but is an adhesion testing method in its own right. In this test, a coated specimen is biaxially stretched a given distance in an appropriate machine. Adhesive tape is applied to the deformed area (the dome) and then pulled off. The amount of coating removed is then compared to a photographic standard to determine the adhesion rating. This testing method is carried out in accordance to ASTM D7093-19 (92).

2.6.2.4 Pull-Off Testing

Sometimes referred to as 'dolly testing', this test involves using an adhesive to stick a 'dolly' or 'stub' to a coating and measuring the force used to pull it off. Failure occurs along the weakest plane within the system comprised of the dolly, adhesive, coating system and substrate and will be exposed by the fracture surface. This method maximises tensile stress as compared to the shear stress applied by other methods such as the scratch or tape test and so results may not be comparable. These tests are classified as being fixed aligned or self-aligning depending on their ability to ensure a vertical pull off force. Best repeatability is obtained when the pull-off force acts perpendicularly to the surface being tested.

This testing methods use is governed by both ISO 4624 and ASTM D 4541; the former dictating the standards for the 'Pull off test for adhesion' and the latter for measuring 'The strength of coatings using portable adhesion testers' (93)(94).

2.6.2.5 Lacquer Coating Durability

Lacquer durability and lacquer adhesion, while interrelated, refer to different properties of a lacquered surface. Durability refers to the ability of the lacquer to resist degradation over time, maintaining its properties and appearance despite exposure to adverse conditions such as UV radiation, corrosion, abrasion, or chemical exposure (95,96). Good durability means the lacquer will have a long lifespan, providing protection and maintaining its aesthetic properties for an extended period. Durability can be measured through accelerated aging tests, which involve exposing the lacquered surface to harsh conditions (like high temperatures, corrosive environments, etc.) for a set period and then assessing any degradation (97). Other tests might involve subjecting the lacquer to mechanical wear (like abrasion tests) to see how well it resists damage (98).

2.7 Literature Review Conclusions

The information analysed in this review dictates the direction of this thesis. The adhesion of protective coatings to packaging materials has been shown to be a multi-faceted topic requiring considerations from both a process and manufacturing point of view. The effect of substrate chemistry has been highlighted.

- A significant quantity of research has been conducted into the replacement of ECCS with TCCT, in particular relating to historic iterations of the material having been produced using a single electrolyte process. This research has primarily focussed on the corrosion behaviour of the materials overall but more recently concentrated on the adhesive behaviour of protective lacquers. Next generation substrate materials require investigation using consistent experimental methodologies for comparison and optimisation.
- The production of TCCT materials has been highlighted as key in ensuring the long-term performance of substrates through inhibiting corrosion and promoting adhesion. For this reason, the effect of process parameters on the deposition of metallic and oxidic chromium coatings presents a unique opportunity in which to conduct research.
- With the ever-changing chemistries of TCCT, as the industry moves closer towards commercially viable products, it is necessary to characterise, both

physically and chemically, novel materials as-well as assessing their performance in simulated industrial conditions.

- Currently, the industry uses a lot of qualitative adhesion testing. They are short tests to determine whether coatings are effective or not 'on-line'. These tests have several problems. The tests frequently depend on the operator and are subjective. Cross hatch testing is therefore not an ideal way of measuring adhesion however scratch testing utilised in more recent literature will prove useful in quantitatively measuring the adhesion force of organic coatings.
- There have been three main areas for research identified: substrate surface chemistry, lacquer adhesive performance and substrate manufacture / electrodeposition.

Chapter 3 – Materials and **Methods**

3 Materials and Methods

Having reviewed relevant literature pertaining to both packaging steel substrates, their manufacturing methods and protective coatings, it is now relevant to state and describe the materials and methods by which these will be both manufactured and investigated with respectively.

3.1 Materials

Blackplate and ECCS were obtained from TATA Steel UK and novel TCCT substrates from TATA Steel Europe (IJmuiden) which were either developmental materials or made in Swansea University laboratories under direction from TATA Steel. Lacquers used in this experimental work were sourced from Metlac and are identical to those used in the food packaging industry.

3.1.1 Substrate Materials

A total of 15 novel TCCT substrates were obtained. The surface chemistries of these materials vary due to the manner in which the substrates were manufactured. This TCCT was produced on a small scale pilot line, typically used for the optimisation of the electroplating process. Table 3.1 details the specific production parameters and XPS derived metallic and oxidic chromium coating weights of the substrates. This information originates from TATA steel Europe (99).

Table 3.1 - 2019 TCCT electroplating parameter information and chromium metal and oxide chemistries for samples acquired for project.

2019 TCCT Sample Set						
Sample Reference	Line Speed (m/min)	Anodes	Charge (C/dm ²)	Current (A/dm ²)	Chromium Metal (XPS) (mg/m ²)	Chromium Oxide (XPS) (mg/m ²)
A	100	7	10	10	131	4
B	100	7	15	14	91	21
C	150	1	3	30	69	17
D	150	6	11	18	73	13
E	150	7	10	14	71	6
F	200	7	10	19	62	8
G	200	6	12	27	65	23
H	200	6	10	22	71	13
I	250	7	8	19	63	3

J	250	5	5	17	58	2
K	250	7	10	24	67	8
L	300	7	10	29	76	10
M	300	7	8	23	65	5
N	350	7	12	40	66	6
O	350	7	10	33	90	9

3.1.2 Organic Coatings

Within the packaging steel industry, protective coatings are applied to the surface of substrates. An epoxyphenolic lacquer was used as a control, against which ideal and current levels of adhesion performance can be compared. In addition, a bisphenol-A non-intent (BPANI) polyester-based lacquer was used. Both materials were manufactured by Metlac, details of which can be found in Table 3.2.

Table 3.2 - Details of the lacquers used.

Manufacturer	Name
Metlac	Gold Epoxyphenolic
Metlac	Gold Polyester BPANI

3.2 Sample Preparation and Processing

The coating of samples and associated experimental processing was undertaken at Swansea University's Pilot Manufacturing Resource Centre, where equipment allowed for the production of a large number of samples. Using larger scale equipment and a greater number of samples reduced the statistical uncertainty that could be associated with smaller scale production. Furthermore, the processes presented here can be directly correlated to full-scale industrial procedures, maximising the impact and relevance of the work presented.

3.2.1 Coating and Curing

An automatic Meyer bar coating system was used to apply both lacquers to metallic substrate materials. The bar was drawn down on A4 sheets of substrate at a constant speed depositing consistent thicknesses of lacquer across the area of the sample.

Figure 3.1 depicts the Meyer bar coating process, demonstrating how the diameter of the wire influences the thickness of the deposited coating. The speed of the automatic coater was sufficiently slow to ensure complete wetting of the lacquer

onto the substrate. A wire grade was chosen to deposit a cured film thickness of 10-12 μm with the coatings being cured for 15 minutes at 215 $^{\circ}\text{C}$ using a Thieme belt dryer. This specification of deposition and curing was specified by the manufacturer (100).

A dry coating thickness of 10-12 μm was confirmed using an Erichsen Depth Borer 518 USB and by following the standardised wedge cut method during which the coating is bored at a defined angle. A high-resolution digital microscope (50x magnification) is then used to obtain an image which is used to determine the absolute thickness of the layer, Figure 3.2.

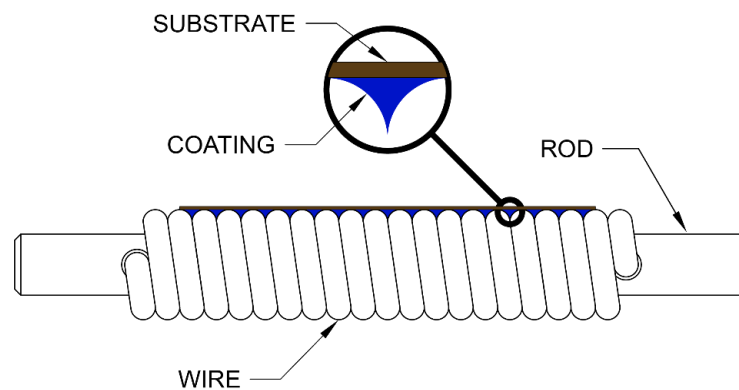


Figure 3.1 - Meyer bar coating method used to coat the substrate materials with lacquers.

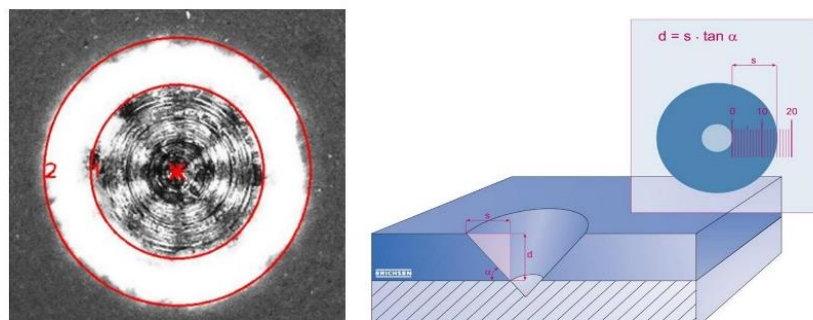


Figure 3.2 - Erichsen depth borer method for measuring coating thickness.

3.2.2 Retort Process

After lacquering, sixteen 40 x 120 mm samples were cut for each of the TCCT variants (Table 3.1). The edges of each sample were sealed with instant epoxy to prevent water ingress beneath the lacquer.

Retort took place in four different simulant solutions to understand how the lacquer / substrate interface may behave when exposed to certain food chemistries, Table 3.3. Four identical samples were placed into each beaker filled with simulant solution, sealed and placed in a CertoClav MultiControl 2 autoclave, Figure 3.3 and Figure 3.4. An industrial retort process was simulated at a temperature of 121 °C at 2 bar for 90 minutes. These processing parameters are consistent with previous work undertaken looking at similar substrate and coating technologies (38). The time and temperature for retort was kept standard throughout investigations, Figure 3.5.

Table 3.3 - Simulant solutions compositions and associated foodstuffs.

Simulant Solution	Concentration	Justification / Simulation
DI Water	-	Control
Citric Acid + NaCl	(0.25 % + 0.25 %) w/v	Salsify
NaCl	1 % w/v	Peas / Beans



Figure 3.3 - Labelled image of the CertoClav Multicontrol 2 used for pressure cooking steel samples.

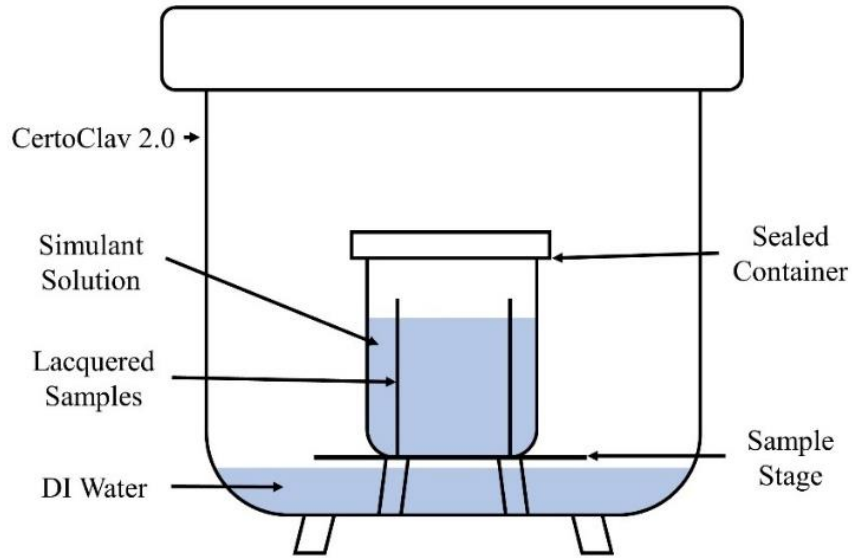


Figure 3.4 - Internal schematic of the CertoClav autoclave.

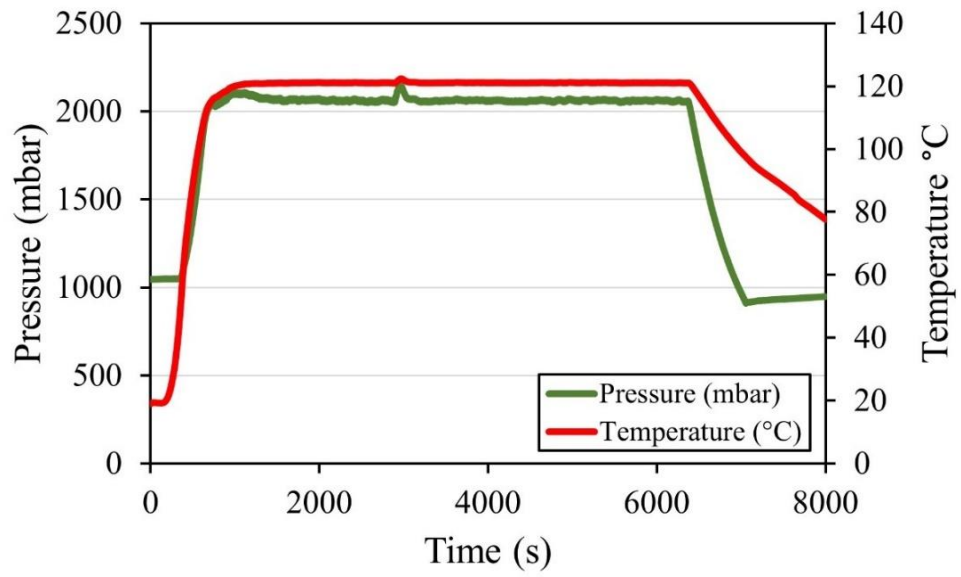


Figure 3.5 - Data logger information for the CertoClav Multicoltrrol 2.

3.3 Analysis Methods

A variety of methods were used to determine both physical and chemical properties of both the packaging steel substrates and their coatings. These observed both physical and chemical properties of the system and in combination served to provide well-rounded, accurate analysis of the substrate itself along with the interaction it has in adhering with the protective coatings. Methods are explained in order of topographic, surface, visual, chemical (and electrochemical) and adhesion.

3.3.1 White Light Interferometry

White light interferometry (WLI) provides a method of assessing the surface topography of materials on a macro scale, highlighting micron scale detail. It is well established as a technique and has been utilised successfully by *Melvin et.al* and *Jones et.al* in the topographical characterisation of packaging steel materials (101,102).

Experimentally, a beam of white light (from a tungsten-halogen bulb) is split by a beam splitter with one half being directed at a reference mirror and the other half being directed at the sample. These beams are then recombined, and an interference pattern (interferogram) is formed, with which a CCD camera uses a series of algorithms to achieve a profile measurement. This technique was used to assess any major differences in surface topography. The advantage of this non-contact technique compared to others such as atomic force microscopy (AFM) is that in materials that display certain levels of anisotropy, like packaging steels, alignment (both substrate and needle) issues are mitigated (103).

A WYKO NT9300 instrument was used to analyse samples. It incorporated three different microscopy lenses, x5, x20 and x50 magnification, along with a table mounted on air bearings to mitigate any vibrational noise from the environment. The table was manipulated through the x, y and z axes ensuring the sample is as flat as possible.

3.3.2 Atomic Force Microscopy

Atomic force microscopy (AFM) is a popular technique commonly used to detail sub-micron scale topographies of materials. A sharp tip connected to the end of a cantilever is raster scanned across the surface of a material to map the topography. The cantilever deflects as the tip interacts with the surface via forces between the sample and the cantilever. This deflection is measured by a laser that is reflected from the upper

surface of the cantilever to a position sensitive detector, allowing the AFM to measure z-direction sensitivity in the order of 0.1 Å. The AFM uses a feedback mechanism to enable tracking, control and position of the probe, as the instrument is very sensitive to surface conditions. This allows the generation and calculation of various roughness parameters, Figure 3.6 (104).

A JPK Nanowizard 3 atomic force microscope was used with samples being cut into 1 x 1 cm squares and mounted on a glass slide. The AFM was operated in alternating contact (AC) mode whereby the tip was vibrated at a frequency of 300 Hz and a scan rate of 0.7 line/s as per previous studies on similar materials (73). AC mode AFM is advantageous because it minimizes damage to the sample and the cantilever, as the cantilever never makes direct contact with the sample surface. Additionally, the amplitude and phase information provide additional insight into the sample's properties, such as its viscoelasticity, and can be used to distinguish between different materials with different surface properties. However, the imaging speed of AC mode AFM is typically slower than other AFM imaging modes (contact), and it requires a more complex experimental setup.

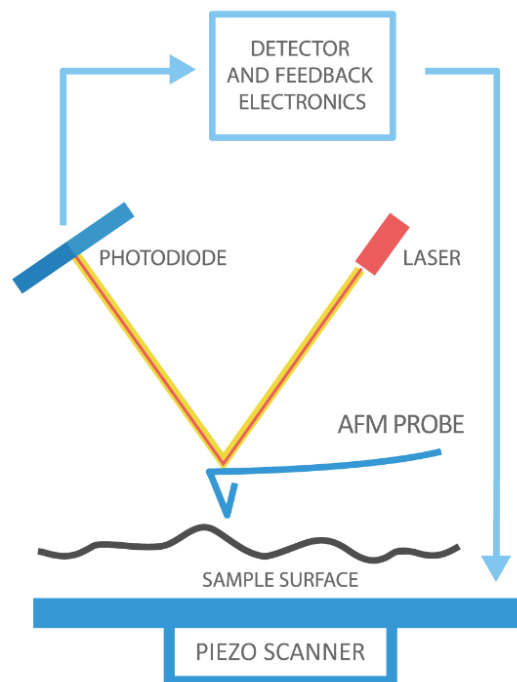


Figure 3.6 - Image detailing the AFM process used.

3.3.3 Surface Tension and Wetting Angle

Measuring the surface tension of the liquid coatings used as well as their wetting properties on substrate materials lends insight into their adhesive performance when subjected to certain environments (105). The sum of all attractive forces acting on a molecule in a liquid's bulk is zero. A surface molecule's cohesion force is a nonzero number acting in the direction of the bulk. This force must be overcome in order to increase the surface area; the energy consumed in this process is referred to as surface energy. Surface tension is measured in terms of surface energy per unit area. After a coating is applied to a surface, surface tension forces act to redistribute the coating layer. Good wetting provides a larger surface area over which adhesive forces may act and so is crucial for good bond formation, good coating homogeneity and ultimately the adhesive performance, as has long been established (106). If wettability is poor, problems such as de-wetting or eyehole formation can occur. De-wetting describes a discontinuous condition of the coating after application whereas eyeholing is usually caused by surface contamination of the substrate.

Contact angle gives a quantitative measurement of wetting by analysing the interface between the solid and liquid mediums. Interfacial surface tension was conducted in the Ossilla software utilising the pendant drop methods by analysing the liquid droplet as it formed into a spherical shape from a pipette. Figure 3.7 illustrates how contact angle is visualised and measured. Images of the droplet were captured via a CCD camera, allowing for computational analysis. For analysis, the last frame before the droplet falls is analysed. Initially, DI water was used to analyse a baseline value.

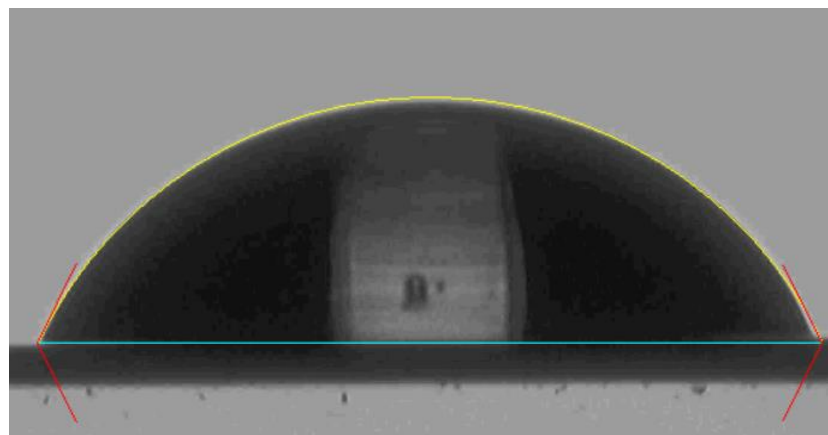


Figure 3.7 - A contact angle measurement of DI water on a metallic surface.

When a drop of liquid rests in equilibrium on a solid surface the Young equation relates the contact angle, θ , to the surface free energies (*Equation 11*). θ_{sg} is the surface free energy of the solid, θ_{sl} is the interfacial tension between the liquid and the solid, θ_{lg} is the surface tension of the liquid and $\cos\theta$ is the contact angle between the liquid-vapour interface and the solid surface.

$$\theta_{sg} = \theta_{sl} + \theta_{lg} \cdot \cos\theta \quad (11)$$

Contact angle analysis was conducted by depositing 20 μ L of each lacquer on to a coupon of TCCT. Images of the droplet were captured via a CCD camera, allowing for computational analysis. Data was recorded after the liquid droplet had settled in equilibrium at approximately 1s and 10s. The rheological properties of the lacquers, specifically the dynamic viscosity was taken from the material SDS data sheets. The goniometer system used comprised of a CCD camera, and contact angle software (Software version 4.0.3.1, Ossilla) (Sheffield, UK) with an error measure of $\pm 1^\circ$ under optimised illumination and optical conditions.

3.3.4 Spherical Spectrophotometry

Spherical spectrophotometers can measure light reflected at all angles to calculate colour measurements that closely match what a human eye would see. One of the key points of a sphere device is its ability to measure in either specular included (SPIN, SCI) or specular excluded (SPEX, SCE) conditions. Specular included mode has the ability to negate the effect of specular reflection off the surface, meaning it only measures the colour - not the appearance. Specular excluded mode includes the surface appearance in the measurement, Figure 3.8.

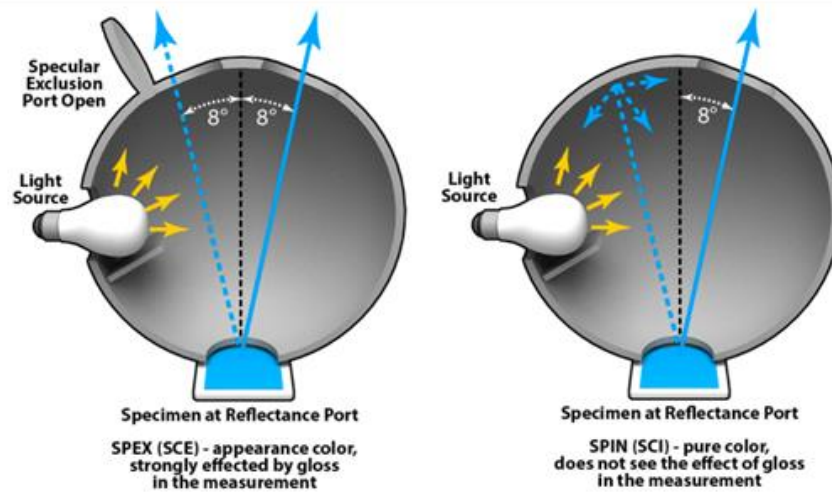


Figure 3.8 - Spherical spectrophotometer - influence of SPEX and SPIN (107).

Characterising a metallically coated substrate in terms of its colour may be a quick way of estimating the quantity of coating there is on the surface. This is specifically relevant in estimating the chromium oxide coating weight as it has been previously documented that this property effects the visual aesthetic of the product (29).

To overcome the limitations of chromaticity diagrams that poorly correlate to visual attributes, the CIE (The International Commission on Illumination) recommend an alternate colour scale: CIE 1976 ($L^*a^*b^*$). This scale is based on the opponent-colours theory of colour vision which says that two items cannot be both green and red at the same time, nor blue and yellow at the same time. When a colour is expressed in CIELAB, L^* denotes lightness, a^* denotes red/green values and b^* the yellow/blue value, Figure 3.9 (108). Before analysis all samples were wiped with acetone to ensure the surface was clean. The instrument used for all measurements of colour was an X-RITE Ci6X spherical spectrophotometer.

Prior to analysis, samples were wiped with acetone and DI water, ensuring the surface of the sample was both free of debris and dry.

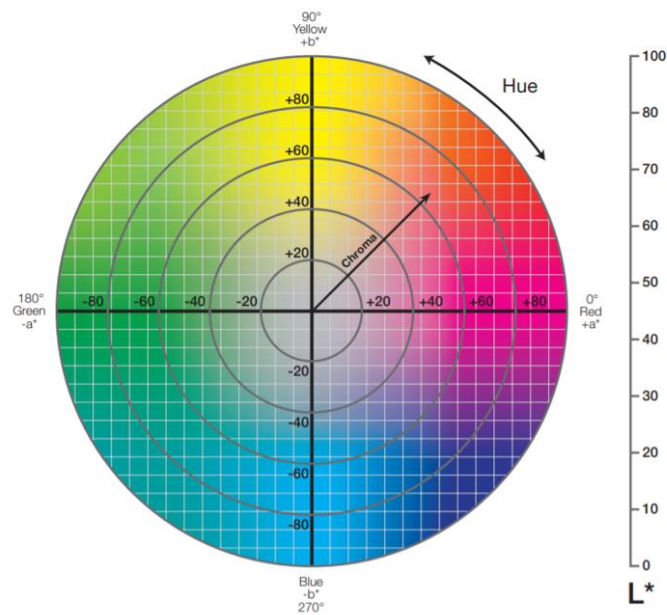


Figure 3.9 - CIELAB colour chart (109).

3.3.5 Gloss Measurement

In the context of packaging steel, gloss is a term that refers to the amount of light that is reflected off of the surface of the coated steel. Gloss is typically measured in terms of gloss units, which are a measure of the specular reflectance of a surface. A surface with a high gloss reflects a lot of light and has a shiny, mirror-like appearance, while a surface with a low gloss reflects less light and has a dull, matte appearance.

Gloss analysis is used to physically characterise the surface of the substrate materials quickly and easily. The gloss of packaging steel can be affected by a variety of factors, including the type of coating applied to the steel, the surface roughness of the steel, and the angle of the light source. A typical glossmeter consists of a fixed mechanical assembly consisting of a standardised light source that projects a parallel beam of light onto the test surface to be measured and a filtered detector located to receive the rays reflected from the surface, Figure 3.10.

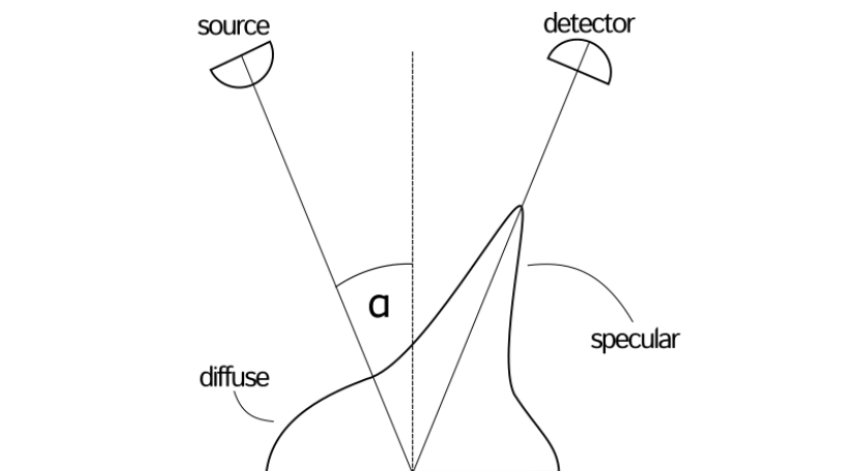


Figure 3.10 - Gloss meter geometry ($\theta=20^\circ, 60^\circ, 85^\circ$) and the specular and diffuse components of surface reflection (102).

The instrument is calibrated using a reference standard made from highly polished plane black glass with a refractive index of 1.567 for the Sodium D line, and this is assigned a gloss value of 100. The measurement angle refers to the angle between the incident and reflected light. Three measurement angles (20° , 60° and 85°) may be used and are specified to cover the majority of industrial coatings applications. The angle selected is based on the anticipated gloss range, as shown in Table 3.4.

For these steel substrate materials, an incident angle of 20° was used as when measuring parallel to the rolling direction, 60° measurements provided gloss readings in excess of 200 GU. This instrument was used in accordance with ASTM D523 (110). Justification of the gloss angle used can be found in Table 3.4.

Table 3.4 - Gloss measurement selection criteria.

Gloss Range	60° Value	Notes
High Gloss	>70 GU	If measurement exceeds 70 GU, change test setup to 20° .
Medium Gloss	10-70 GU	
Low Gloss	<10 GU	If measurement is less than 10 GU, change test setup to 85° .

Prior to analysis, samples were wiped with acetone and DI water, ensuring the surface of the sample was free of debris and dry.

3.3.6 Scanning Electron Microscopy

Scanning electron microscopy (SEM) was used to investigate the surface characteristics of substrate materials. Images were taken using a Hitachi TM 3000 microscope and a JEOL 7800F FEG-SEM. Accelerating voltages of 15 and 20 kV were used respectively. These relatively high voltages allow for a more detailed analysis of the material's microstructure and surface features. Additionally, high accelerating voltages enhance the signal-to-noise ratio resulting in a clearer image with less background noise. Working distances in all cases were between 6 and 10 mm. Samples were mounted onto a stub and held in place with copper tape, improving conductivity of the samples. EDX analysis was done using Quantax 70 software on the Hitachi TM 3000 microscope. The EDX scans were run for 15 minutes.

3.3.7 Differential Scanning Calorimetry and Thermogravimetric Analysis

Differential scanning calorimetry (DSC) measures the heat absorbed or released by a sample as it is heated or cooled at a controlled rate. During a DSC experiment, the sample is heated and cooled through the glass transition temperature, and the heat flow is measured as a function of temperature. The T_g is determined by analysing the heat flow curve and looking for a change in the slope, which indicates the onset of the glass transition.

Thermogravimetric analysis (TGA) is a technique used to measure the weight change of a sample as it is heated or cooled under controlled conditions. TGA can be used to determine the decomposition temperature of a polymer, as well as the weight loss or gain due to thermal degradation. By analysing the TGA and DSC curves together, it is possible to determine the mechanisms of thermal degradation and the thermal stability of the polymer.

Coatings were deposited on a Teflon substrate before curing and peeling. Approximately 20 mg of coating was removed and analysed in a ceramic pan. Repeatability for this device is given as ± 0.1 mg, representing $\pm 5\%$ of the analysed sample mass (111).

DSC and TGA was performed using a Perkin Elmer Pyris 1 TGA thermogravimetric module. Results were obtained using a heating rate of $10\text{ }^\circ\text{C} / \text{min}$ from $30\text{ }^\circ\text{C}$ to $500\text{ }^\circ\text{C}$. Paired with DSC, this technique was used to identify the glass transition temperatures the lacquers used for substrate coating (47).

3.3.8 Fourier Transform Infra-Red Spectroscopy

Fourier transform infra-red spectroscopy is a powerful tool used to characterise the chemical composition of coating materials. In the context of this work, this technique is useful in understanding the behaviour of lacquer coatings before and after the retort process. Spectra represent the molecular fingerprint of materials illustrating radiation which is either absorbed or transmitted through the material (112).

A Perkin Elmer Spectrum 100 FTIR Spectrometer with a UATR accessory was used to determine changes in the chemical bonding of the lacquer. This method utilises attenuated total reflectance (ATR) where a beam of light is passed through a crystal such that it reflects off the surface which is in contact with the sample. An acquisition time of 30 seconds, with an interval of 4 cm^{-1} and a scan range of 4000 to 450 cm^{-1} was used (113). This technique can be used to analyse coatings while in situ on the surface of a substrate, hence enabling the samples to be analysed with minimal preparation.

3.3.9 X-Ray Fluorescence

X-ray fluorescence (XRF) is a spectroscopic technique, based on the fluorescence of atoms in the X-ray domain, providing qualitative or quantitative information on the elemental composition of a sample.

X-rays have the energy to expel tightly held electrons from the atom's inner orbitals. When an electron is removed in this manner, the atom's electronic structure becomes unstable, and electrons in higher orbitals "fall" into the lower orbital to fill the hole left behind. This process releases energy in the form of a photon, the energy of which equals the energy difference between the two orbitals involved. As a result, the material emits radiation with the energy of the atoms present (114,115).

An Oxford Instruments X-met 7500 XRF was used with a scan time of 3 s per sample, measuring elemental content in parts per million (PPM). Apart from the obvious time advantage, this technique differs from XPS in the fact that the atoms both absorb and emit X-rays as opposed to absorbing X-rays and emitting electrons. Prior to analysis, samples were wiped with acetone and DI water, ensuring the surface of the sample was free of debris and dry.

3.3.10 X-Ray Photoelectron Spectroscopy

X-ray photoelectron Spectroscopy (XPS) was used to detail and quantify the outermost surface chemistry of substrate materials which is useful in identifying the precise chemical make-up of surfaces. This technique is non-destructive in nature and provides a quantitative analysis based on the elemental composition of a given surface.

In a sample, incident X-rays cause photoemission; electrons are collected and their kinetic energies are measured. The resulting spectra contain characteristic peaks that can be used to identify chemical species present on the sample surface. To allow unscattered electrons from the sample to reach the detector, the technique must be performed under ultra-high vacuum (UHV) conditions. XPS is limited by the fact that it cannot detect very light elements such as helium or hydrogen, however compounds containing these elements can be identified through the chemical shifts which occur within the compounds themselves (116).

Upon irradiation with photons of sufficient energy, electrons are ejected from the surface of a material via the photoelectric effect according to Figure 3.11 and *Equation 12*.

$$E_k = hv - E_b - \phi \quad (12)$$

E_k is the kinetic energy of the electron after being ejected, hv is the energy of the X-ray (wavelength multiplied by Plank's constant), E_b is the binding energy of the electron in the material and ϕ is the work function of the material.

To remove contaminants, samples of approximately 1 cm^2 must be degreased and cleaned. The generated X-rays have a superficial impact on the surface as well as a penetration depth, which is typically greater than 1000 \AA (117). Surface analysis is carried out by accounting for electrons that escape without inelastic energy loss. Auger peaks are also visible on the XPS spectra, indicating when electrons with lower kinetic energy collide with other atoms on their path of ejection.

For this research a Kratos Axis Supra instrument was used which was fitted with a monochromated $1486 \text{ eV Al K}\alpha$ source and large area slot mode detector. The analysis area was $300 \mu\text{m} \times 800 \mu\text{m}$. Binding energies were calibrated to the main hydrocarbon peak (284.8 eV). Spectra were subsequently analysed in CASA software

with Shirley backgrounds. The models used in the analysis were based on that successfully used for previous studies of chromium coated substrates (34,101).

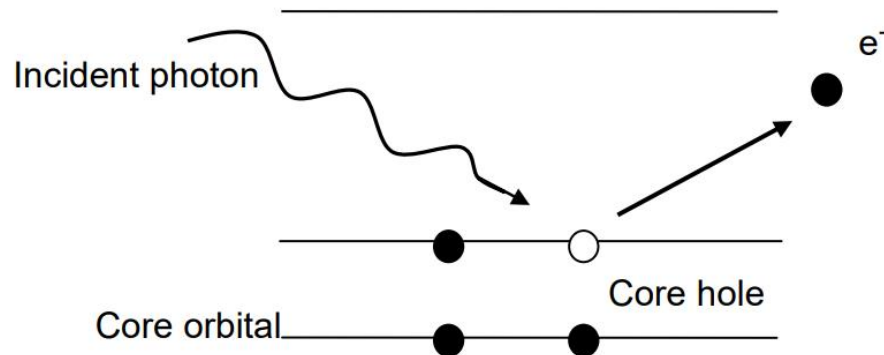


Figure 3.11 - Visualisation of the XPS method of excitation; the photoelectric effect.

3.3.11 Glow Discharge Optical Emission Spectroscopy

Glow discharge optical emission spectroscopy (GDOES) is a destructive analytical technique that quickly and sensitively determines the bulk elemental composition of solid materials and layers as well as their surface / depth profile. Metallic samples are used as a cathode in a direct current plasma process and the surface is sputtered away. A downstream spectrometer records the characteristic wavelengths of photons as they are emitted along with excited waves, and these wavelengths are then quantified. If the sample is flat over the sputtered area, the technique can achieve great depth resolution (nm level) very quickly (118,119).

A HORIBA Jobin Yvon GD Profiler 2 Spectrometer was used for all GDOES measurements taken. This instrument does not have a laser source built in and so an external Cu anode laser is used. To generate a laser beam using a Cu anode, an electrical discharge is used to vaporise a small amount of Cu, which is then ionised to create a plasma. The plasma is then excited by an additional electrical discharge, which causes it to emit laser light. The laser beam can then be directed onto the surface of the coating being analysed using mirrors and other optical components. The laser beam is absorbed by the coating, causing a small amount of material to be removed from the surface, or ablated. Copper vapor lasers (CVLs) are commonly used for ablation of metallic coatings, as they are able to generate short pulses of high-energy laser light. The crater size made by this instrument is 5 mm in diameter.

3.3.12 Cyclic Voltammetry

Cyclic voltammetry is an electroanalytical technique used to study the reduction and oxidation reactions of electroactive species in solution. It involves applying a voltage ramp to an electrode immersed in a solution containing the species of interest and measuring the resulting current. Cyclic voltammetry can be used to study the kinetics of these reactions, as well as the nature of the species involved. This method is useful in identifying any electrolyte contaminants prior to the electrodeposition of chromium coatings.

Prior to analysis samples were scrubbed with acetone and rinsed with DI water. A Metrohm Autolab PGSTAT302N potentiostat was used to scan repetitively between the onset of hydrogen evolution cathodically and oxygen evolution anodically and was run until a stable cyclic voltammogram (CV) was acquired. The working electrode was a mirror polished platinum electrode. All potentials were reported vs. a Hg / Hg₂Cl₂ / KCl (saturated) electrode. The cyclic voltammograms were recorded with a scan rate of 100 mV.s⁻¹ (31).

3.3.13 Scanning Vibrating Electrode Technique (SVET)

The primary method which has been identified for the investigation of the corrosion of packaging steel substrates is the Scanning Vibrating Electrode Technique (SVET). This technique has been used in many studies and represents a method by which the electrochemical activity of a corroding surface can be mapped and quantified (73,120–122).

This technique involves scanning a microtip electrode, which is vibrated mechanically at a constant amplitude and frequency, using a simple electromagnetic or piezoelectric driver, over the surface of a material. The microtip electrode registers an alternating potential at the vibration frequency which is proportional to electrical field strength or potential gradient in the direction of vibration. One advantage of this technique is its ability to spatially resolve and quantify (used indirectly), localised differences in surface reactivity and reaction rate. Spatial resolution is of particular interest when considering metallic corrosion and the various electrochemical reactions involved are often heterogeneous (i.e. occur on different regions of the metal surface) and the corrosion is localised in nature (121). A drawback of this technique is that the acquired data may be complicated and may contain noise and interference.

The scanning vibrating reference electrode technique (SVRET), which is often abbreviated to scanning vibrating electrode technique (SVET) due to the use of a pseudo reference electrode, is a derivative of the scanning reference electrode technique (SRET) (123). The SRET was the initial method of scanning used to study corrosion in aqueous environments (124). The device measures potential differences in solution which occur as a result of ionic currents generated by the corroding surface (123). When a metal corrodes in an electrolyte, a current flows from a localised anode to a more generalised cathode. This current of ions can be thought of as current flux lines travelling through the electrolyte from the anode to the cathode, the circuit being completed by the flow of electrons through the metal. These lines of current flux can be seen in Figure 3.12. The high conductivity of metals renders their resistance negligible, resulting in the metallic surface being viewed as a plane with constant potential. Conversely, the electrolyte is characterized by high resistance. As a result, miniature dipoles generate ohmic potential gradients that develop as the current flows (125). These gradients are represented by lines of equipotential perpendicular to lines of current flux.

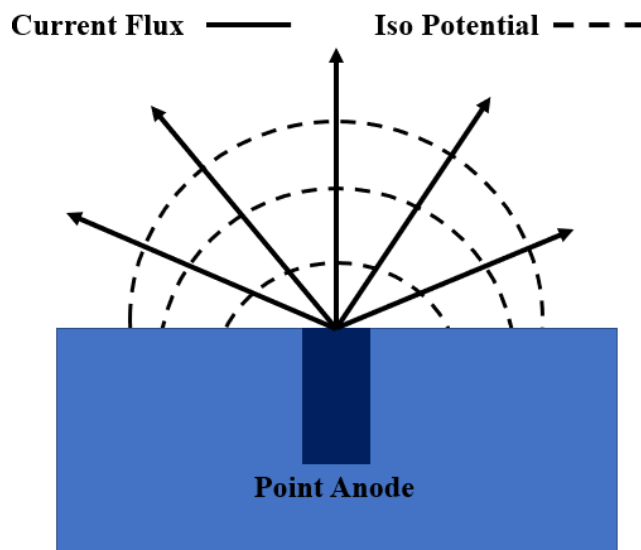


Figure 3.12 - A schematic showing the lines of current flux and equipotential through an electrolyte in which a metal is corroding.

The Laplace equation and Ohms Law can be used to calculate the potential and current distributed within the solution (*Equations 13 and 14*) (126)

$$\nabla^2 E = 0 \quad (13)$$

$$i = -k\nabla E \quad (14)$$

Where E is the electrical potential i is the current and k is the solution conductance. Solutions to Ohm's law equation are non-trivial with no analytical solution possible. Solutions may be obtained when considering the simplest case of a point current source.

For a point source of current, i , located at height $z = 0$ on a non-conducting x, y plane, with the current drain at infinity it may be shown that the potential at any point (x, y, z) in solution is inversely proportional to the distance from the source and is given by *Equation 15* (126)

$$E = \frac{i}{2\pi k \sqrt{x^2 + y^2 + z^2}} \quad (15)$$

The Scanning Vibrating Electrode Technique (SVET) contrasts to the SRET in that it measures an alternating potential at the vibration frequency of the microelectrode tip, this being proportional to the electric field strength of potential gradient in the direction of vibration. The SVET technique makes use of a scanning micro-tip electrode which is vibrated mechanically at a constant amplitude and frequency above the sample. An alternating potential is therefore detected when scanning above a sample which is corroding. The potential is proportional to the electric field strength or potential gradient that occur as a result of the ionic currents, in the direction of the vibration. Therefore, the signal can be related to the ionic current in the electrolyte lying in the direction of the probe, and therefore normal to the sample surface. The microtip resides at a set distance above the surface and thus the signal measured is not proportional to the surface current density but the vector component of the current density in the electrolyte at the height of the probe.

When still considering an anodic point source, the tip measures the electric field strength or potential gradient, F , and is given by the z differential of E (*Equation 16*) (126)

$$F = \frac{dE}{dz} = \frac{iz}{2\pi k(x^2 + y^2 + z^2)^{1.5}} \quad (16)$$

The maximum field strength (F_{max}) occurs directly above the point source, or origin ($x=0, y=0$) and is given by *Equation 17*.

$$F_{max} = -\frac{i}{2\pi kz^2} \quad (17)$$

A characteristic peak is therefore seen above the current source during an SVET scan. Due to the inverse square relationship between the height and maximum field strength it is important that the height is controlled and remains constant during measurements using the SVET. When using this technique samples are typically flat and are levelled before experimental scans take place. However, the recent development of the 3D SVET allows for scanning of non-flat samples. When using the 3D SVET the device is used in ‘height scanning mode’ to obtain a profile of the sample surface. The profile is stored before a scan is conducted.

The SVET can detect extremely small potential changes which exist over the surface of an electrochemically active sample. By measuring the potential gradients using a fine tipped vibrating microelectrode the SVET allows us to spatially characterise corrosion activity and detect areas of anodic and cathodic activity on the substrate. Nevertheless, a significant limitation of the technique is the resolution of localised corrosion features. Resolution refers to the minimum distance between two features that can be detected by the microtip and is calculated using the signal peak width at half maximum peak height (whm). Considering a quantity r as the distance from a point current source on the x,y plane then:

$$r = (x^2 + y^2)^{\frac{1}{2}} \quad (18)$$

The value of r at which the value of F falls to half of its maximum value (i.e. $0.5F_{max}$) is obtained by combining *Equations 18 and 19* giving *Equation 20*. The width of the SVET response peak is therefore $whm = 2r = 1.533z$ (126)

$$F_{max} = \frac{iz}{2\pi k(r^2 + z^2)^{1.5}} \quad (19)$$

$$r = z(2^{\frac{2}{3}} - 1)^{1.5} \quad (20)$$

When using a typical scan height of $100\mu\text{m}$, a spatial resolution of $153\mu\text{m}$ is calculated. This is a theoretical value and differs from the actual value due to the dimensions of the probe, typically a $125\mu\text{m}$ platinum disc. Consequently, the SVET cannot resolve two point current sources if they are not separated by a distance which is greater than the value of whm. Additionally, when anode-cathode distance $> h$, current flux lines cross the plane of scan and are detected by SVET but when anode-cathode distance $\ll h$ (e.g. general corrosion), current flux lines do not cross the plane of scan and are not detected by SVET, Figure 3.13.

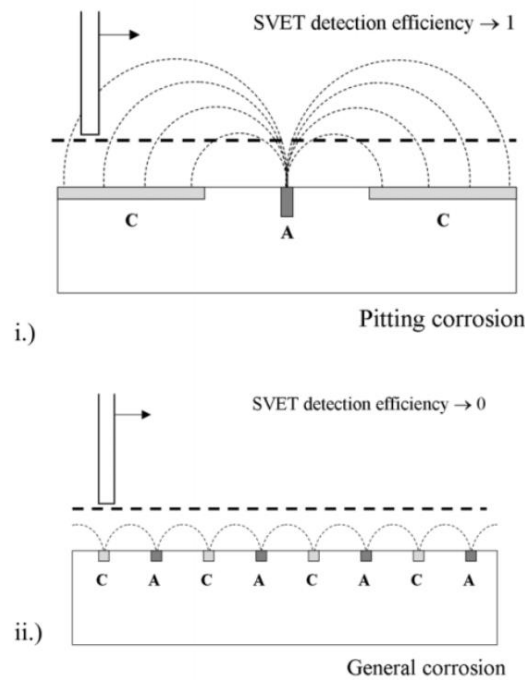


Figure 3.13 - Schematic showing limitations of the SVET with respect to spatial resolution i.) anode-cathode distance is greater than scan height and localised corrosion can be resolved and ii.) anode-cathode distance is smaller than scan height and localised corrosion cannot be resolved (72).

Prior to analysis, 20×20 mm samples of substrate material were cut using a guillotine ensuring that the test specimens were as flat as possible. PTFE tape was used to expose a 10×10 mm area for analysis. The surface of the samples were cleaned using ethanol swabs before being secured in the test beaker. Amplitude and frequency of tip vibration were kept consistent at approximately $25\mu\text{m}$ and 140 Hz respectively.

SVET scans were measured and analysed on bespoke equipment and software (Surfer) made and developed in Swansea University.

3.3.14 Scratch Testing Adhesion

The principle of scratch testing is to score the surface of a coated substrate using a weighted, pointed stylus to assess the adhesion characteristic, and is therefore relevant in the testing of lacquered packaging steel substrates. This method provides a quantitative measurement of adhesion in terms of weight and therefore force. The adhesion force is measured at the highest weight at which the substrate / lacquer interface would still ‘pass’ – i.e. no electrical contact between the stylus of the scratch tester and the substrate. Previous work highlights the need to keep samples in solution for as long as possible prior to analysis; this research was noted, and samples were kept submerged for as long as possible (113). There are no chemical interactions using this method making it suitable for the thin film systems tested here.

A discrete static load is placed on the vertical pole of the scratch tester in 25g increments. The machine then scratches the sample with a 1 mm tungsten carbide tip for 100 mm at a constant speed (35 mm/sec). The failure force is found when the tip penetrates the coating and electrical conductivity is noted on the instrument gauge, Figure 3.14 and Figure 3.15.

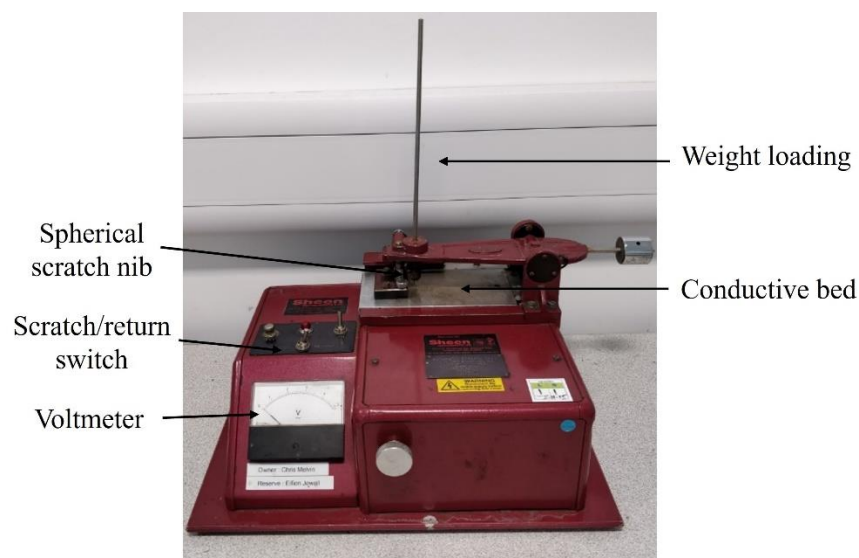


Figure 3.14 - The Sheen Instruments scratch tester used for adhesion investigations.

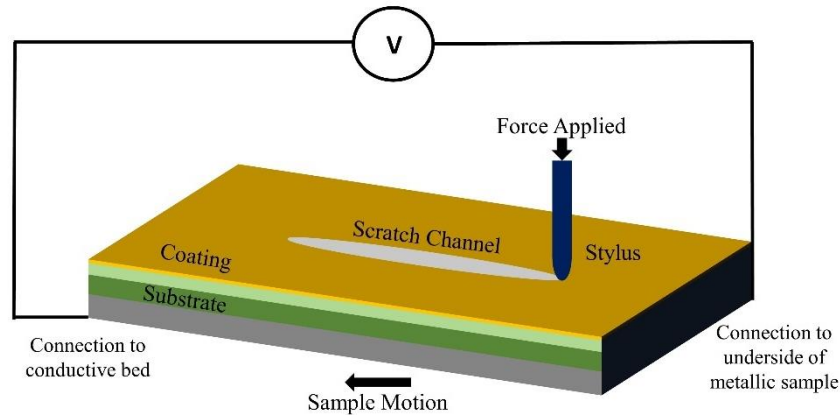


Figure 3.15 - Schematic of a scratch testing process.

From reviewing the relevant literature, it is clear that when using scratch testing as a method to assess the adhesion failure forces of lacquers, there are clear values at which it is evident that the coating / substrate system ‘pass’ the test. This ‘pass’ would indicate that the lacquer / substrate system would provide enough of a protective barrier between the canned foodstuff and metallic substrate. Adhesion forces measuring ≥ 10 N are acceptable and still remain intact, providing an adequate barrier. Ideally, the adhesion force needs to be higher than this to ensure maximal performance, therefore a 10 N failure force would be the lower bound of acceptability. Adhesion forces measuring ≤ 4 N represents very poor adhesion, and these materials are often seen to be peeling off the substrate materials indicating total failure of the lacquer / substrate system.

The adhesion of lacquers to substrate materials was measured using a Sheen Instruments BS3359 scratch tester, operated in accordance with ISO 1518-1:2011 (87).

3.4 Conclusion

Within this section of work, materials have been sourced and detailed along with key experimental methodologies being explained and examined. This now gives direction and focus to the research to be conducted which will focus on the characterisation of substrate materials and protective coatings along with the manufacture of novel TCCT substrate materials.

Chapter 4 – Characterisation of
TCCT Packaging Steel Substrates:
The Effect of Chromium Oxide
Coating Weight

4 Characterisation of TCCT Packaging Steel Substrates: The Effect of Chromium Oxide Coating Weight

4.1 Introduction

As discussed previously, Cr (III) based substrates such as TCCT have been developed as a REACH compliant alternative to ECCS. ECCS has historically been well researched and characterised since its inception in the 1980's, with its manufacturing process having been optimised for decades. TCCT is yet to be made commercially available, so characterisation of iterative pre-production substrate materials is necessary in order to both predict the performance of the substrate and to critique the manufacturing process.

The adhesive performance of lacquers to packaging steel substrates can be affected profoundly by the physical characteristics of materials (roughness and wetting of coatings) as well as the chemical composition of the metallic coatings. It is for this reason that characterisation has been necessary on a large sample set, specifically looking at effect of chromium oxide coating weight. It is this feature which has been shown to dictate both the lacquer adhesion performance and the electrochemical passivity of the material. Chromium oxide coating weight is a key parameter in ensuring good adhesive performance of the substrate / lacquer system as it provides OH^- sites with which the lacquers can initially bond too as well as serving to passivate any iron present on the surface / within the chromium metal layer (127,128)

The aesthetic quality of the substrate material is also vital in ensuring customer satisfaction and so spherical spectrophotometry and gloss measurements are regularly used for quality control processes industrially (102). In this research these techniques illustrate the effect of varying oxidic coating weights.

Characterisation is an important step in understanding the quality of the materials. Importantly, the techniques used here will be replicated in the evaluation of the Swansea University manufactured TCCT. This is so that the results between industrially made samples and samples made independently can be directly compared. This work will provide insight into the final adhesive performance of lacquers in simulated industrial conditions along with the commercial viability of this iteration of TCCT.

4.2 Materials and Methodology

The characterisation of TCCT substrates has been limited to the pre-production designs of the substrate. Iterations of TCCT manufactured by TATA Steel IJmuiden on their full-scale pilot line currently represent their latest version of substrate material (at the time of writing).

A set of 15 TCCT substrates were received from TATA Steel IJmuiden R&D. The surface chemistries are detailed in Table 3.1 Chapter 3. Their production comprised of a systematic change in electroplating parameters with the aim of depositing varying levels of chromium oxide ($2\text{-}23\text{ mg/m}^2$) onto the surface of a pre-coated chromium metal substrate. ECCS sourced from TATA Steel UK is used as a control substrate, coated with 9 mg/m^2 of chromium oxide. For the purposes of characterisation techniques, 3 TCCT samples were used to look at the effect of chromium oxide coating weight alphabetically referenced as I, H and G as per Table 3.1 and henceforth will be referred to as TCCT samples with low (3 mg/m^2), medium (13 mg/m^2) and high (23 mg/m^2) chromium oxide coating weights.

This investigation is separated into the following sections: the effect of surface topography, the effect of the adhesive interface, metallic coating morphology, substrate colour and reflectance analysis and chemical characterisation.

4.3 Physical Characterisation

Topographical information provides substrate surface data crucial in the understanding of the adhesive mechanisms of the protective lacquer that the substrate will eventually support. Examining the wetting characteristics of lacquers used industrially will help explain the role the metallic coating plays in the ultimate performance of the substrate / coating system. Visualising the substrate aids in assessing the continuity of the samples as well as providing an overview as to the homogeneity of the metallic coatings and the likely acceptance/rejection of substrates from a customer due to aesthetic.

Utilising experimental techniques to characterise TCCT samples in terms of their surface topographies (both on a macro and micro scale), wetting properties, and their aesthetic lends insight into the future adhesive performance characteristics of the substrates as well as their quality.

4.3.1 The Effect of Surface Topography

The base blackplate substrate, onto which the TCCT coating is deposited, is cold rolled which dictates its surface topography. Due to the fact that chromium metal and oxide coatings are further electroplated onto this surface, there is potential for the roughness characteristics to change impacting the wetting of lacquers and therefore the eventual adhesion performance of the lacquer / substrate system. It is for this reason that it is necessary to investigate the substrate topographies.

The surface topographies of all 15 TCCT substrates were first investigated using white light interferometry. 2D and 3D plots at x20 magnification are illustrated in Figure 4.1 (a-e) representing blackplate, low (3 mg/m²), medium (13 mg/m²) and high (23 mg/m²) chromium oxide coating weights of TCCT respectively and ECCS (9 mg/m²). Using this magnification, the sampling area is 232 x 310 µm with the smallest resolvable feature size being 0.03 µm (129). Surface roughness values Ra (arithmetic average of the absolute values of the profile heights), Rt (the vertical distance between the highest and lowest points of the profile) and Rz (the average of the successive values of Rt) are given, Table 4.1.

Table 4.1 – Surface topographical data Ra, Rt and Rz values for blackplate, TCCT substrates coated with low CrOx – 3mg/m², medium CrOx – 13 mg/m² and high CrOx - (23 mg/m²) and (e) ECCS.

Sample	Surface Topography Characteristic (µm)		
	Ra	Rt	Rz
Blackplate	0.49	4.87	4.26
TCCT Low CrOx (3 mg/m ²)	0.41	4.77	4.36
TCCT Medium CrOx (13 mg/m ²)	0.38	4.73	3.78
TCCT High CrOx (23 mg/m ²)	0.42	4.38	3.97
ECCS	0.39	5.41	4.17

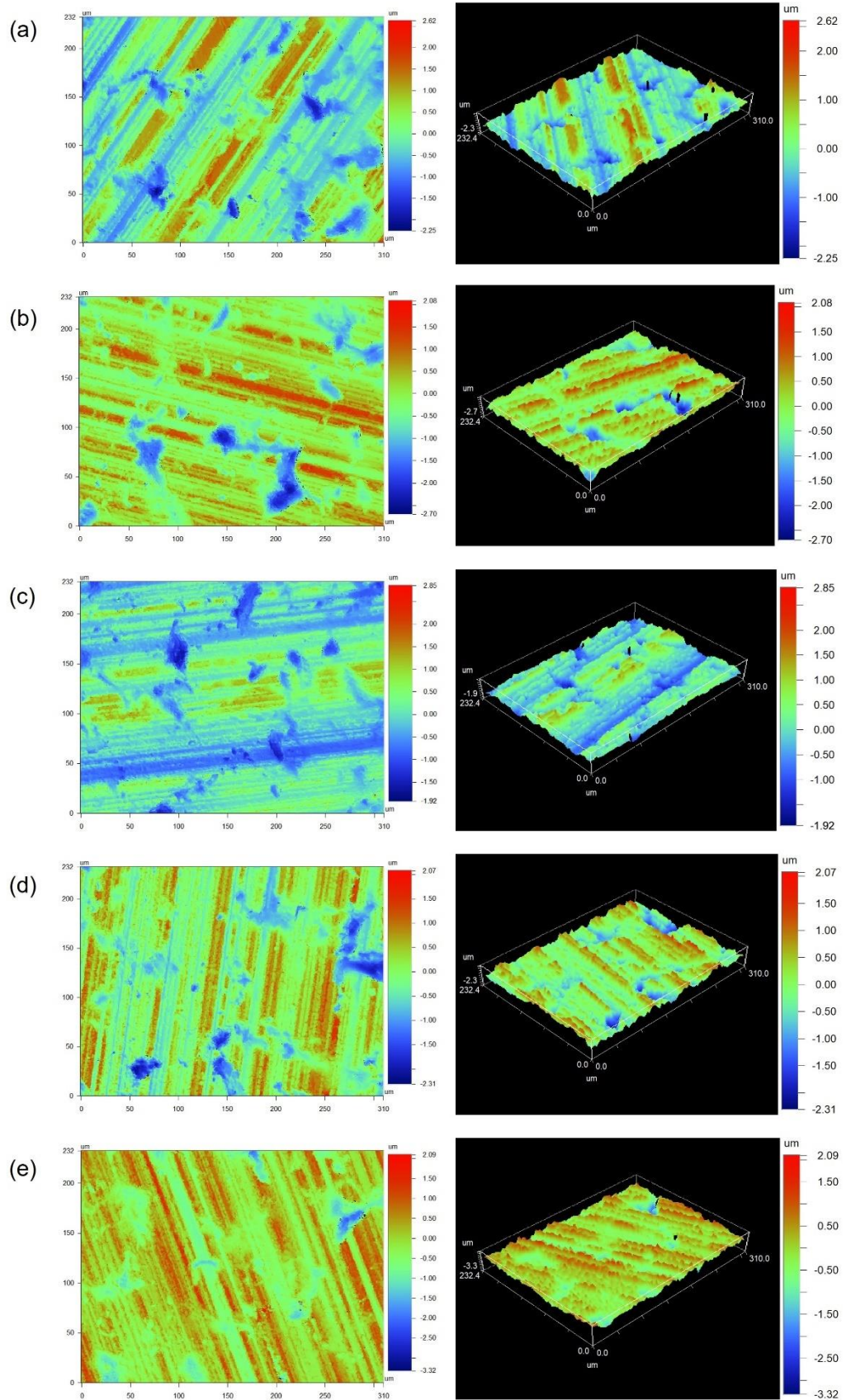


Figure 4.1 - White light interferometry 2D and 3D plots of (a) blackplate, TCCT substrates coated with (b) low CrOx (3mg/m^2), (c) medium CrOx (13 mg/m^2) and (d) high CrOx (23 mg/m^2) and (e) ECCS (9 mg/m^2).

The main surface roughness values of Ra, Rt and Rz are all very similar to each other and represent no particular pattern. The dominant topographical features are that of the underlying substrates rolling direction with peaks and troughs measuring between approximately 2-3 μm in depth spaced approximately 0.1 μm apart. This is evidenced by the comparison of maximum and minimum depths witnessed between blackplate and the TCCT samples. Larger pits in the substrates surface can be seen across all samples, including blackplate, measuring anywhere between 20 and 50 μm across, Figure 4.1 (b) and (d).

Surface roughness (Ra) measurements were also taken for the whole sample set at magnifications of x5, x10 and x20, Figure 4.2. No trend is witnessed in these results with Ra roughness values differing between ~ 0.32 - $0.56 \mu\text{m}$. The Ra of blackplate and ECCS was measured at 0.49 and 0.39 μm respectively at x20 magnification. The variation in these results is in line with literature pertaining to roughness's of cold rolled packaging steel substrates, stating that typical Ra values vary between 0.3 and 0.6 μm (130).

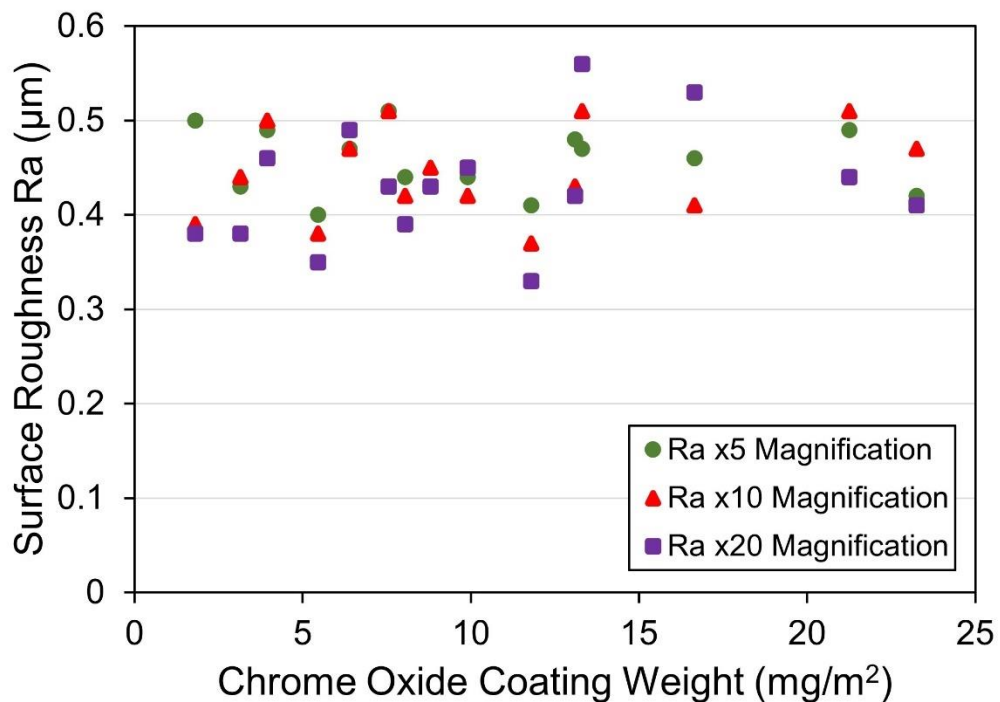


Figure 4.2 - Surface roughness data as measured by white light interferometry for 15 TCCT samples and ECCS at x5, x10 and x20 magnifications.

Further investigation was undertaken using AFM in order to assess the topographies of the three previous TCCT samples along with ECCS and blackplate as per the methodology outlined in section 3.3.2, Figure 4.3 and Table 4.2. Scans were taken over a 10 x 10 μm area. With the instruments vertical and horizontal resolution measuring nanometres. The aim of this was to establish whether the surface roughness of substrates remain comparable or differ on a smaller scale since the white light interferometry results were inconclusive.

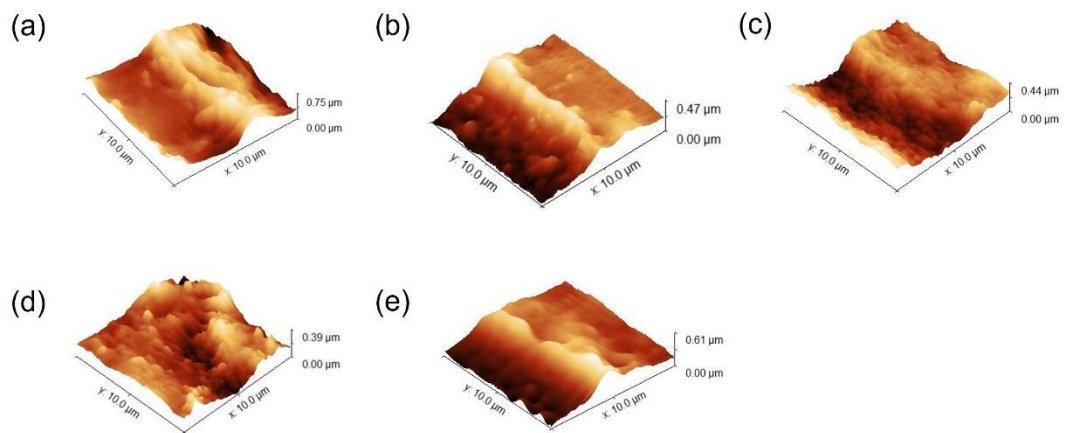


Figure 4.3 - AFM plots illustrating the 3D topographies of (a) blackplate, TCCT substrates coated with (b) low CrOx (3 mg/m^2), (c) medium CrOx (13 mg/m^2) and (d) high CrOx (23 mg/m^2) and (e) ECCS (9 mg/m^2).

Table 4.2 - AFM surface roughness's (R_a) of blackplate, TCCT substrates coated with low CrOx (3 mg/m^2), medium CrOx (13 mg/m^2) and high CrOx (23 mg/m^2) and ECCS (9 mg/m^2).

Sample	Roughness (R_a)
Blackplate	$0.20\ \mu\text{m}$
TCCT Low CrOx (3 mg/m^2)	$0.17\ \mu\text{m}$
TCCT Medium CrOx (13 mg/m^2)	$0.21\ \mu\text{m}$
TCCT High CrOx (23 mg/m^2)	$0.11\ \mu\text{m}$
ECCS (9 mg/m^2)	$0.18\ \mu\text{m}$

These results show that there is still no noticeable trend in the surface roughness values on a micro scale, Table 4.2. The difference in measured surface roughness is due to the prominent features seen on this scale such as the rolling direction and large pits / pores which are indicative of the features left by the cold rolling process. This is evidenced in the images shown in Figure 4.3.

Having investigated the surface topographies of substrate materials both on a macro and micro scale, it is clear that the metallic and oxidic coatings applied during the TCCT manufacturing process have no effect on the surface roughness values at these scales, within the limits of sampling and measurement used. It is proposed that this is due to the thickest duplex coating investigated measuring ~20 nm in thickness, and that therefore there are no measurable differences in roughness on this scale. This is a key finding, suggesting that mechanical interlocking as a mechanism of adhesion of the lacquers to the substrate is not affected by the chromium oxide coating weight (131).

4.3.2 The Effect of the Adhesive Interface – Surface Tension and Contact Angle

Prior to can forming, substrate materials are coated with a protective lacquer which is applied in liquid form through a roller coating process; this coating is then cured at elevated temperatures. Having investigated the effect of substrate materials topographies, it is necessary to assess the effect of the adhesive interface between the substrate and protective coating that will be applied. The method by which surface tension and contact angle measurements were undertaken is detailed in chapter 3 section 3.3.3.

Good wetting provides a larger surface area over which adhesive forces may act and so is crucial for good bond formation, good coating homogeneity and ultimately the adhesive performance, as has long been established (106). If wettability is poor, problems such as de-wetting or eyehole formation can occur. De-wetting describes a discontinuous condition of the coating after application whereas eyeholing is usually caused by surface contamination of the substrate.

Generally, a surface with low surface energy will cause poor wetting and therefore a high contact angle. This is due to the surface not being capable of forming strong bonds, so there is little energetic reward for the liquid to break bulk bonding in favour of interacting with the surface, and so it follows that the critical surface energy of the substrate should be higher than the critical surface tension of the adhesive. In the case of lacquers and packaging steel substrates, the high surface energy of chromium oxide coupled with the low critical surface energy of epoxies makes for good wetting; however, the varying quantities of chromium oxide on the substrates coupled with the need to investigate BPANI lacquers means that investigation is required.

4.3.2.1 Surface Tension

The surface tension of a liquid is a measure of the cohesive forces between molecules within the liquid. It is a measure of the strength of the liquid's "skin," and it determines how the liquid will behave when it comes into contact with other materials. In general, a liquid with a high surface tension will have a greater tendency to bead up and form droplets, rather than spreading out. This is because the cohesive forces between the molecules are stronger, causing the molecules to be more strongly attracted to each other. A liquid with a low surface tension, on the other hand, will tend to spread out more readily when it comes into contact with other materials. If a coating's surface tension is greater than the substrate's, the coating may be prone to incomplete surface wetting and defects (132,133).

The pendant drop method was used to measure the surface tension of the liquid lacquers. It involves suspending a small volume of the liquid in the form of a pendant drop from a capillary tube or needle and measuring the dimensions of the drop. The surface tension of the liquid can then be calculated based on the dimensions of the drop and the applied force. It was necessary to use a larger needle to produce a drop that was large enough to measure accurately because these materials high solvent contents caused the drop to evaporate quicker when using a smaller needle, making it difficult to obtain a stable measurement. The last frame before the droplet falls is examined for analysis.

DI water was initially used to determine a baseline calibration value before examining epoxyphenolic and BPANI lacquers. Three repeat measurements were taken of each liquid with error bars illustrating one standard error, Figure 4.4.

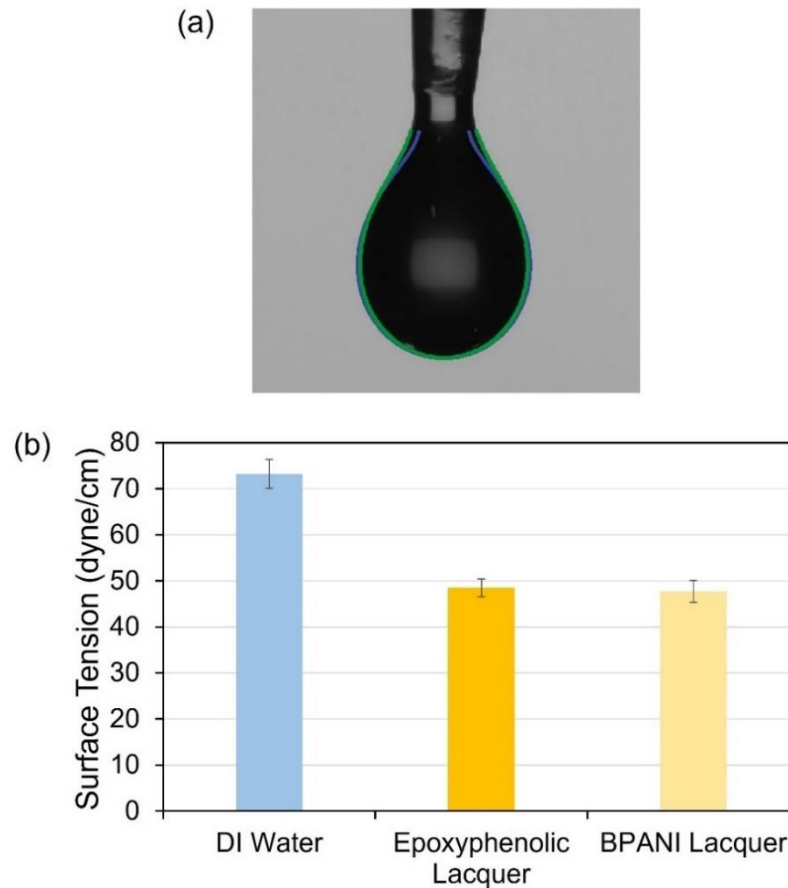


Figure 4.4 - Image showing the pendant drop method of measuring surface tension (a) and graphical depiction of the surface tensions of DI water, epoxyphenolic and BPANI lacquers.

The average surface tension value of DI water was 72.25 mNm^{-1} , this measurement acted as calibration for the system and is in line with expectations (134). The average surface tension of epoxyphenolic and BPANI lacquers were 48.5 and 47.75 mNm^{-1} , respectively. These values allude to both the epoxyphenolic and BPANI lacquer demonstrating equal ability in wetting a surface and are similar to those published elsewhere (135).

4.3.2.2 Contact Angle

Wetting of both smooth and rough surfaces is governed by Young, Wenzel and Cassie-Baxter equations with the latter two taking into consideration the surface roughness of the substrate material. As established from section 4.3.1 there is no significant change in the roughness of this sample set and therefore the Young equation is used in calculating the wetting characteristics of these substrates (105).

When a drop of liquid rests in equilibrium on a solid surface the Young equation relates the contact angle, θ , to the surface free energies (*Equation 21*). θ_{sg} is the surface free energy of the solid, θ_{sl} is the interfacial tension between the liquid and the solid, θ_{lg} is the surface tension of the liquid and $\cos\theta$ is the contact angle between the liquid-vapour interface and the solid surface.

$$\theta_{sg} = \theta_{sl} + \theta_{lg} \cdot \cos\theta \quad (21)$$

It has been established that the first 10 Å of the material thickness dictates the contact angle of a fluid on a surface (136). It is therefore the effect chromium oxide coating weight which will be shown by these measurements. Initially the contact angle of DI water on a range of TCCT samples with varying chromium oxide coating weights was analysed, Figure 4.5.

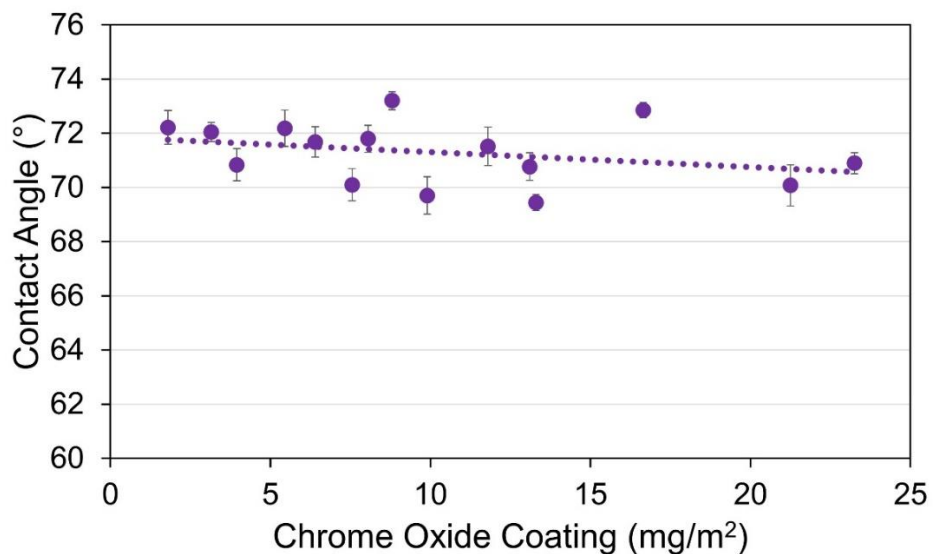


Figure 4.5 - Relationship between chromium oxide coating weight of TCCT substrates and contact angle of DI water.

The contact angle of DI water on this range of TCCT substrates can be seen to decrease slightly as chromium oxide coating weight increases, Figure 4.5. This may be explained by thicker layers of chromium oxide exhibiting higher surface energies and therefore allowing the DI water to wet more easily onto its surface. All thicknesses of chromium oxide exceed 10 Å and so even considering the standard errors and

spread of results, it can be concluded that the contact angle of DI water on these substrate materials is not affected by the coating weights of chromium oxide deposited. The contact angle is relatively consistent measuring between approximately 69° and 73°.

As was done for surface topographical analysis conducted in section 4.3.1; low, medium and high chromium oxide coated samples (3, 13 and 23 mg/m² respectively) were investigated for how epoxyphenolic and BPANI lacquers wet onto them, Table 4.3. Contact angles of the lacquers were measured after being left to relax on the substrates surface for 10 s. Values are rounded to the nearest degree and represent an average of three readings, standard errors are shown in parentheses.

Table 4.3 - Contact angle measurements of TCCT substrates coated with low CrOx (3mg/m²), medium CrOx (13 mg/m²), high CrOx (23 mg/m²) and ECCS (9 mg/m²).

Sample	Liquid		
	DI Water	Epoxyphenolic Lacquer t=10 s	BPANI Lacquer t=10 s
TCCT Low CrOx (3 mg/m ²)	72 (0.6)	36 (0.7)	34 (0.6)
TCCT Medium CrOx (13 mg/m ²)	70 (0.6)	33 (1.4)	30 (1.0)
TCCT High CrOx (23 mg/m ²)	73 (0.8)	35 (0.7)	32 (0.8)
ECCS (9 mg/m ²)	67 (0.6)	33 (0.8)	33 (0.8)

From Table 4.3 it can be seen that the contact angle measurements of all three fluids are not affected profoundly by the chromium oxide coating weights. A slight decrease in contact angle is seen as the chromium oxide coating weight is increased, Figure 4.5. This increase is not significant due to the effect of substrate surface being the outermost first 10 Å.

4.3.2.3 Glass Transition Temperature

The glass transition temperature (T_g) of a polymer is the temperature at which the polymer transitions from a brittle, glassy state to a rubbery, viscous state. This transition is a result of the motion of the polymer chains, which become more flexible and mobile as the temperature increases. The T_g of a polymer depends on various factors such as the type of polymer, the molecular weight, the degree of crosslinking,

and the presence of any plasticizers or other additives. Polymers that have a high T_g tend to be more rigid and brittle, while those with a lower T_g are more flexible and elastic.

This value is significant in the context of packaging steel coatings due to the elevated temperatures and pressures (121 °C and 2 bar) the system experiences during the retort process. Previous work has characterised epoxy based packaging steel lacquers as having T_g values between 94 and 107 °C (137). Both the epoxyphenolic and BPANI lacquers were investigated for their glass transition temperatures with view to illustrating the temperature at which the materials soften and start becoming more amorphous. Lacquers were coated onto a Teflon sheet and fully cured as per the manufacturer's instructions, later being peeled off. The T_g values and the DSC data from which they were calculated for the epoxy and BPANI lacquer is shown in Table 4.4 and Figure 4.6 (a-b). The T_g is typically determined by measuring the midpoint of the transition, which is the temperature at which the heat flow is at a maximum.

Table 4.4 – Glass transition temperatures (T_g) for the epoxyphenolic and BPANI lacquers.

Lacquer	Glass Transition Temperature (T_g)
Epoxyphenolic	96.2 °C
BPANI	100.5 °C

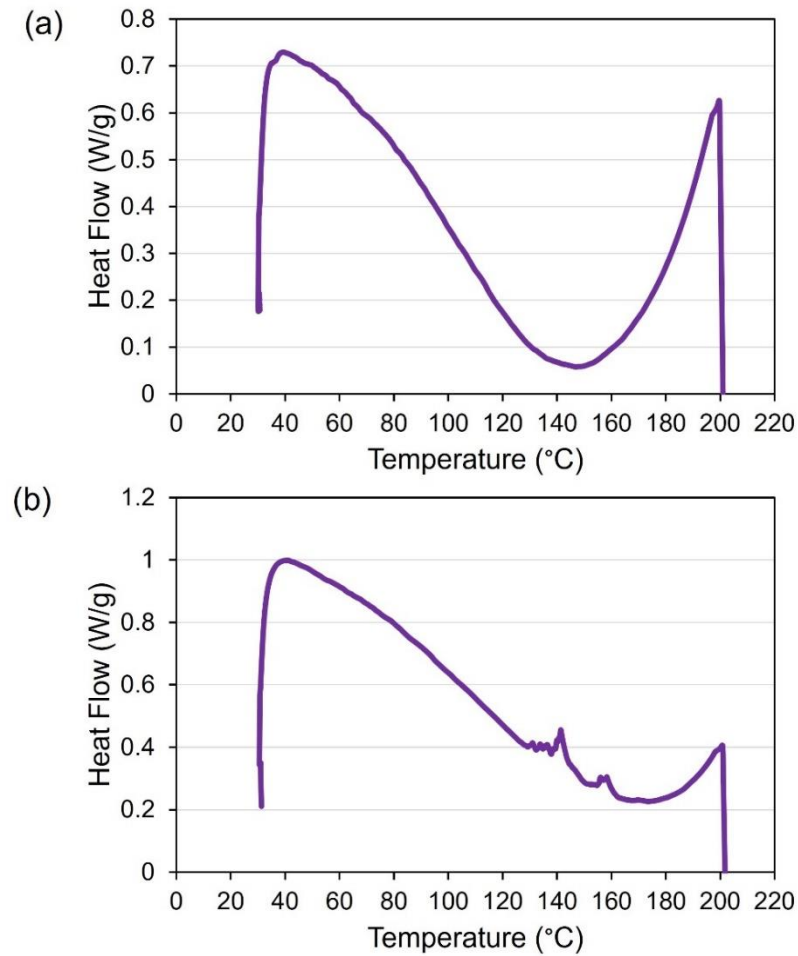


Figure 4.6 - DSC data for the (a) epoxyphenolic and (b) BPANI lacquers.

The T_g values for epoxyphenolic and BPANI lacquers are 96.2 °C and 100.5 °C respectively. These values are in-line with literature which details the glass transition temperatures for a range of epoxy-based lacquers (49). It may be argued that DSC is not the best method with which to measure this parameter, however, research has shown that other techniques such as dynamic mechanical analysis (DMA) yield similar results (138). Significantly the T_g values of both lacquers are below the operating temperature of the retort process, 121 °C. This means that during the retort process, for 90 minutes, the lacquers exhibit lower localised viscosities and are more mobile from a polymer chain perspective. Consequently, their barrier properties may be compromised.

4.3.3 Metallic Coating Morphology

The homogeneity of the metallic coatings deposited on packaging steel substrates is of paramount importance, not only to provide good adhesive characteristics for the lacquers applied but to mitigate iron present in the underlying blackplate substrate. Coating porosity has previously been noted on previous iterations of TCCT substrates and so it is relevant to investigate coating morphologies in order to visualise the affect that the electroplating parameters have had, specifically the applied current density (34,59).

SEM imagery of low, medium and high chromium oxide coating weight samples along with ECCS are illustrated in Figure 4.7 (a-d) respectively. All images in this section were taken on a JEOL FEG-SEM as per the method described in section 3.3.6.

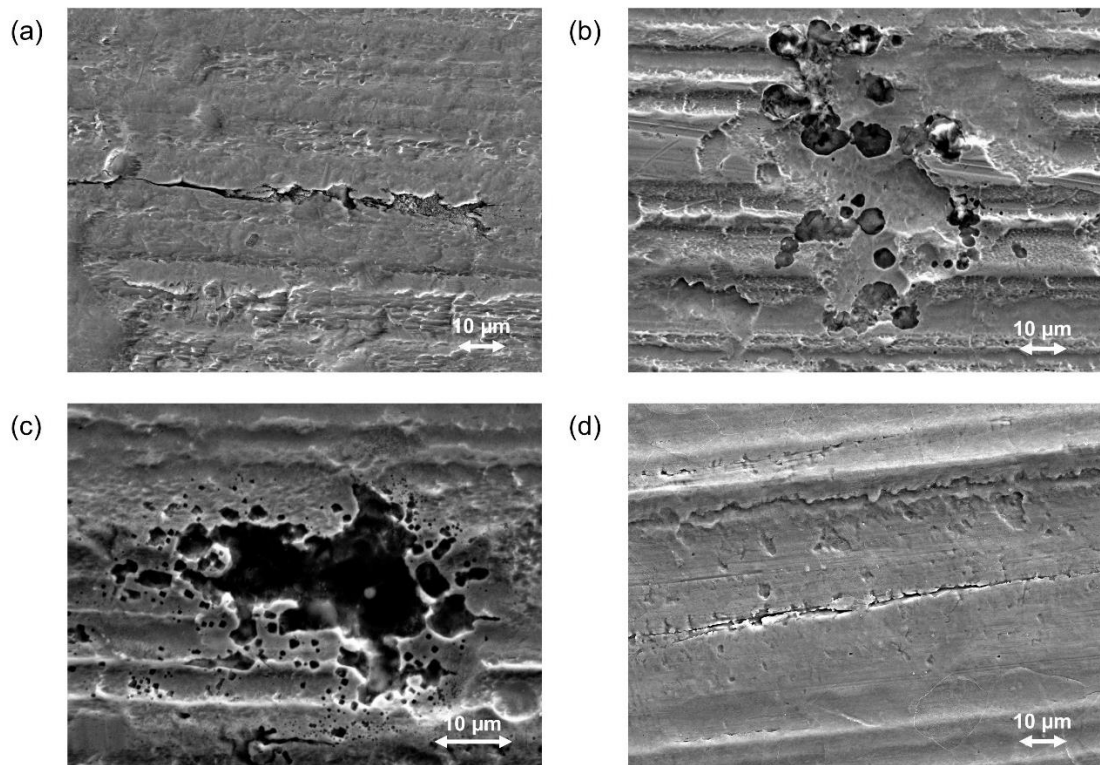


Figure 4.7 - SEM imagery showing the surfaces of TCCT substrates coated with (a) low CrOx (3 mg/m^2), (b) medium CrOx (13 mg/m^2), (c) high CrOx (23 mg/m^2) and (d) ECCS (9 mg/m^2).

Figure 4.7 (a-c) shows that the surfaces of TCCT samples exhibit significant cracking and porosity when compared with ECCS (Figure 4.7 (d)), on which the metallic coating seems more homogenous. The defects seen in Figure 4.7 (b-c) appear to be both pitting in nature and surrounded by smaller bubble like pinholes. It is

proposed that the increased number of defects observed at higher chromium oxide coating weights are due to the fact that the substrate acts as the cathode in the electroplating process, and so hydrogen is evolved on its surface during electrodeposition (139). The surfaces of the low (3 mg/m^2) and high (23 mg/m^2) chromium oxide coated samples were further imaged at higher magnifications in order to visualise any differences, Figure 4.8.

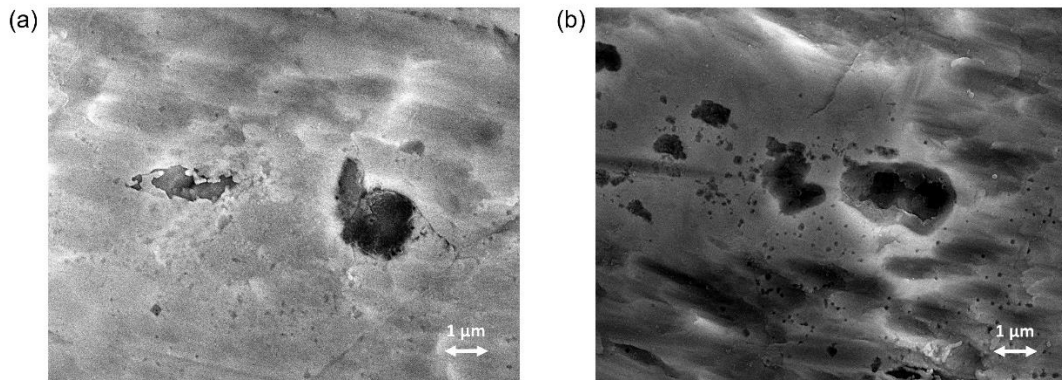


Figure 4.8 - SEM imagery showing the surfaces of TCCT samples coated with (a) low CrOx (3 mg/m^2), and (b) high CrOx (23 mg/m^2) at magnifications of 10000x.

Figure 4.8 shows variation in surface morphology between these two substrates. This variation is represented by differences in the depth of pitting defects ($\sim 1\text{-}5 \text{ }\mu\text{m}$ in diameter) and smaller pinholes ($< 0.1 \text{ }\mu\text{m}$ in size). It is proposed that the larger defects are products of the surface topography of the chromium metal deposition which may not be mitigated by the chromium oxide subsequently plated on top. It is hypothesised that the smaller, nano scale ‘pinholes’ are a product of hydrogen evolution from the electroplating process.

4.3.4 Characterising Thin Chromium Oxide Films Aesthetically - Substrate Colour and Reflectance Analysis

The aesthetic of packaging substrate materials is key in ensuring customer satisfaction. Historically the highest number of complaints to the manufacturers of packaging steel substrates are for aesthetic reasons, which seems counter intuitive considering aesthetic rarely has any influence over the overall performance of the product (102). For this reason, the full range of 15 TCCT substrates listed in section 3.1 were measured colorimetrically in order to determine whether the chromium oxide coating weight has a notable effect on the aesthetic of the substrate. It has been noticed in the

past that at high chromium oxide coating weights, sulphide staining causes black streak like lines on substrates which tend to be in line with the rolling direction (140). This is due to the currents necessary to deposit a thick layer. This work is complimented by gloss measurements illustrating how shiny or dull the substrates are, with all results being compared to ECCS.

Using colour and reflectance analysis has proven to be useful in illustrating the aesthetic change in the substrates and also therefore in estimating the chromium oxide coating weight which may be useful in work described in later chapters. All 15 TCCT samples were measured using an XRITE Ci6X spherical spectrophotometer and the corresponding $L^*a^*b^*$ values were plotted against chromium oxide coating weight with results shown excluding specular light, Figure 4.9 (a-b). Excluding the specular light means that the $L^*a^*b^*$ values are not influenced by the effects of surface texture and similar variables such as haze that can affect the accuracy of the measurements. This haze is caused by microscopic surface textures that diffuse light adjacent to the main specular component of reflected light. ECCS was also measured with results tabulated along with the three TCCT samples representing low, medium and high chromium oxide coating weights respectively, Table 4.5.

Table 4.5 - Numerical spherical spectrophotometry data for TCCT substrates coated with low CrOx (3 mg/m²), medium CrOx (13 mg/m²), high CrOx (23 mg/m²) and ECCS (9 mg/m²).

Sample	Colour Component		
	L*	a*	b*
TCCT Low CrOx (3 mg/m ²)	82.87	0.03	2.55
TCCT Medium CrOx (13 mg/m ²)	84.38	0.16	2.93
TCCT High CrOx (23 mg/m ²)	76.68	0.57	8.54
ECCS (9 mg/m ²)	79.6	-0.71	-1.53

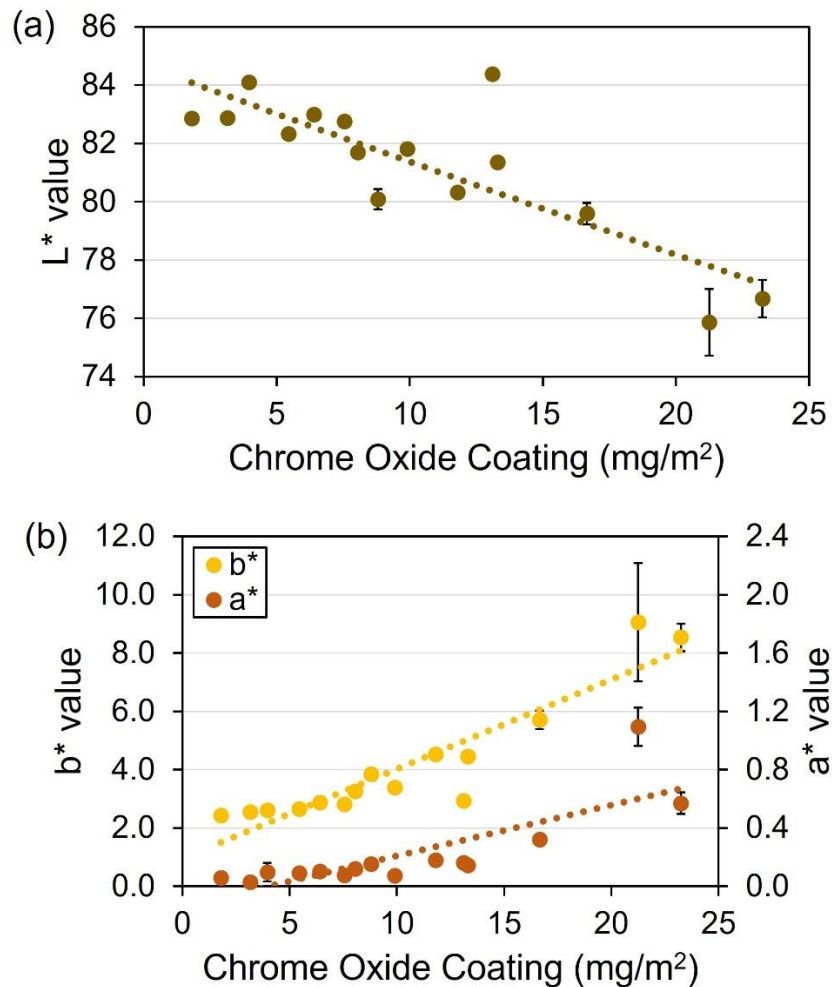


Figure 4.9 - Spherical spectrophotometry data for TCCT sample set: L* values, measured with specular light excluded.

The chromium oxide coating weight has a significant effect on the colour of the substrate. As the chromium oxide coating weight increases, the substrate gets darker (L* value decreases), Figure 4.9 (a). The human eye can detect a change in lightness (L* value) of approximately 1, therefore illustrating the significance of the substrate darkening (141,142).

The amount of chromium oxide has no significant effect on the a* value, Figure 4.9 (b); though it could be argued that at higher chromium oxide levels the a* value increases illustrating a 'redder' appearance of sample, rising from approximately 0.1 to 0.6 at the extremes of the sample set.

The b* value shows a much higher dependency on the chromium oxide coating weight than the a* value; its Y axis being magnified by a factor of 10 in comparison, Figure 4.9 (b). This is in line with the visual observation that the colour becomes more

yellow / brown at high chromium oxide levels, compared to the ‘blueish’ metallic hue of steel itself. The b^* value begins to increase linearly from approximately 2.5 up to 9 at a chromium oxide coating weight of 8 mg/m^2 . This suggests that this is the optimal coating weight of oxide above which, notable changes in colour are visible.

In comparison to these samples, ECCS exhibits a ‘lighter’ surface (as evidenced by a relatively low L^* value of 79.6) along with negative a^* (-0.71) and b^* (-1.53) values. This suggests that ECCS is ‘greener’ and ‘bluer’ than TCCT, exhibiting a more metallic finish.

Along with assessing the colour characteristics of the TCCT substrates, measuring the gloss of the surface of substrate materials lends insight into whether the product may be visually appealing to a customer by quantitatively as this value describes and quantifies shine or lustre. The whole TCCT sample set was measured as per the methodology outlined in section 3.3.5 along with ECCS, Figure 4.10.

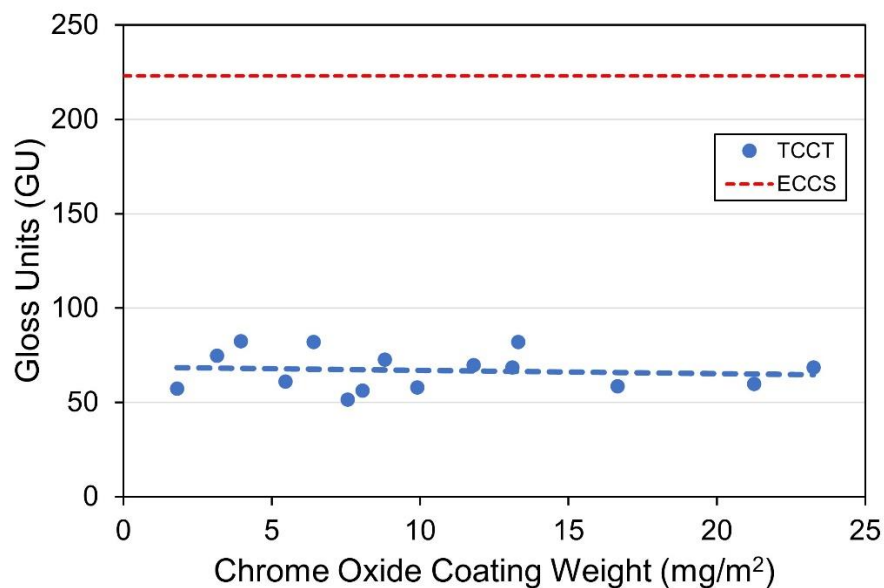


Figure 4.10 - Gloss measurements of TCCT sample set and ECCS taken at a 20 degree angle of reflectance.

The gloss values measured for all TCCT samples are within 40 GU of each other, illustrating a fairly constant gloss level across all chromium oxide coating weights. This is compared to ECCS which has a gloss value of 223 GU which is significantly higher, the difference of which is clearly visible to the human eye.

The marked difference in gloss values between TCCT[®] and ECCS substrates is most likely not due to the surface roughness as it has been shown that all materials have consistent R_a values which are comparable to that of the underlying blackplate

material (0.3 – 0.6 μm). As has been shown in section 4.3.3, pitting defects are present on the surface of TCCT[®] materials (not seen on ECCS) and so may act to lower the gloss level of the substrates by lowering the specular reflectance. It is also possible that the chromium species on the surface of ECCS and TCCT[®] substrates have different optical densities which would inherently change the refractive index of the surface (143). Additionally, the thickness of the chromium oxide layer can also affect the optical properties, with thicker layers generally having higher absorption and therefore lower refractive index values and lower gloss values.

4.4 Chemical Characterisation

From the SEM imagery of the TCCT materials, it is clear that the substrate materials have both micro and nano scale defects on their surface. This suggests that the metallic coatings deposited may not be homogenous and therefore may not fully mitigate the iron content in the base substrate. For this reason, the chemical compositions of these coatings are required both superficially and through their cross section.

4.4.1 XPS Surface Scans

The surfaces of three TCCT substrates representing low, medium, and high chromium oxide coating weights (3, 13 and 23 mg/m^2 respectively) were analysed using XPS. ECCS was analysed for comparison purposes. Scans were obtained with view to quantifying the outermost layer (~ 0.5 nm) of the electro-deposits and to visualise the contribution of surface chemistry as it is this which dictates the bonding sites available for the lacquer adhesion. ‘Wide’ generalised scans were first taken of each sample over the whole range of binding energies to characterise the elemental constituents present on the material, Figure 4.11. Data presented in Table 4.6 is not necessarily calculated from the specific wide scans shown in Figure 4.11, rather the best of a collection of scans.

The chromium peaks on all samples at 575 eV and 584 eV are clearly visible along with its neighbouring peak of oxygen at 530 eV. The peak to the right of oxygen (~ 284 eV) shows that carbon is present, most likely in the form of environmental contamination (DOS oil, fingerprints etc) as these are surface scans. The iron peak is visible for all substrates at 706-710 eV, however, they are more defined on the low chromium oxide sample and the ECCS sample due to the lower total layer thicknesses.

This data is complimented with high resolution scans which quantifies the surface chemical constituents of the substrate, Table 4.6.

Figure 4.12 (a-b) shows the breakdown of iron and chromium into their constituent peaks allowing the accurate analysis of metal and oxide contributions. The iron peak is broken down into Fe_2O_3 and Fe-metal with the chromium peak being broken down into Cr_2O_3 , $\text{Cr}(\text{OH})_3$, Cr_3C_2 and Cr-metal as per previous studies (34).

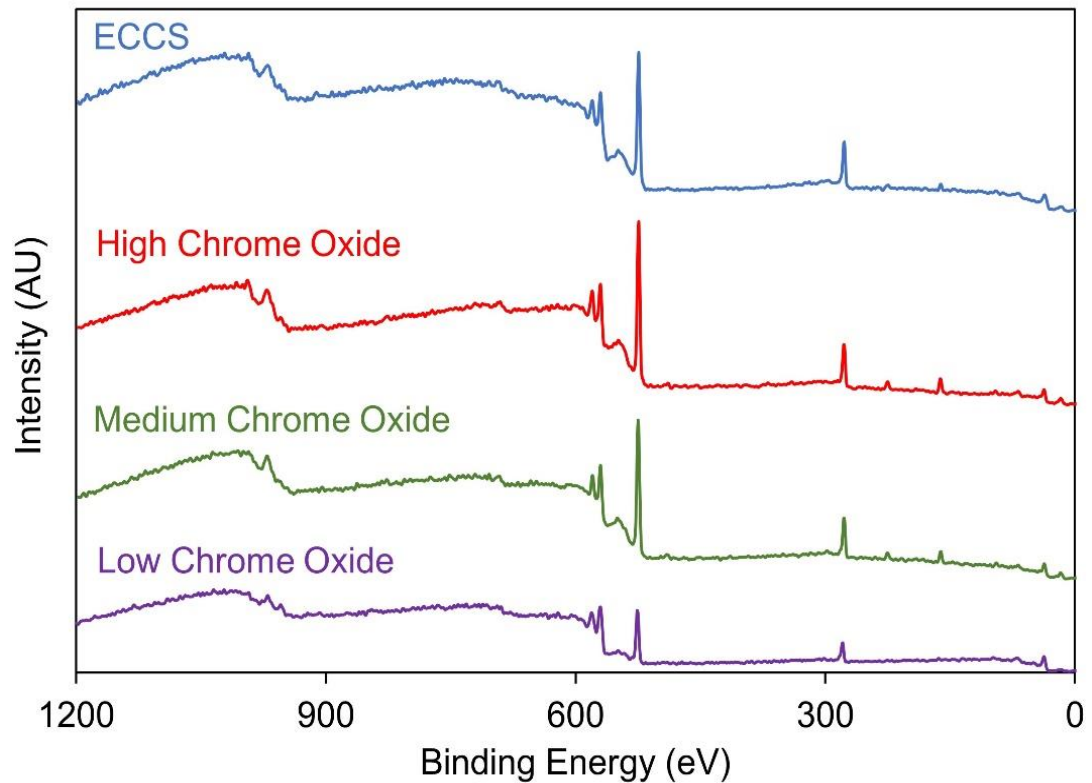


Figure 4.11 - XPS wide scans of TCCT substrates coated with low CrOx ($3\text{mg}/\text{m}^2$), medium CrOx ($13\text{mg}/\text{m}^2$), high CrOx ($23\text{mg}/\text{m}^2$) and ECCS ($9\text{mg}/\text{m}^2$).

Table 4.6 - XPS chemical constituents of low (3mg/m²), medium (13 mg/m²) and high (23 mg/m²) chromium oxide coated TCCT samples and ECCS.

	Depth (nm)	C-org	Carbide	Cr(OH)₃	Cr- metal	Cr₂O₃	Cr₃C₂	Fe- metal	Fe- Oxide	OH	Oxide	SO₄-	Total
TCCT High CrOx (23 mg/m ²)	0.5	50.7%	0.3%	3.8%	0.4%	1.0%	0.7%	0.0%	0.2%	37.5%	0.5%	4.9%	100.0%
TCCT Medium CrOx (13 mg/m ²)	0.5	14.6%	3.7%	15.6%	0.4%	4.6%	10.2%	3.7%	1.1%	24.0%	21.0%	1.1%	100.0%
TCCT Low CrOx (3 mg/m ²)	0.5	38.4%	6.3%	5.3%	4.1%	9.7%	0.0%	0.1%	2.0%	33.5%	0.0%	0.6%	100.0%
ECCS (9 mg/m ²)	0.6	3.7%	0.7%	7.0%	0.4%	8.3%	20.5%	28.4%	2.2%	12.5%	15.9%	0.4%	100.0%

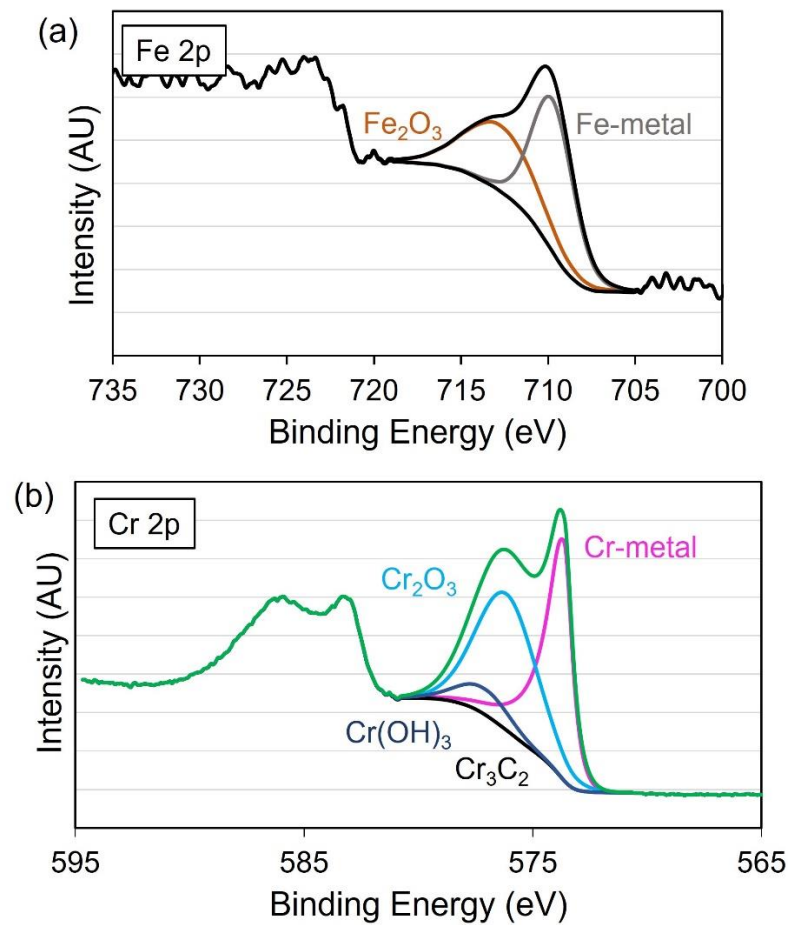


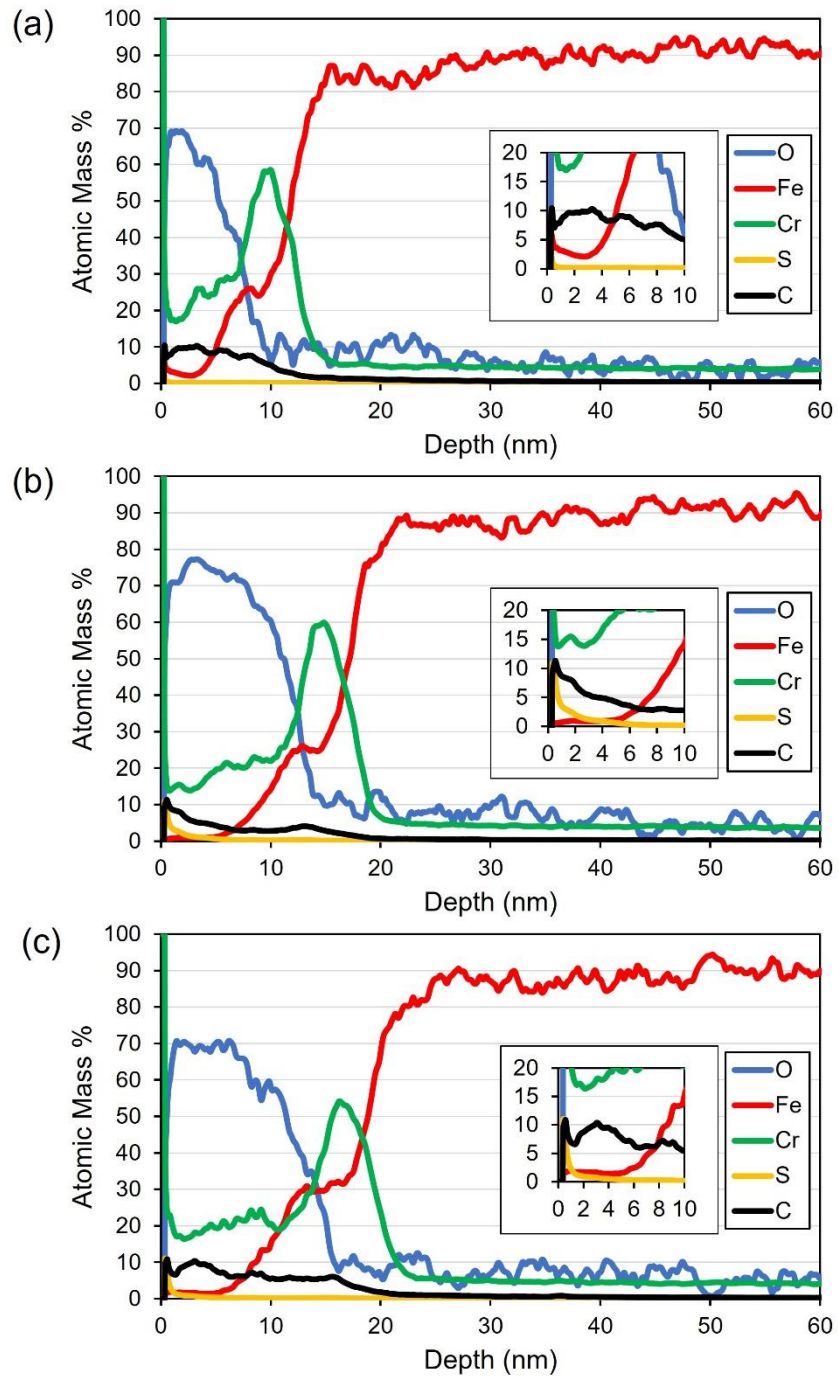
Figure 4.12 - Peak fitting components of (a) Fe 2p and (b) Cr 2p used for XPS analysis.

The outer surface of the TCCT coatings are enriched in oxide with the layer itself made up of chromium metal, chromium oxide and chromium carbide. A notable quantity of iron is detected on ECCS which it is assumed is an anomalous result which was unable to be repeated. All samples have a very high level of carbon contamination on their surfaces, however, the key OH and Cr₂O₃ groups are still measured and a broad picture of the surface chemistry of these substrates is presented.

4.4.2 GDOES Depth Profiles

It is necessary to chemically characterise these substrates through the depth of their coatings (up to 30 nm) to prove the hypothesis of iron being present. GDOES depth profiling was carried out on the same four samples as in the XPS analysis, Figure 4.13. Each sample was etched for 90 s with data being calibrated against XPS depth profiles undertaken by Tata Steel IJmuiden R&D to ensure accuracy. These depth profiles

characterised the absolute thickness of the materials metallic coatings and so could be used as reference when scaling the x axis.



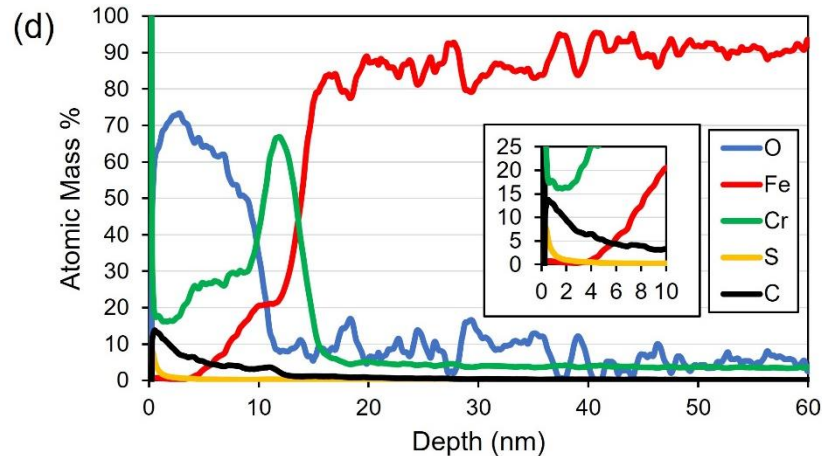


Figure 4.13 - GDOES depth profiles of TCCT substrates coated with (a) low CrOx (3 mg/m^2), (b) medium CrOx (13 mg/m^2), (c) high CrOx (23 mg/m^2) and (d) ECCS (9 mg/m^2).

The differences in chromium coating weights are clearly visible from the oxygen and chromium peaks in Figure 4.13, represented by the blue and green lines respectively. Due to the GDOES measuring elemental composition as opposed to compound and elemental compositions like XPS, the oxygen peak may not be fully quantitative of the chromium oxides present on the surface; instead, they will be spread between the oxygen and chromium peaks. In the case of all samples the chromium metal peak can be seen increasing rapidly once the oxide rich layer (peaking at 70% atomic mass in all cases) has been ablated. For the TCCT samples these signals peak at between 55-60% however for the ECCS sample, the chromium metal peaks at 68%.

The red lines represent iron metal. It is noted that on the surface (first 5-10 nm) of TCCT samples, there is a small but notable signal of approximately 2-4%, especially on the low chromium oxide sample (Figure 4.13 (a)) which has a thin metallic coating, this is not the case on the ECCS sample, for which this signal seems to be approximately 1%. The graphical inserts help visualise this. This finding is broadly comparable to the findings of the XPS surface scans in Table 4.6. The iron signal grows in intensity through the chromium metal layer in the case of the TCCT samples, intersecting the chromium metal peak at $\sim 10\text{ nm}$. In the case of ECCS this intersection is delayed to $\sim 15\text{ nm}$.

On each sample there is approximately 10% carbon signal within the outer 10 – 20 nm of material which, similarly to the XPS surface scans, can be mainly attributed to environmental contamination. A small quantity of sulphur is also present in each sample, originating from the sulphate-based electrolytes that are used.

This analysis has shown a quantifiable difference in both the chromium oxide and chromium metal coating weights for TCCT and ECCS samples. It has illustrated that iron is present on the surface of all TCCT substrates and that there appears to be less iron in the chromium metal layer in the ECCS samples. This agrees with the hypothesis that defects on the surface of TCCT substrates are providing a route for free iron on the surface and that ECCS has a more homogenous metallic coating in comparison.

4.5 Conclusions

Within this section of work, the physical and chemical characterisation of novel TCCT substrate materials has been undertaken with view to illustrating the topographical, wetting, colour and gloss and chemical differences. These characteristics play a role in describing the future performance of these substrates in simulated industrial conditions and their potential acceptance by customers. The work can be summarised into the following conclusions:

- TCCT packaging steel substrates with chromium oxide coating weights of up to 23 mg/m^2 were not found to vary significantly in surface roughness either on a macro or a micro scale. The dominant features included the rolling direction along with structures imparted due to the substrates cold rolling process prior to metallic coating.
- The measured surface tension of both lacquers being investigated (epoxyphenolic and BPANI) exhibit similar physical properties in their liquid state. The contact angle of DI water on the TCCT sample set decreases slightly with increasing chromium oxide coating weight illustrating that increased levels of chromium oxide leads to increased surface energies, allowing liquid coatings to 'relax' more efficiently on their surface. This finding is replicated when the lacquers contact angle are measured on a range of TCCT substrate materials with varying chromium oxide coating weights.
- The glass transition temperatures (T_g) of both the epoxyphenolic and BPANI lacquers have been investigated and found to both be below the temperature of the $121 \text{ }^\circ\text{C}$ retort process (96.2 and $100.5 \text{ }^\circ\text{C}$ respectively). This is significant in that it illustrates that these lacquers become more amorphous during the

retort process and so will act as less of a barrier between the food chemistry and metallic substrate material.

- Surface pits and pores were identified (1-10 μm in size) on the surface of these substrates using SEM, illustrating inhomogeneity in their metallic coatings. Both pitting defects and pinhole defects have been identified.
- XPS surface scans have illustrated the main chemical compound and elemental compositions of a sub-set of TCCT materials and ECCS.
- GDOES depth profiling has enabled a measurement of the absolute thicknesses of the metallic coatings have been visualised along with the profile with which iron moves through said coatings.
- Colorimetric measurements have clearly shown that the chromium oxide coating weight of TCCT substrates cause the lightness, 'yellowness' and 'redness' to vary significantly. All TCCT substrates exhibit significantly less of an aesthetic appeal when compared to ECCS as objectively measured by spherical spectrophotometry. This methodology can therefore be used to estimate the chromium oxide coating weight of substrate materials without the use of x-rays (XRF / XPS).
- Gloss measurements have shown that the lustre of TCCT substrate materials is significantly duller than that of ECCS by many orders of magnitude. This signifies that the aesthetic quality of the TCCT samples investigated may not satisfy customer expectations should it be made commercially available at this stage.

Chapter 5 - The Adhesive
Performance of Protective Coatings
on Novel TCCT Substrates with
Varying Chromium Oxide Coating
Weights

5 The Adhesive Performance of Protective Coatings on Novel TCCT substrates with Varying Chromium Oxide Coating Weights

5.1 Introduction

As established, packaging steel used for canning applications is often coated with a layer of lacquer. This provides protection not only for the substrate material, but also for the canned contents from any contamination from the substrate. There are many mechanisms of lacquer adhesion as detailed in section 0 with deadhesion being influenced by the properties of both the lacquers and the substrates, as characterised in section 4.

The epoxyphenolic and BPANI lacquers used exhibit porosity which has previously been reported upon (144) This porosity acts as a means of ion transport for chemistries within solution to move through the polymer layer to the interface of the substrate and the lacquer, potentially initiating corrosion reactions (68). This porosity may well be exacerbated by the fact that the retort process is approximately 20 °C above the glass transition temperatures, T_g , of the lacquers used as evidenced in section 4.3.2.3. The extent to which these coatings enable the transport of solution can be limited by ensuring the substrate has limited free iron on its surface with which wet chemistries can react. This ion transport through the lacquers is initiated during the canning process where the retort cycle inflicts high temperatures and pressures on the filled cans.

The role of the TCCT duplex metallic chromium coating is both to passivate the iron based substrate but also to provide a surface with which protective lacquers can bond. Subsequently, ensuring continuous layers of both chromium metal and chromium oxide is key in determining the eventual adhesive performance of the lacquer / substrate system.

This section of research aims to characterise the adhesive performance of iterative TCCT substrate materials coated with both epoxyphenolic and BPANI lacquers in simulated industrial conditions. At all times the performance of these substrates are compared to that of ECCS. This investigation is undertaken with view to evaluating the durability and functionality of these TCCT materials in simulated industrial, and real-life conditions.

5.2 Materials and Methodology

The substrate materials used in this chapter were TCCT and ECCS samples consistent with those used in Section 4. This TCCT represented an iterative step forward in bath chemistry and conditions and were manufactured with view to changing the coating weights of chromium oxide by varying on-line line parameters such as line speed (m/min) and applied current density (A/dm^2).

TCCT substrates were parametrically studied to identify the optimum coating weight of chromium oxide (mg/m^2) for the adhesion of lacquers. This was done by assessing their adhesive performance in retort conditions then quantitatively measuring failure forces when scratch tested. Scratch testing was used as the primary method of assessment for the adhesion of the lacquers to the substrates, section 3.3.14. Previous work in this field has used methods such as crosshatch testing to assess the adhesion of these substrate / coating systems, however, due to their subjective nature, have been ignored in this research. The systems used for sample preparation and coating along with the method used for experimental processing and analysis is detailed in 3.2 and was kept consistent in all cases.

Each result, or data point, in the graphs that follow represents an average of four repeats that were undertaken to ensure statistic validity. From these results, standard errors were calculated which are shown in the form of error bars in the plotted charts. Each graph includes a linear line of best fit.

5.3 Adhesion Performance

Each TCCT substrate material has been coated with both epoxyphenolic and BPANI with their adhesion being investigated in dry conditions and post retort in three different simulant solutions (Table 3.3). These results have been compared with ECCS subjected to the same conditions defining a benchmark level of performance. The trends witnessed allude to the failure mechanisms of the lacquers and form the foundation on which further investigation was carried out.

5.3.1 Dry Adhesion – Failure Characteristics Pre-Retort

Dry adhesion measurements characterise the performance of the substrate / lacquer interface in its original coated state without the influence of any procedures such as transport, storage, or retort processes. This information can be used to predict the performance of the substrates through the various processing stages and is used in

industry as a quality control measurement. Dry adhesion measurements indicate if the lacquer curing process has been effective and also whether any surface contaminants are present on the surface of the substrate, Figure 5.1.

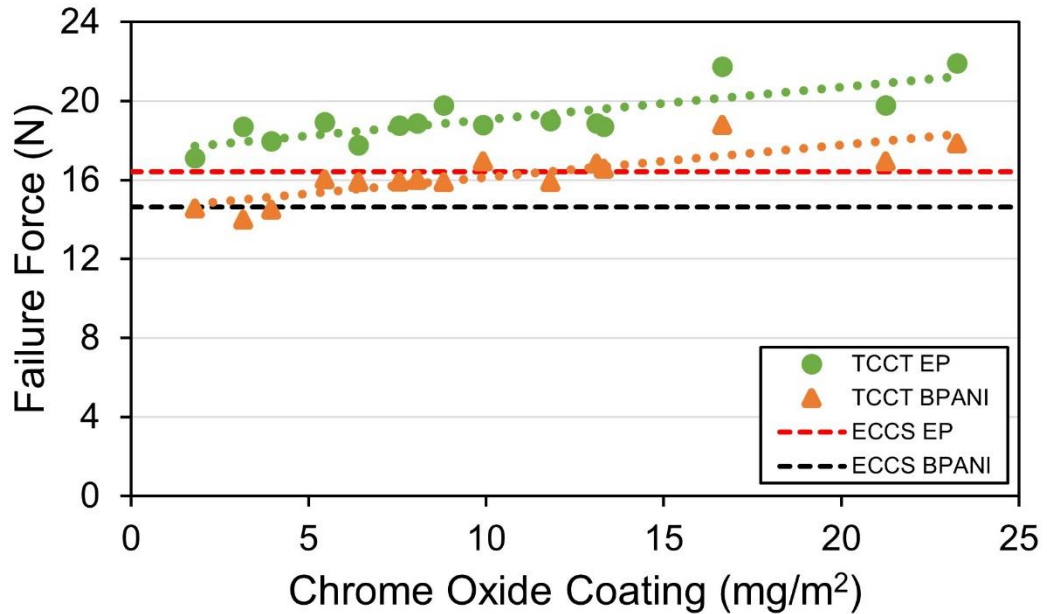


Figure 5.1 - Dry adhesion measurements of TCCT substrates and ECCS coated with both epoxyphenolic and BPANI lacquers.

All TCCT samples with the exception of one, exhibit equal or higher failure forces than ECCS coated with BPANI lacquer. All epoxyphenolic coated TCCT samples perform better than their ECCS counterpart. The chromium oxide coating weight at which BPANI coated TCCT samples surpasses the performance of epoxyphenolic coated ECCS is approximately 13 mg/m². It is also noted therefore that there are sufficient oxide bonding sites for the lacquer in dry conditions on substrates with chromium oxide coating weights as low as 3 mg/m².

The performance of BPANI coated substrates is consistently 2-5 N poorer than epoxyphenolic coated systems. This finding is in line with previous work, initially on tinplate, and more recent work on TCCT systems (38,101). There is a general trend of increasing failure force with increase in chromium oxide coating weight. It is proposed that this is due to there being more hydroxide (OH⁻) bonding sites available for the lacquer to adhere to as previously suggested by Melvin et.al (33)

5.4 Failure Characteristics Post Retort in Simulant Solutions

The wet adhesive characteristics of these lacquers are key in defining a substrate's overall effectiveness commercially and in identifying the mechanisms by which the lacquers adhesion fails. The lacquer adhesion measurements presented in this section were taken after a retort process at 121 °C for 90 minutes, simulating industrial conditions. The method used is outlined in Section 3.2 with the simulant solutions and their justifications detailed in Table 3.3.

TCCT substrates have previously been studied for their lacquer adhesion performance post retort in similar simulant solutions that have been used here. However, the chemistries by which these substrates were manufactured is different and therefore the sample set investigated in this research represents novel iterations which have been made with view to moving towards the commercially stable manufacture of TCCT substrates. Each simulant solution is presented and discussed individually.

5.4.1 Simulant Solution: De-Ionised Water

There is a significant interaction between the substrate / coating interface and retort simulant solution, as evidenced by research pertaining to previous iterations of TCCT substrate materials (113). DI water is perhaps the most benign of all simulated can chemistries and represents both a control for the experiment and a baseline for the performance and witnessed failure mechanisms of the lacquer. Results are illustrated in Figure 5.2.

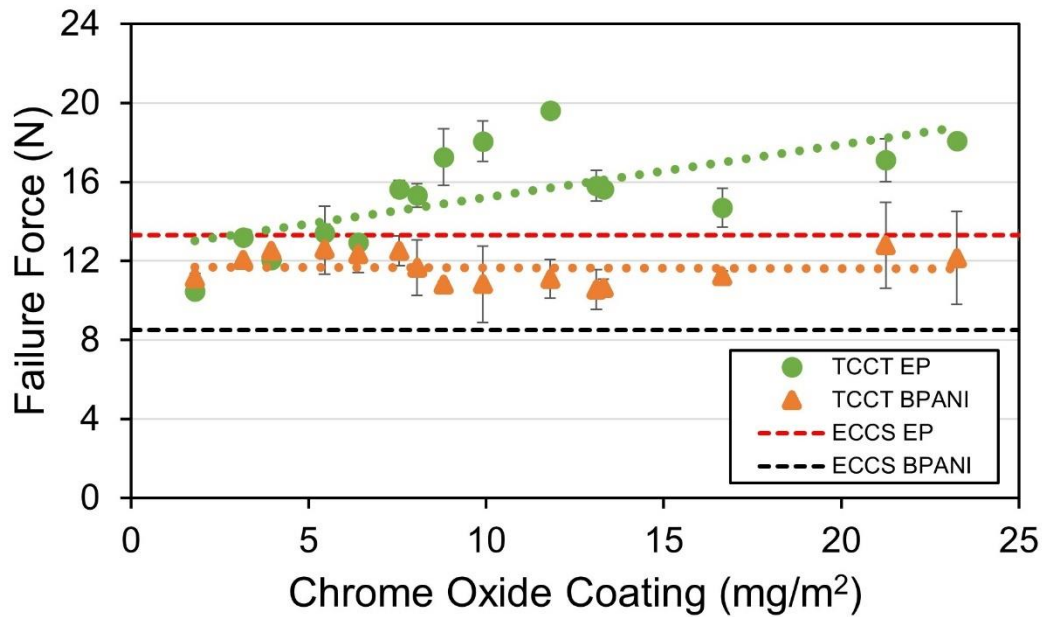


Figure 5.2 - Adhesion measurements of TCCT substrates and ECCS coated with both epoxyphenolic and BPANI lacquers after a retort in DI water simulant solution.

The failure forces of epoxyphenolic coated TCCT peaks at a chromium oxide coating weight of approximately 12 mg/m^2 , exhibiting a failure force of 19.7 N . For chromium oxide coating weights of 6 mg/m^2 or more, the epoxyphenolic coated TCCT out-perform ECCS. The performance of BPANI coated TCCT remains relatively constant throughout the sample set but is always higher than BPANI coated ECCS. Compared to the dry adhesion results, lower adhesive failure forces are generally observed.

5.4.2 Simulant Solution: NaCl

Sodium chloride (1% w/v) is a common chemistry found in canned goods which has proven to be extremely detrimental to the adhesion of lacquers post retort, often causing blistering and by extension, coating delamination (68). The understood mechanism whereby the deadhesion occurs is identical to the corrosion mechanism previously described. The adhesive performance of TCCT and ECCS substrate materials in this 1 % w/v NaCl solution is presented in Figure 5.3.

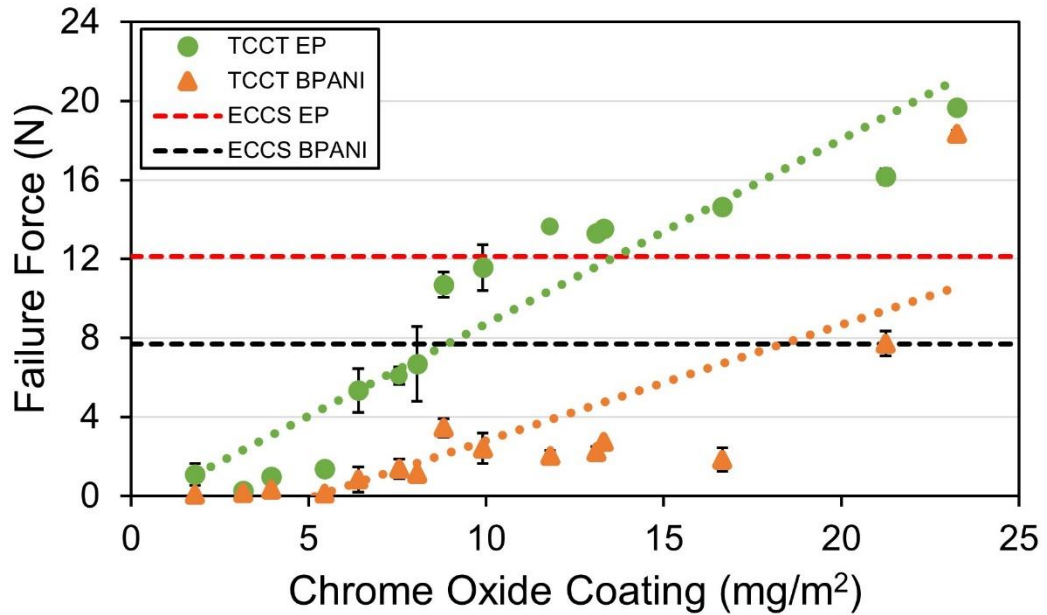


Figure 5.3 - Adhesion measurements of TCCT substrates and ECCS coated with both epoxyphenolic and BPANI lacquers after a retreat in 1 % w/v NaCl simulant solution.

The 1 % NaCl solution impacts the performance of the lacquers considerably – to a point where for some samples coated with BPANI lacquer had completely de-adhered and so presented no failure force to measure. The chromium oxide coating weight at which the epoxy coated TCCT system performs in line with its ECCS counterpart is approximately 13 mg/m², with the BPANI coated TCCT system requiring 18 mg/m².

5.4.3 Simulant Solution: Citric Acid + NaCl

Including a secondary organic acid into the NaCl solution, in this case citric acid, has been shown to reduce the impact of the NaCl on similar substrate materials. The mechanism by which this occurs involves the citric acid neutralising the corrosion potential of free iron (forming iron citrate) on the surface and further oxidising the chromium coating(73). The adhesive performance of TCCT and ECCS substrate materials in this Citric acid + NaCl solution is presented in Figure 5.4.

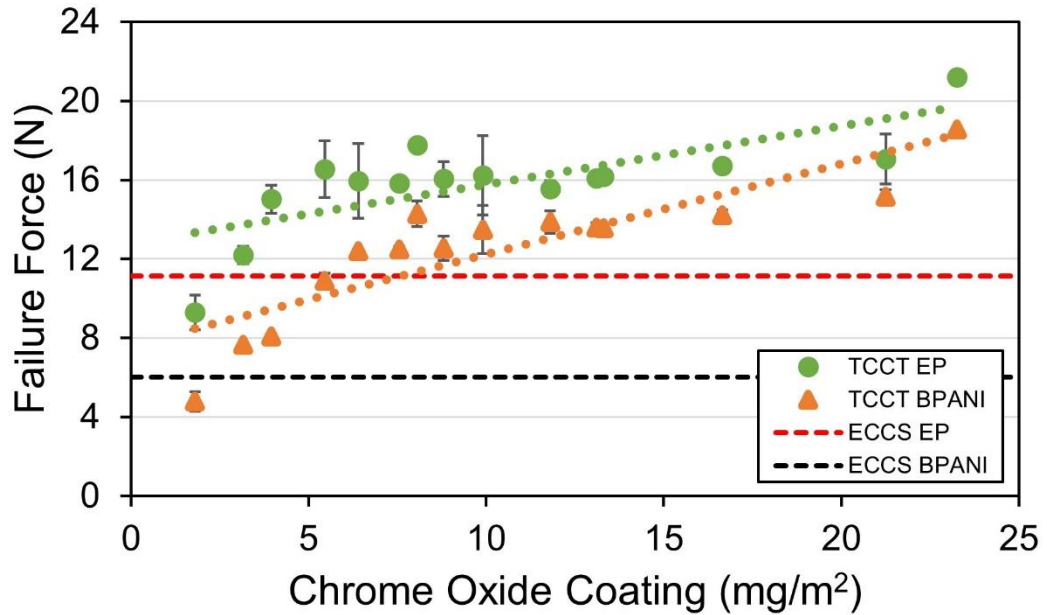


Figure 5.4 - Adhesion measurements of TCCT substrates and ECCS coated with both epoxyphenolic and BPANI lacquers after a retort in citric acid + NaCl (0.25 % + 0.25 % w/v) simulant solution.

ECCS exhibited lower adhesive failure forces by approximately 1-2 N compared to those in the NaCl solution however, the impact of this solution on TCCT samples was seen to be significantly less than the NaCl solution. Both the epoxy and BPANI coated TCCT samples equal and surpass the performance of ECCS at a coating weight of approximately 5.5 mg/m² of chromium oxide and again, BPANI coated systems always perform worse than the epoxy coated systems. The trend in these data suggest that the effect of this secondary organic acid in solution is limited as there is a plateau in the failure forces, both at a coating weight of approximately 5.5 mg/m².

5.5 Failure Mechanisms and Post-Retort Visualisation

Post-retort, the visual quality of TCCT samples varied from looking completely unaffected, in DI water simulant solution, to comprehensively destroyed with corrosion product present on the surface after being retorted in NaCl solution; particularly the samples with lower chromium oxide coating weights (< 8 mg/m²). It is evident from both the scratch testing results and the visual state of the lacquer / substrate system that the retort process has a significant effect on the adhesion properties of the lacquers. For this reason, a selection of samples coated with 3 mg/m² of chromium oxide were visually inspected post retort process using optical microscopy to ascertain the true integrity of the lacquer / substrate boundary and to

picture any lacquer deadhesion mechanisms, or lack thereof. These images are detailed in Figure 5.5.

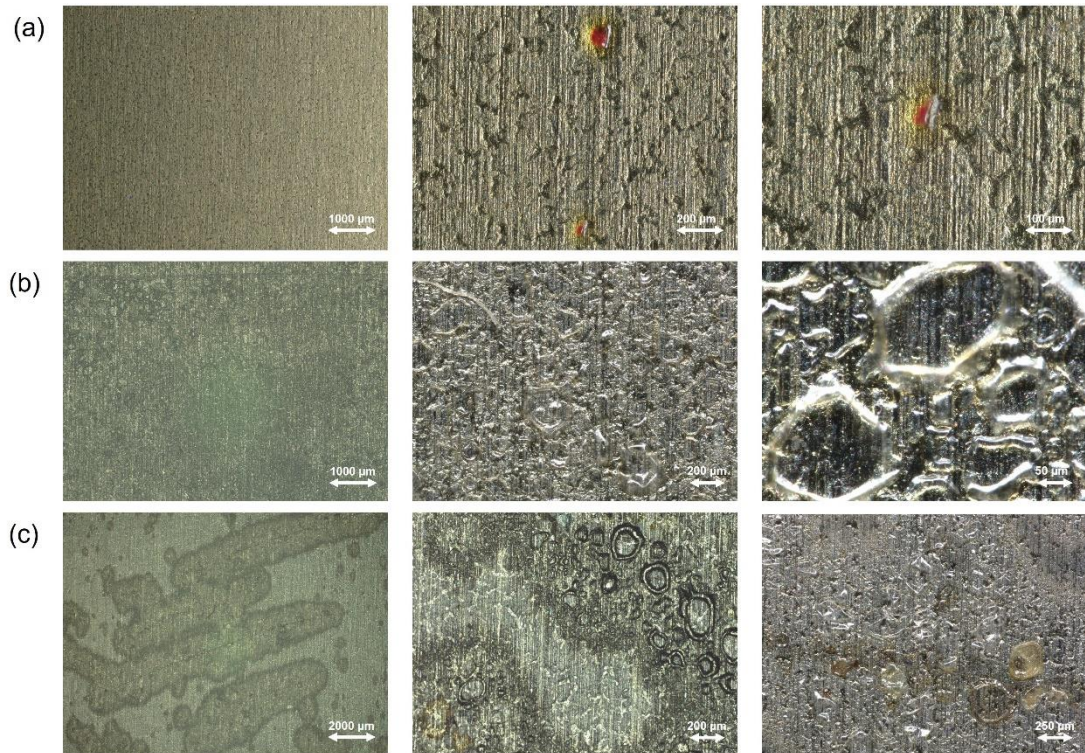


Figure 5.5 - TCCT substrate with chromium oxide coating weight low (3 mg/m^2) post-retort in (a) DI water, (b) NaCl and (c) Citric and NaCl solutions visualising lacquer failure mechanisms.

After retort in DI water, the lacquer's surface post retort looks to still be homogenous, apart from the occasional medium sized blister like defect, which in this case measures between 20 and $50 \mu\text{m}$. Due to the sporadic nature of these abnormalities, they are likely caused by defects in the lacquer coating (from sub-optimal coating / curing procedures). The lacquer coating remains fully intact, Figure 5.5 (a).

Post-retort in a NaCl solution, the samples appear to have been severely impacted by blistering from underneath the lacquers surface (Figure 5.5 (b)). This supports the theory that localised corrosion is taking place and gas (hydrogen) is therefore being evolved at the lacquer / substrate interface. The lacquers surface is destroyed, and in some areas, blisters have pierced the lacquer layer causing complete adhesive failure. These blisters are observed over the entire area of the substrate, Figure 5.5 (b). There is clear rust which has been formed (although not pictured).

Including citric acid in the NaCl retort solution seems to limit this blistering effect to some degree. Approximately 50% of the samples area is covered in blisters,

however, they seem to be focussed over perceived lines on the substrates surface. It is hypothesised that these lines are pits which become passivated due to the citric acid. However, no further investigation has been undertaken due to time constraints, Figure 5.5 (c).

5.5.1 Water Uptake assessment of Polyester Based (BPANI) Lacquer

A common trend through all of the adhesion data, both dry and wet, is that the BPANI lacquer consistently performs poorer than its epoxyphenolic counterpart. This difference is far more significant after a retort process. It is proposed that this variance in measured failure force is primarily caused by the polyester readily absorbing H₂O into the polyester bulk with oxygen, water, and ionic species having the potential to migrate through the coating. This acid / alkaline hydrolysis reaction occurs when water molecules penetrate the surface of the lacquer and react with the ester groups (-CO-O-) in the polyester resin. This reaction degrades the polymer into its alcohol / carboxylic acid components (-COOH) breaking the polymer chains, causing the lacquer to become weaker and lose its properties (145,146). Thermogravimetric analyses of coated substrate samples that have been gradually exposed to DI water at 121 °C revealed a gradual rise in coating mass with increasing retort time (38). The adhesion strength in these conditions was found to be reversible, and so it is assumed no corrosion took place. This adhesion strength would not have been reversible if corrosion had been initiated on the surface as hydrogen would have been evolved and localised blistering would have occurred therefore de-adhering the lacquer from the surface of the substrate.

Having witnessed the severe effect of NaCl simulant solution on these TCCT substrate materials, it is clear that there is a considerable corrosive deadhesion mechanism and so it follows that the adhesion force will not be recoverable. In order to determine any physical or chemical changes in this polyester based BPANI lacquer post retort, a Perkin Elmer Spectrum 100 FTIR Spectrometer with a UATR accessory was used. TCCT samples representing low, medium and high chromium oxide coating weights (3, 13 and 23 mg/m²) were coated and retorted in DI water, 0.5 % NaCl and 1 % NaCl. Their absorbance spectra post retort is illustrated in Figure 5.6.

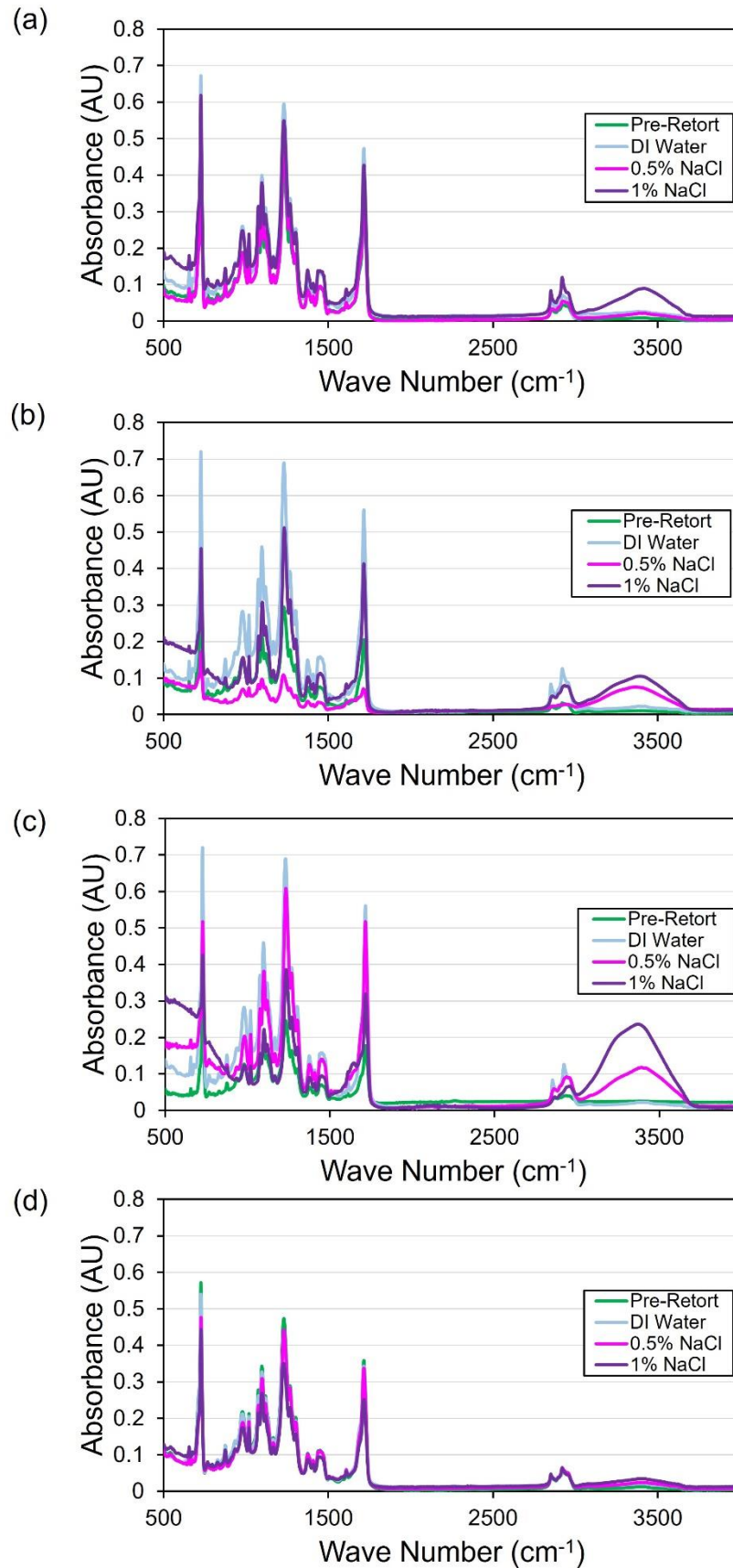


Figure 5.6 - FTIR graphs representing TCCT samples coated with (a) high CrOx (23 mg/m²), (b) medium CrOx (13 mg/m²), (c) low CrOx (3 mg/m²) and (d) ECCS (9 mg/m²) pre retort and post retort in DI water, 0.5% NaCl and 1% NaCl.

FTIR has identified that water is present within all coatings across all samples which is shown by the increasing absorbance of the O-H peak at 3400 cm^{-1} (147,148). This water uptake is far more prevalent in samples with the lowest chromium oxide coating weights. This is evident from the magnitude in the areas under the absorbance band at 3400 cm^{-1} in Figure 5.6 (c) compared to those in Figure 5.6 (a) which are later quantified. On the TCCT sample with the lowest chromium oxide coating weight, water ingress under the coating was visible to the eye in 0.5 % and 1 % NaCl solution, illustrating the delamination of the lacquer. The absorbance of the remaining functional peak at 1700 cm^{-1} (C=O stretching frequency) was not seen to change throughout the sample set. In addition, the peak at 2900 cm^{-1} which is characteristic of a methyl or ethyl ester group, is present in all spectra in (149). These groups are composed of carbon-carbon (C-C) and carbon-hydrogen (C-H) bonds, which are relatively stable and resistant to oxidation or degradation. This finding therefore suggests that the NaCl solution does not initiate a chemical reaction with the polyester coating but rather the substrate underneath (150).

These findings are complimented by using the FTIRs Perkin Elmer software to integrate the areas under the O-H stretching peaks at 3400 cm^{-1} (after normalising each sample against their own carbonyl peak (C=O) at 1700 cm^{-1} ensuring accuracy). After comparison with the 'dry' sample scan this allows estimation of the percentage increase in water uptake of the coating, Figure 5.7 and Table 5.1.

It's important to note that this method assumes that the coating is homogeneous and that the water uptake is uniform throughout the coating. The accuracy of this method depends on the quality of the reference spectrum and the consistency of the sample preparation and measurement. As only a pinpoint of the surface has been measured, the implication is that these findings may not be as accurate as if many repeats had been taken and averages made. This was not possible due to time constraints. The clear trends in the data, however, lend credence to the theory that these findings are scientifically valid.

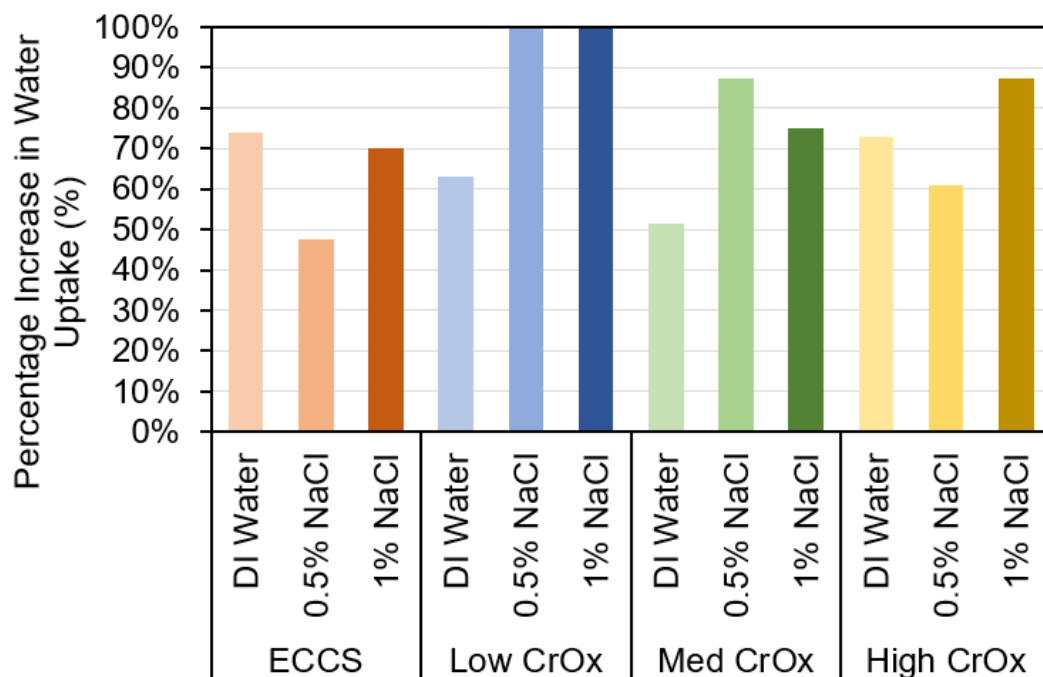


Figure 5.7 - Quantification of water uptake of BPANI coated TCCT samples coated with low CrOx (3 mg/m²), medium CrOx (13 mg/m²) and high CrOx (23 mg/m²) and ECCS (9 mg/m²) post retort in DI water, 0.5% NaCl and 1% NaCl illustrating a percentage of the coatings in

Table 5.1 – Numerical quantification of water uptake from FTIR data shown in section 5.5.1 as a percentage of the coatings initial O-H stretching quantity for TCCT samples coated with low CrOx (3mg/m²), medium CrOx (13 mg/m²), high CrOx (23 mg/m²) and ECCS (9 mg/m²).

Sample	Retort Status	Water Uptake
TCCT Low CrOx (3 mg/m ²)	Pre	0%
	DI Water	63%
	0.5% NaCl	99%
	1% NaCl	100%
TCCT Medium CrOx (13 mg/m ²)	Pre	0%
	DI Water	52%
	0.5% NaCl	87%
	1% NaCl	75%
TCCT High CrOx (23 mg/m ²)	Pre	0%
	DI Water	73%
	0.5% NaCl	61%
	1% NaCl	87%
ECCS (9 mg/m ²)	Pre	0%
	DI Water	74%
	0.5% NaCl	48%
	1% NaCl	70%

The percentage increase in water uptake of the BPANI lacquer for the TCCT samples increases to 100% for the lowest chromium oxide coated samples, Figure 5.7. This quantity of water uptake is prevented by increasing the chromium oxide coating weight, however, ECCS still exhibits the lowest level of total increase in water uptake overall in all simulant solutions.

5.5.2 Copper Sulphate Study Identifying Surface Iron

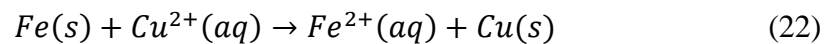
It has been established through XPS and GDOES that iron is present on the outermost surface of TCCT packaging steel substrates (section 4.4). The FTIR investigation (section 5.5.1) of both TCCT and ECCS samples suggests that the NaCl retort solution does not initiate a chemical reaction with the polyester coating but rather the substrate underneath. It is hypothesised that these factors have a potentially catastrophic effect to the adhesion of protective coatings through localised corrosion enabled by the porosity of the lacquers, in particular that of the BPANI coating. This porosity acts as a route for ion transport through the lacquer to the substrate, initiating this corrosive mechanism of deadhesion. It is hypothesised that this is corroborated by images shown in Figure 5.5 where blisters are present in the lacquered coating post retort, alluding to gas evolution at the substrate / lacquer interface.

In order to lend further credibility to this theory, and to investigate the finding of ECCS potentially having a more homogenous coating of chromium oxide than TCCT materials, defects in the chromium oxide layer have been visualised and quantified using a copper sulphate test. Samples investigated here are consistent and include TCCT samples with a low (3 mg/m²), medium (13 mg/m²) and high (23 mg/m²) chromium oxide coating weights with ECCS (9 mg/m²) being used as a control. These samples were dipped in a copper sulphate solution, the composition of which can be found in Table 5.2, and left for 60 s before being rinsed under a stream of DI water and left to drip dry. This method is adapted from the Preece test used to evaluate the integrity of zinc coatings; it has also been used in the context of packaging steel (151,152).

Table 5.2 - Composition of copper sulphate solution used to visualise defects in chromium oxide layer on chromium oxide coated substrate materials.

Constituent	Weight / Volume
Copper Sulphate Pentahydrate	8 g
Sulphuric Acid	2 ml
DI Water	500 ml

In this basic reaction, iron displaces copper ions from an aqueous solution of copper sulphate. It is a single displacement reaction of one metal by another metal which is realised through iron placing above copper in the reactivity series of materials; this therefore makes iron more reactive. Metallic iron is converted into ferrous ion (Fe^{2+}) and cupric ions (Cu^{2+}) are converted into metallic copper, *Equation 22*.



Due to this being a quick displacement reaction, and not copper plating, the copper formed is a precipitate and so is not formally adhered to the surface of the substrate. For this reason, it is important not to wipe the samples dry after the $CuSO_4$ dip and instead let them drip dry as the deposited nodules are easily removed mechanically. SEM imagery of precipitated copper on substrates surfaces and optical imagery of these copper nodules and their relative sizes is shown in Figure 5.8.

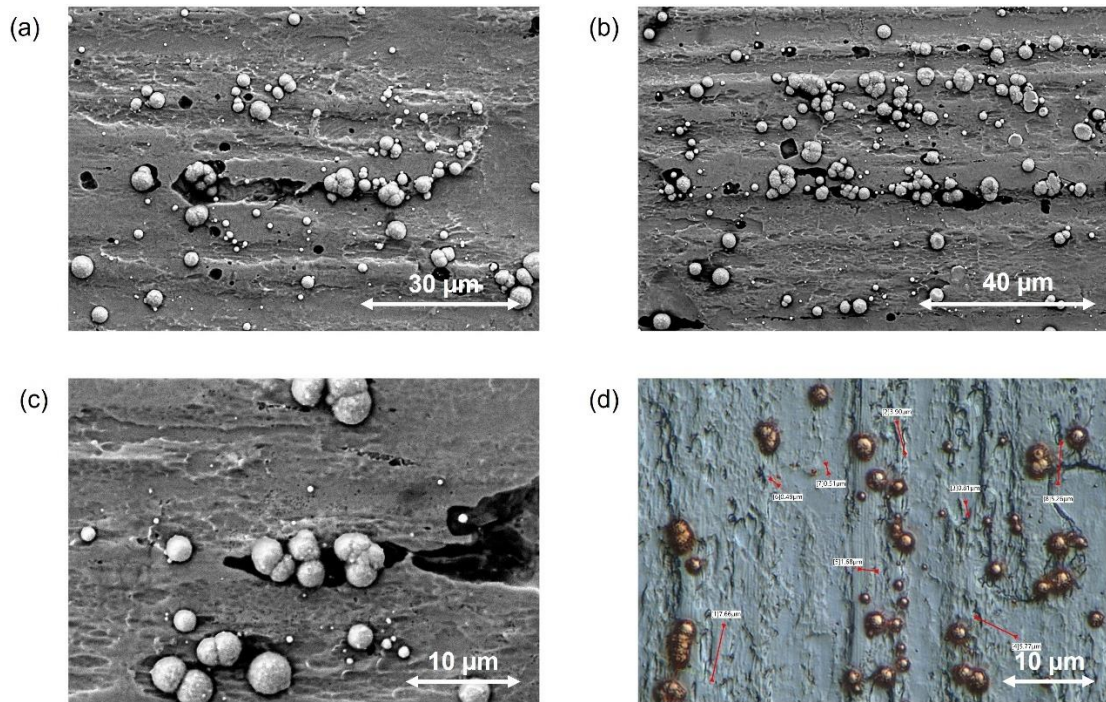


Figure 5.8 - SEM and optical imagery of a TCCT substrate with low CrOx coating weight (3 mg/m^2) showing copper on its surface after a CuSO_4 dip.

As seen in Figure 5.8, the copper nodules have a characteristic ‘mushroom’ shape, being circular in most cases, with a significant height profile from the substrate surface. SEM imagery has shown that the shape of these defects is not consistent, so it is noted that this shape of copper precipitation is independent of the defect or iron it may precipitated in or on.

In order to ensure that the nodules witnessed on the surface on these substrates were in fact copper, XRF measurements were taken of each sample, including 3 repeats, Figure 5.9. An EDX map was also plotted for the sample with the lowest coating of chromium oxide (3 mg/m^2), Figure 5.10.

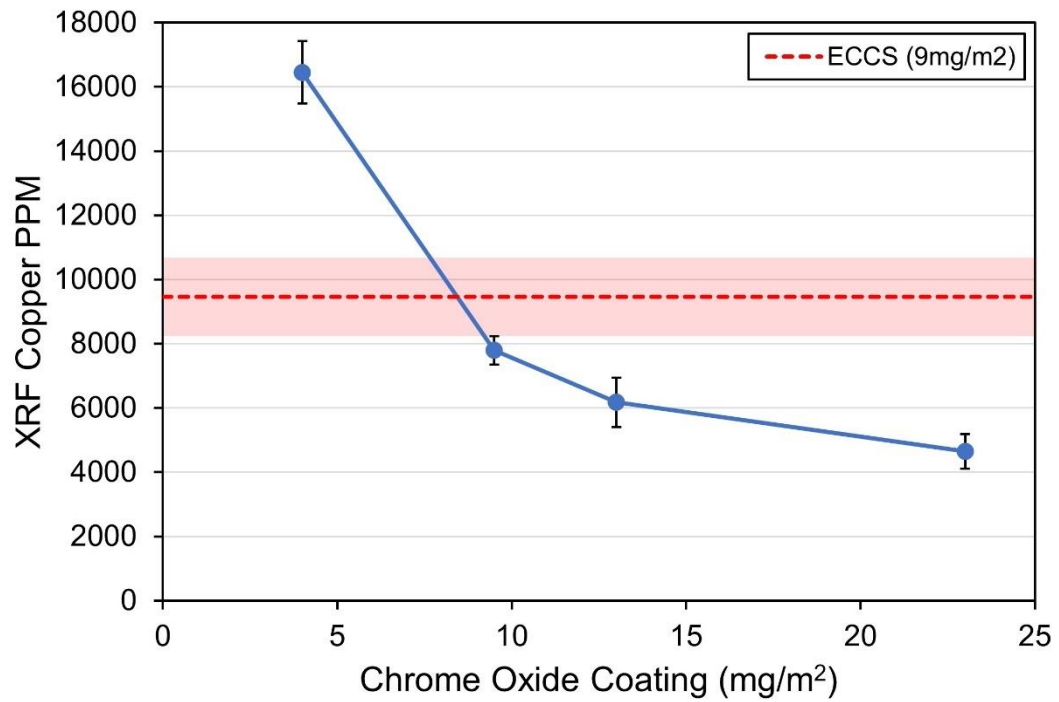


Figure 5.9 - XRF data for the TCCT substrates coated with low CrOx (3mg/m^2), medium CrOx (9 and 13mg/m^2) and high CrOx (23mg/m^2) after dipping in CuSO₄ with ECCS (9mg/m^2) used as a control. Data is represented in PPM of copper.

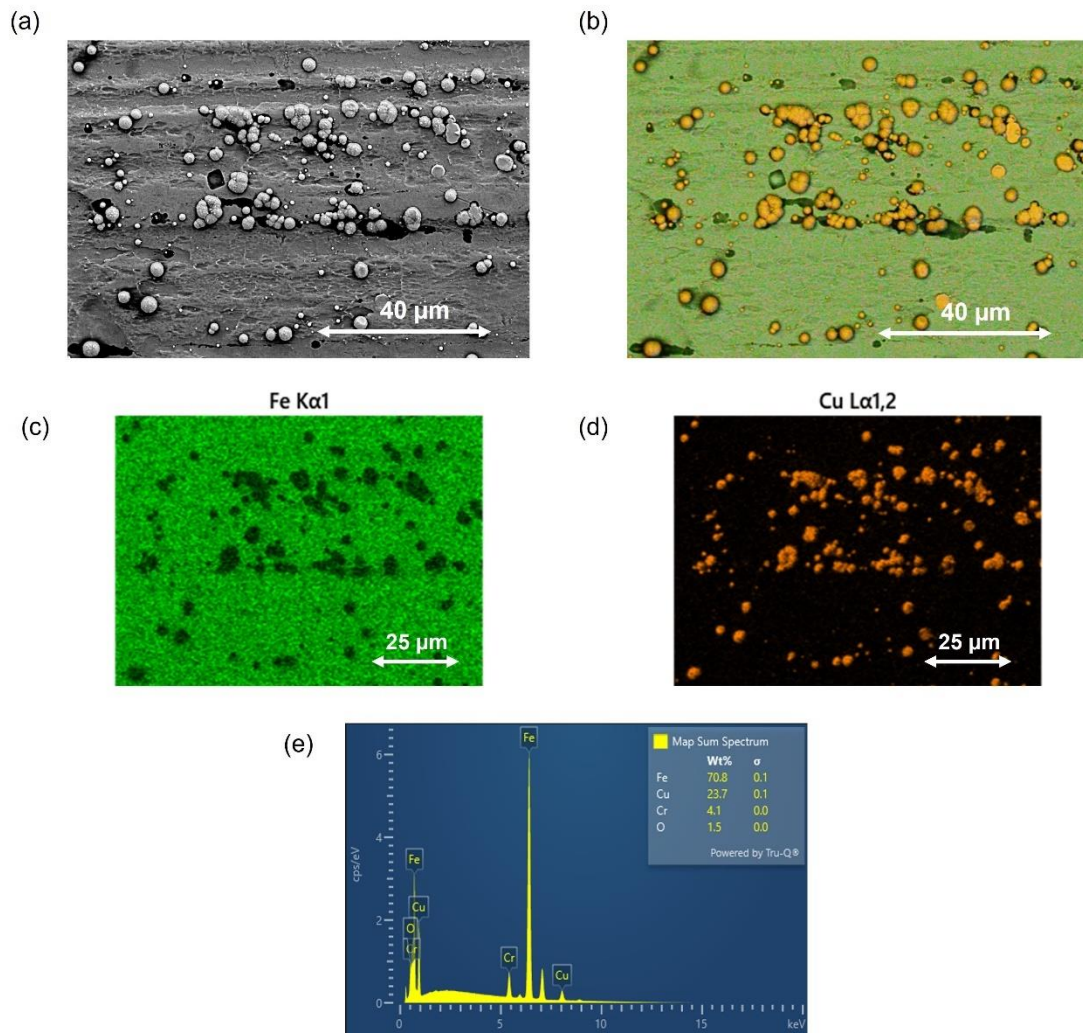


Figure 5.10 - EDX map and corresponding images of the iron and copper plot for a TCCT sample with chromium oxide coating of 3 mg/m², highlighting copper on the substrate surface.

By varying light settings and contrast on the Keyence optical microscope, it is possible to define these copper nodules more clearly using a colour contrast tool. This allows the calculation of the area average of copper on a given sample, Figure 5.11.

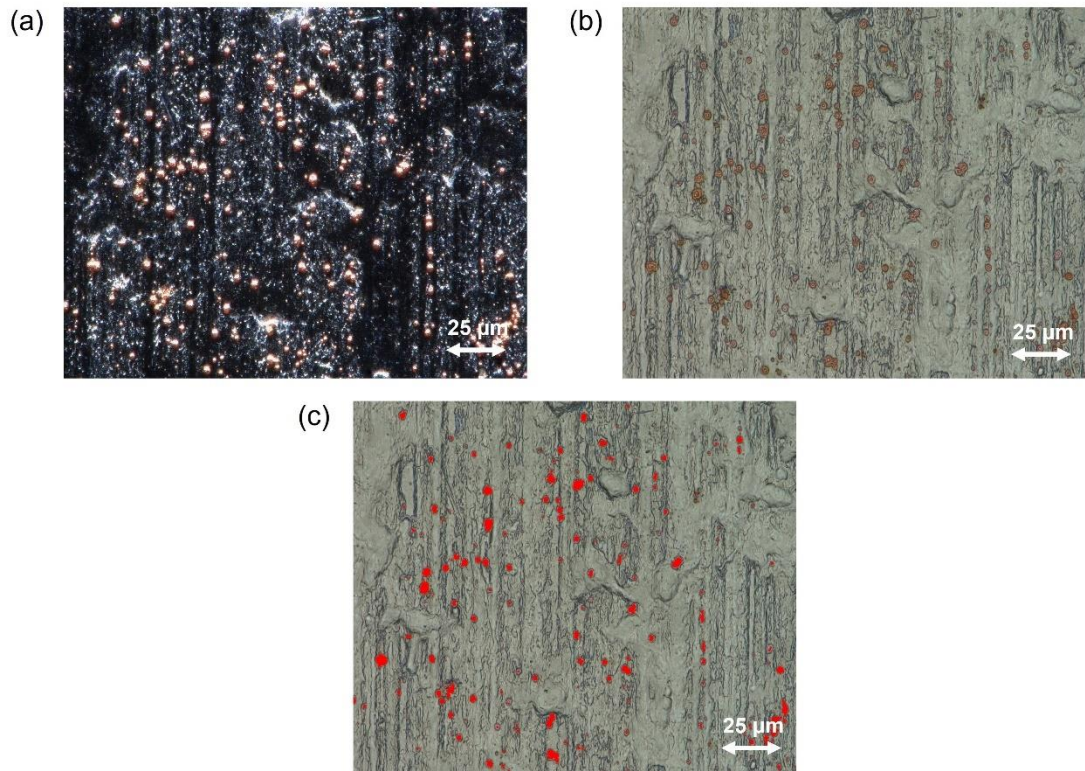


Figure 5.11 - Light microscope images (a-c) showing the quantification of copper area on substrate materials with differing light and contrast settings.

The copper nodules on a given surface can be quantified by using the colour contrast software. This was done for TCCT samples with a low (3 mg/m^2), medium (13 mg/m^2) and high (23 mg/m^2) chromium oxide coating weights along with ECCS (9 mg/m^2). The results of this investigation are shown in Table 5.3 and Figure 5.12. The standard errors of measurements are tabulated due to Figure 5.12 having a dual Y-axis.

Table 5.3 - Area ration of copper on the surface of TCCT and ECCCS substrate materials highlighting differences in site density and therefore chromium oxide layer homogeneity.

Sample and Corresponding Chromium Oxide Coating Weight	Area Ratio Cu %	Site Density
TCCT (3 mg/m ²)	5.6 (0.1)	3900 (110)
TCCT (13 mg/m ²)	3.2 (0.1)	2500 (100)
TCCT (23 mg/m ²)	2.2 (0.2)	2200 (180)
ECCS (9 mg/m ²)	1.8 (0.1)	1600 (170)

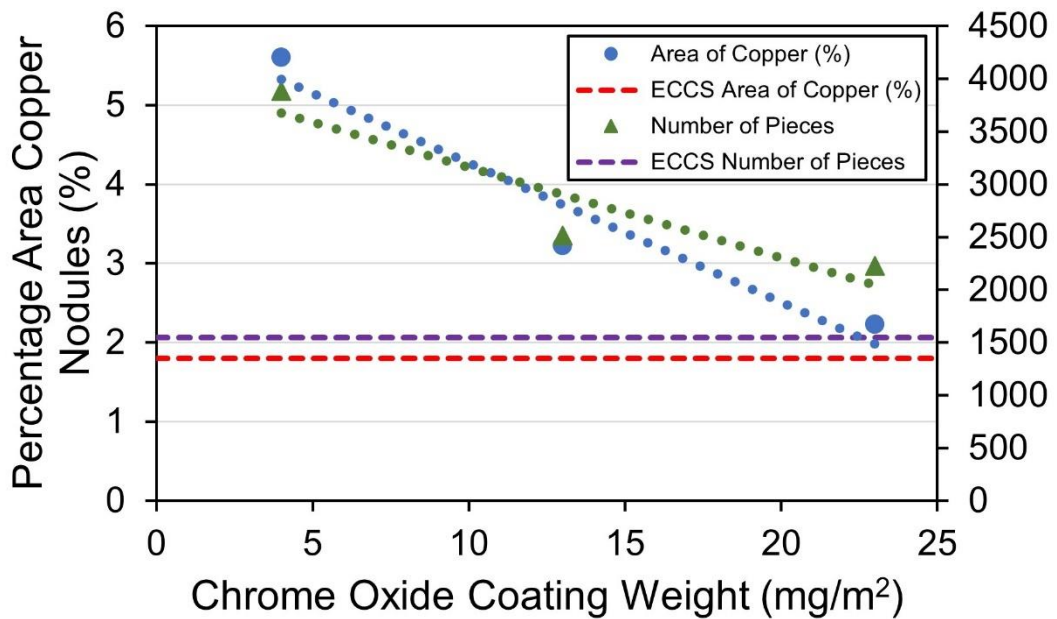


Figure 5.12 - Area ratio of copper on the surface of TCCT and ECCCS substrate materials plotted with their respective site densities.

The lowest chromium oxide coated TCCT has a 5.6% area ratio of Cu after the CuSO₄ dip test with as many as 3900 sites present (in all cases the site densities are rounded to the nearest 100). Both of these values decrease with increasing chromium oxide coating weight and fall to 2.2% area ratio of Cu and 2200 sites in the case of the highest chromium oxide coated TCCT sample. However, even though ECCS has a mid-level of chromium oxide coating (9mg/m²) in comparison, it still exhibits the

lowest area ratio of Cu and number of sites after the CuSO₄ dip (1.8% and 1600 respectively). This confirms the theory stated previously of ECCS having a more homogenous layer of chromium oxide on its surface than all TCCT substrate investigated.

5.5.3 Corrosion Resistance of the Substrate

It has now been established that chromium oxide coating weight has a significant effect on the adhesive performance of lacquers both pre and post retort. This is due to the oxide / hydroxide layer providing sites for the lacquer to bond with, as well as pacifying any iron which may be on the surface on the substrate / incorporated in the chromium metal layer. This has been both visualised and quantified using a range of techniques including optical microscopy, FTIR and CuSO₄ dip testing. Although useful in proving that iron is present on the surface of, and through, the metallic coatings, this testing does not provide any information as to what effect this iron may have.

The scanning vibrating electrode technique (SVET) was used to assess the local current density distributions across the surface of the same samples as section 5.5.2; TCCT with chromium oxide coating weights of 3, 13 and 23 mg/m² respectively along with ECCS (9 mg/m²). The design, calibration and operation has been well documented elsewhere (62,121). This testing was conducted in order to assess the mechanisms of corrosion on these substrates' surfaces.

Acetone and ethanol were used to clean 50 mm x 50 mm samples, with a 10 mm x 10 mm central square left exposed and the remainder of the sample taped off using, allowing data collection from the exposed area only. Samples were immersed in a 0.171 mol dm⁻³ NaCl electrolyte solution at 20°C. The SVET microtip was held 100 µm above the samples surface. Every hour for 24 hours, including hour 0, the SVET tip was scanned over the surface of the sample measuring and quantifying areas of dissimilar electrochemical activity. The collected data was processed to add the calibration factor for each scan point. Surfer™ from Golden Software was used to create colour maps of the current density values.

Shown in Figure 5.13 to Figure 5.15 are SVET scans of TCCT samples coated with 3 mg/m², 13 mg/m² and 23 mg/m² of chromium oxide respectively using ECCS as a control. The scans presented are at 6 hour intervals with all scale bars being measured in A/m².

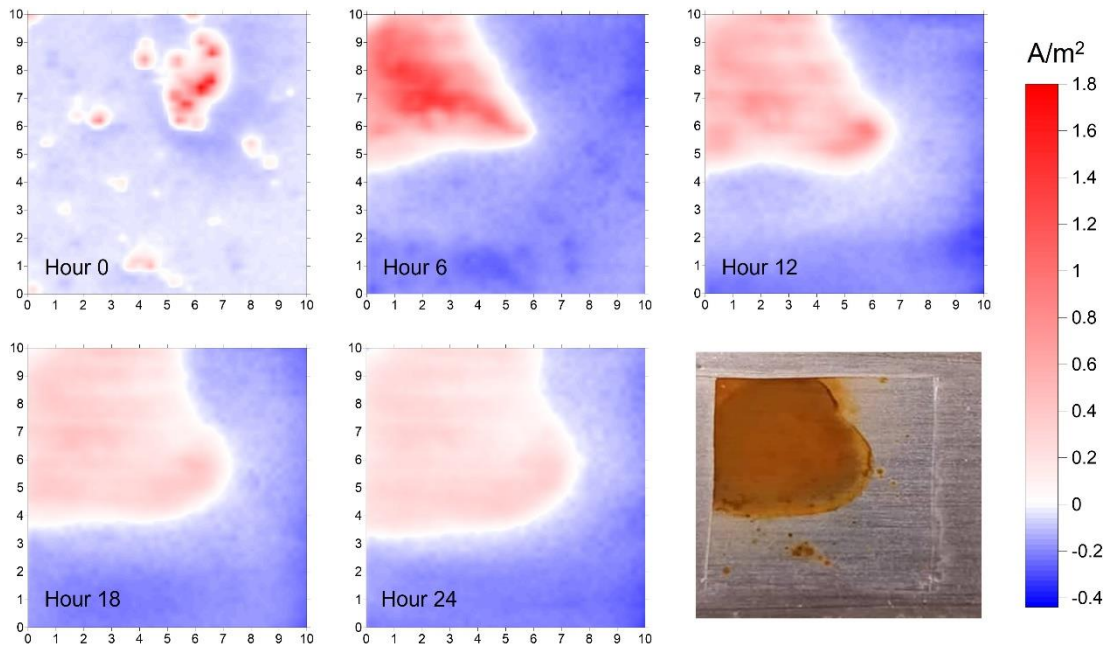


Figure 5.13 - SVET colour charts representing TCCT coated with 3 mg/m^2 of chromium oxide and image of sample post-process.

Figure 5.13 represents a TCCT sample with 3 mg/m^2 chromium oxide coating weight. It is evident from this data that the surface of the substrate has corroded significantly. Initially localised pits form between hours 0 and 5, after which corrosion becomes more generalised in nature, spreading across the samples surface with current density of 1.8 A/m^2 . The corrosion seems to reduce in intensity after hour 6 with the final appearance of the substrate appearing to be coated with corrosion product. After this scan it appears that although corroded, no penetrating defects are present. Minor pits are visible in the substrate.

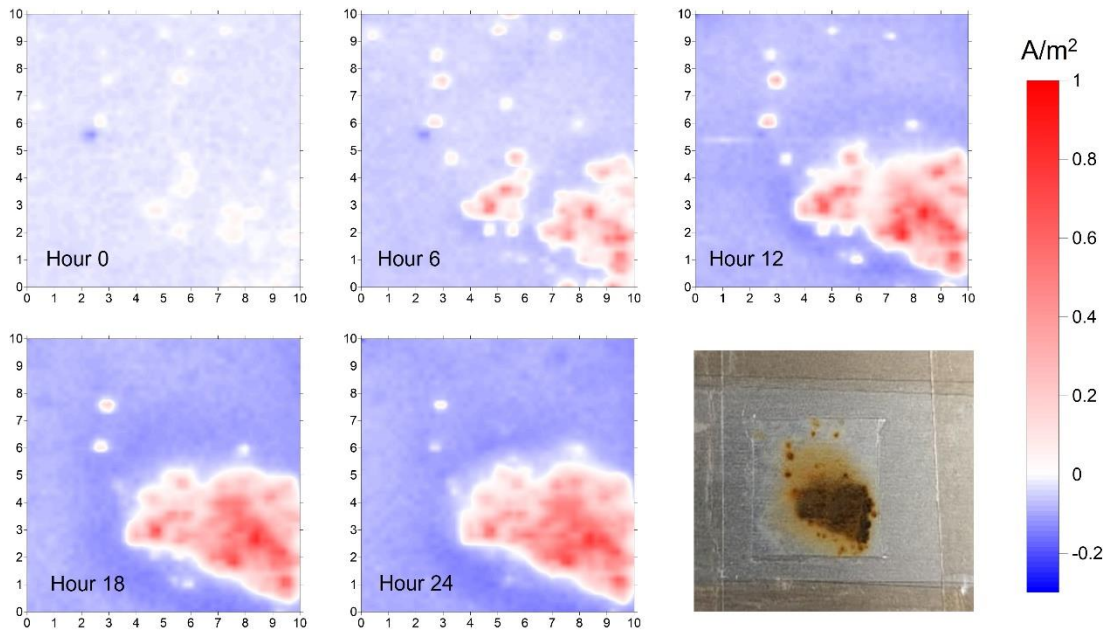


Figure 5.14 - SVET colour charts representing TCCT coated with 13 mg/m² of chromium oxide and image of sample post-process.

Figure 5.14 represents a TCCT sample with 13 mg/m² chromium oxide coating weight. Unlike the sample with the lowest chromium oxide coating, this materials anodic current peaks at the 24th hour in this scan but is consistent in that the substrate is acting as the cathode. This shows that corrosion is actively taking place throughout the whole time of the scan. The mechanism of corrosion is a mix between generalised scaring and pitting, with the anodic current density peaking at 1 A/m². Corrosion product has been deposited onto the samples surface as well as deeper pits being visible which are black, signifying the coating is completely destroyed in that region.

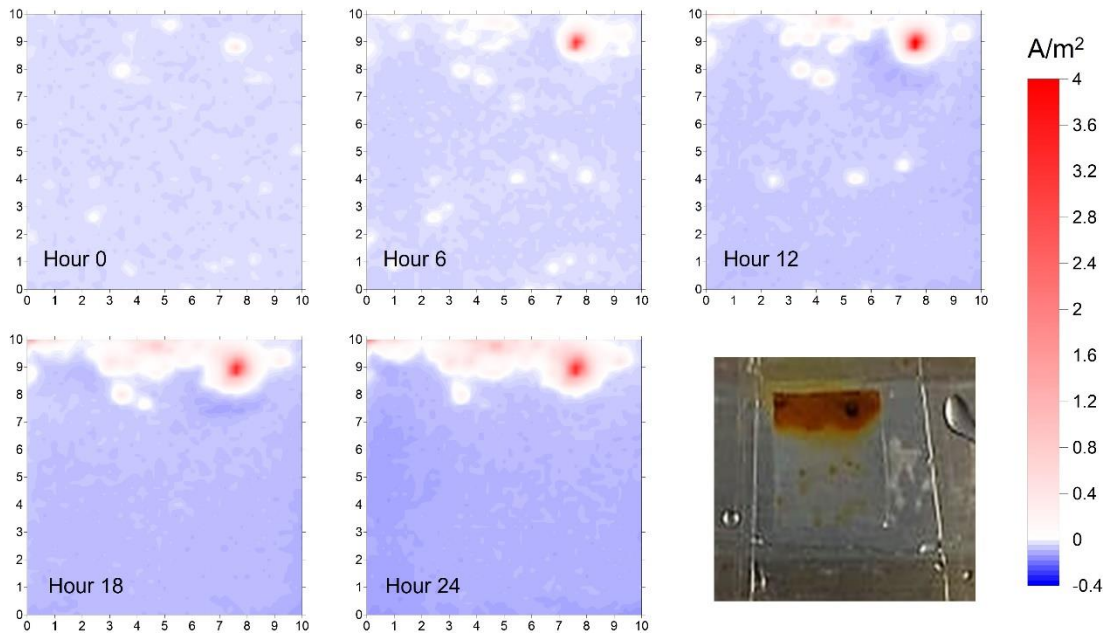


Figure 5.15 - SVET colour charts representing TCCT coated with 23 mg/m^2 of chromium oxide and image of sample post-process.

Figure 5.15 represents a TCCT sample with 23 mg/m^2 chromium oxide coating weight. From the colour charts it is immediately clear that the surface area affected by anodic metal dissolution, which in this case is iron, is significantly less than the previous two scans of TCCT substrates with 2 and 13 mg/m^2 of chromium oxide respectively. However, the anodic current density peaks at 4 A/dm^2 happening at hour 24. Once again, the substrate is acting as the cathode. The nature of the main anodic activity is a severe pit which destroys the metallic coating in that area.

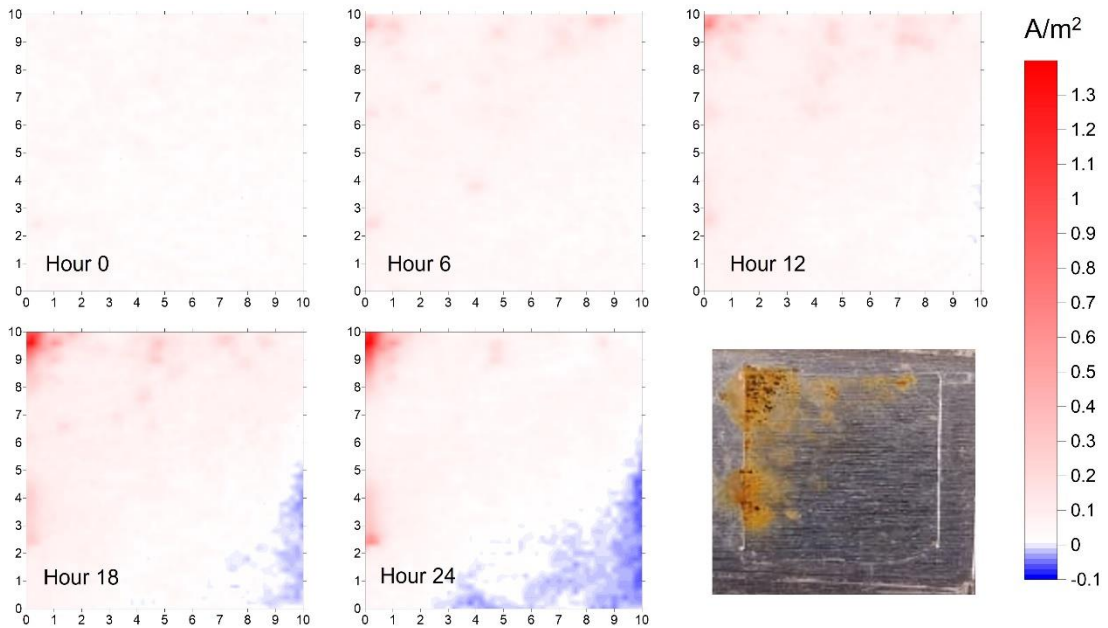


Figure 5.16 - SVET colour charts representing ECCS coated with 9 mg/m^2 of chromium oxide and image of sample post-process.

Figure 5.16 represents ECCS with 9 mg/m^2 chromium oxide coating weight. What is immediately clear from these colour plots is that the anodic activity is dominating the majority of the samples surface area, with only a small section of the sample acting cathodically. The anodic activity peaks at 1.3 A/m^2 with only small pit like defects being witnessed. This peak occurs as hour 11 but remains fairly constant, only falling to approximately 25% of this value by hour 24. The overall quality of the substrate post scan is visually the least damaged with the metallic coating appearing to be almost fully intact across the surface area of the substrate. Corrosion product is limited to the top and left-hand side of the sample where the anodic activity was concentrated. Small pits have developed but, as evidenced by the low peak of anodic activity compared to the TCCT substrates, the coating remains intact. Smaller pits have not been resolved individually as their size is below the resolution of the equipment used.

Repeats of TCCT samples with low chromium oxide coating (3 mg/m^2), high chromium oxide coating (23 mg/m^2) and ECCS (9 mg/m^2) were completed and compared although not pictured in this main body of work. Appendix I visualises additional samples tested, confirming the scarring and pitting mechanisms of corrosion witnessed in the TCCT samples.

5.5.3.1 SVET - Corrosion Mechanism Discussion

The corrosion mechanisms which have been highlighted in the previous section of work are scarring and pitting. To assess these, it is helpful to look at the total anodic and cathodic data for each scan at each hour, Figure 5.17 and Figure 5.18.

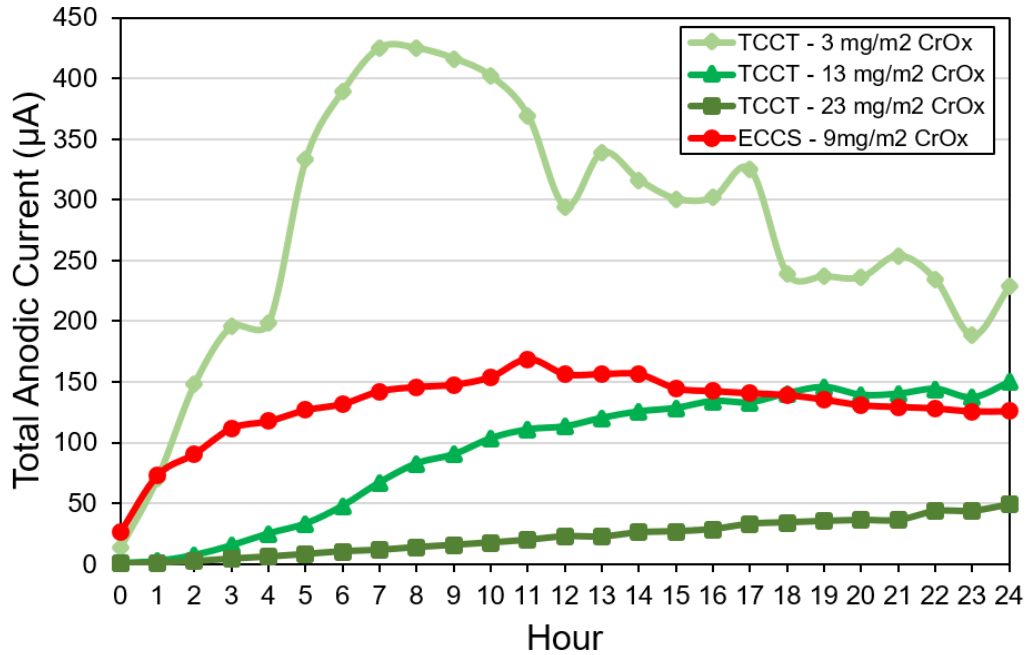


Figure 5.17 - SVET anodic data for TCCT substrates coated with low CrOx (3 mg/m²), medium CrOx (13 mg/m²), high CrOx (23 mg/m²) and ECCS (9 mg/m²).

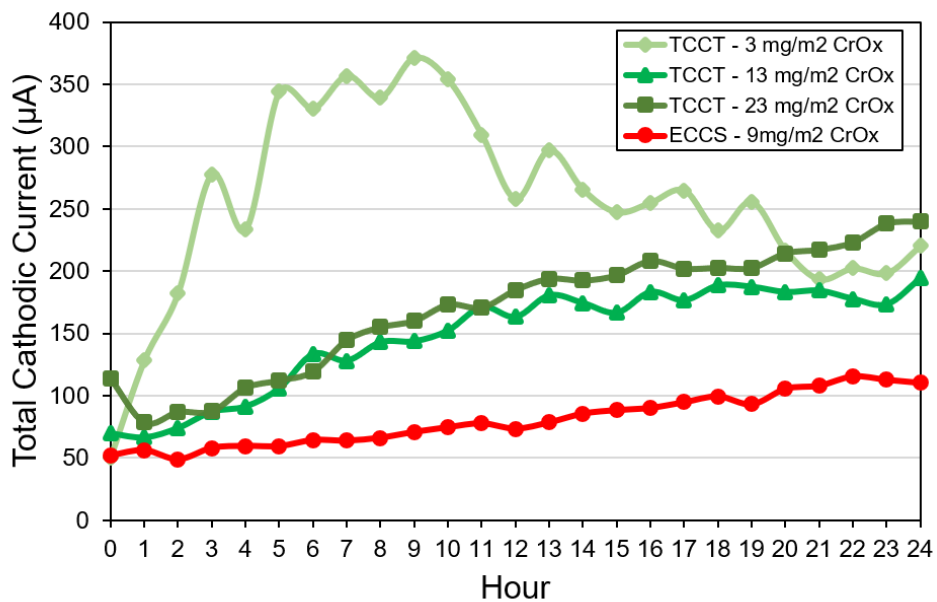


Figure 5.18 - SVET cathodic data for TCCT substrates coated with low CrOx (3 mg/m²), medium CrOx (13 mg/m²), high CrOx (23 mg/m²) and ECCS (9 mg/m²).

As expected, the total anodic and cathodic activity of the samples roughly balance throughout the duration of the scan. The scarring mechanism witnessed on the lowest and mid-range chromium oxide coated TCCT samples is explained by a large surface area of sample acting anodically for the duration of the scan. What is notable however is that the anodic activity for the 3 mg/m² chromium oxide coated TCCT sample peaks at hour 9 and then gradually decreases until the end of the scan. This is explained by the Fe₂O₃ plated cathodically onto the substrate as seen in Figure 5.13 and then acting to self-limit the corrosion process by insulating the substrate. This is not the case for the other TCCT samples but is notable, but to less of a degree, on ECCS.

The pitting mechanism stems from a metallurgical defect on the substrates surface acting as a site for preferential attack. This corrosion mechanism is seen to dominate TCCT samples with a mid-level and high chromium oxide coating and is not as simple to describe mechanistically. Oxygen is consumed within the pit with ions being transported to achieve a balance charge, however, the gradual build-up of corrosion product typically makes the inward diffusion of oxygen more difficult meaning that a pit may well stabilise itself. Within the SVET measurement process, however, the vibration of the tip is driving small quantities of oxygen to the surface of the substrate, therefore allowing this pitting corrosion to continue when it may not otherwise in more subtle environments. The effect of this oxygen diffusion due to tip vibration may be notable due to the pitting mechanism being controlled by mass transport. It has been noted, however, that the SVET microtip influences the O₂ reduction current minutely (< 5%) in the context of other corrosion mechanisms (153). It is therefore hard to establish if the destruction of the metallic coatings, as observed in the images of the samples post-scan, would be a true prediction of this substrate's performance in real-life conditions. It is noted that this pitting corrosion witnessed represents unstable pitting as evidenced by the continual positive gradient of the anodic activities of each substrate, Figure 5.17.

5.5.3.2 SVET – Sample Mass Loss

When using the SVET to measure the electrochemical activity of a substrates surface, it is possible to infer the mass loss from the surface of the substrate over the period of the scan, Figure 5.19. This value is calculated by inputting the mass of iron and referencing the corresponding anodic activity of the scan, as it is in this process where

iron is dissolved, *Equation 6*. Therefore, the trend in this data closely follows that of the total anodic activity shown in Figure 5.17.

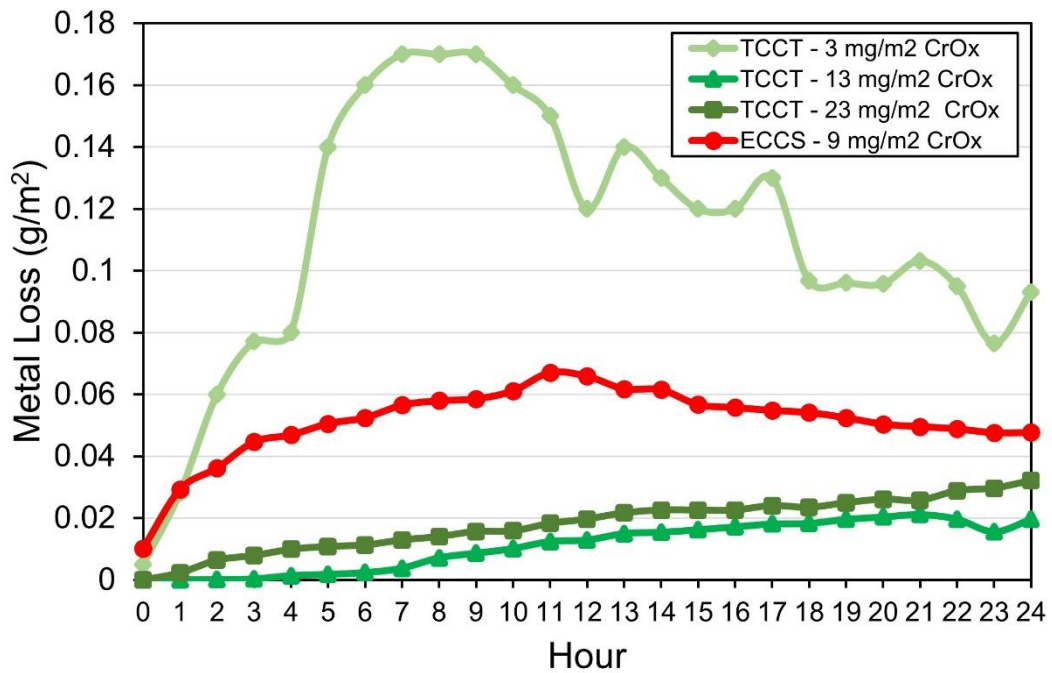


Figure 5.19 - SVET mass loss data for TCCT substrates coated with low CrOx (3 mg/m²), medium CrOx (13 mg/m²), high CrOx (23 mg/m²) and ECCS (9 mg/m²).

From the data shown in Figure 5.19 it is clear that the TCCT sample with the lowest chromium oxide coating weight (3 mg/m²) loses the highest quantity of mass over time, peaking at approximately 0.17 g/m². The total quantity of mass loss decreases with increasing chromium oxide coating weight, apart from the TCCT samples coated with 13 and 23 mg/m² of chromium oxide respectively.

Whilst this data agrees with the previous research undertaken within this body of work illustrating the incomplete oxide layer on substrates coated with lower quantities of chromium oxide (section 5.5.2), some limitations of this technique must be mentioned.

1. The SVET microtip may not be detecting all the current as flux lines may be being generated below the scan height (in this case 100 μm).
2. The resolution of the SVET in this case is approximately 155 μm as per *Equation 18* and so smaller features, as evidenced from SEM imagery, which may be corroding will not be being measured and quantified.

All being considered this semi-quantitative method is still legitimate to use as, although the absolute values of metal loss may not be reliable, they are valid for comparison purposes within the sample set.

5.6 Conclusions

The results shown in this section of work show promise that TCCT substrates have the ability to compete with the current industrial standard of epoxyphenolic coated ECCS for packaging steel applications.

- The studies pertaining to the adhesion of lacquers to these substrates have highlighted the importance of optimal chromium oxide coating weight on the substrates surface. This is seen in Figure 5.1 to Figure 5.4 where there is a positive correlation between failure force and chromium oxide coating weight in all conditions both dry and wet.
- Changing just the lacquer alone from epoxyphenolic to BPANI has a severe effect on the adhesion performance of the substrate. This is validated by the drop in adhesion force between the ECCS / epoxy and ECCS / BPANI system. In all cases it seems that increasing the level of chromium oxide increases the failure force of the coating / substrate system. The difference in performance between the epoxy and BPANI systems are lower at lower chromium oxide levels in the DI and NaCl simulant solutions which then increases as chromium oxide levels increase.
- BPANI lacquers perform poorer than epoxy based lacquers in all conditions, and it is hypothesised that this is due to their inherent porosity providing a transport route for solution to the substrates surface. Water uptake in BPANI lacquered substrates is exacerbated by the retort process and the presence of increasing concentrations of salt. This is as a result of physical diffusion of water molecules as opposed to a chemical reaction of the lacquer as shown by FTIR. The loss of adhesion of the BPANI lacquers due to the retort process is attributed to surface substrate corrosion. It was postulated NaCl does not interact chemically with the lacquers and hence this has been subsequently proven. The impact of NaCl in solution is profound for both the TCCT and ECCS materials. The addition of citric acid to the NaCl solution limited the

corrosion of the surface of the substrate and therefore it is proposed that this chemistry has served to passivate free surface iron.

- Chemically comparing the surfaces of TCCT and ECCS, it is plausible that the primary mechanism which lowers the adhesion performance of TCCT substrates is the presence of small (1-3 micron) defects in the substrate which provides access to the iron in the underlying steel substrate. Whether these defects are a result of the fundamental Cr (III) deposition process chemistry or whether they are associated with pilot manufacture which, by its nature is less consistent compared to a commercial production line, is yet unknown.
- A CuSO_4 dip test has illustrated the presence of iron on the surface of all TCCT samples and ECCS. This has subsequently been characterised and quantified through use of XRF and optical microscopy. Area averaging has proven that in the case of TCCT, chromium oxide coating weight is directly proportional to the quantity of copper and therefore iron on the substrates surface. In this experiment, ECCS was shown to have the most homogenous chromium oxide layer with only 1.8% of its surface measured as being copper. This is compared to TCCT with the highest chromium oxide coating weight of 23 mg/m^2 having a copper area of 5.3%.
- Using the SVET, it has been shown that TCCT samples with low chromium oxide coating weights exhibit a scarring mechanism of corrosion which is characterised by significant quantities of insulating corrosion product (Fe_2O_3). This makes the process self-limiting and therefore not destructive to the metallic coating. TCCT samples with medium and high chromium oxide coating weights exhibit an unstable pitting mechanism of corrosion whereby the metallic coating is destroyed through the continual diffusion of oxygen to surface defects as evidenced by their positive gradients within the anodic activity data. ECCS is shown to exhibit a limited corrosion effect characterised by small corrosion potential which is well balanced.
- Total mass loss of these samples has been estimated using SVET, all be it semi-quantitatively. The most mass is lost on samples with the lowest chromium oxide coating weights, as expected.

Chapter 6 - Laboratory
Electroplating of TCCT Substrate
Materials: Chromium Metal and
Chromium Oxide Deposition

6 Laboratory Electroplating of TCCT Substrate Materials: Chromium Metal and Chromium Oxide Deposition

Having physical and chemically characterised TCCT substrates manufactured in an industrial pilot line setting, it is relevant to examine their production parameters and to attempt to replicate their production in the interest of process optimisation. Systematically being able to change the chromium metal and chromium oxide coatings will aid in identifying the impact of various electroplating parameters and make it easier to study the process discreetly.

6.1 Introduction

The use of Cr (III) in the electroplating of packaging steel is a relatively recent development. However, Cr (III) has been used for a long time in the decorative coating industry where hard chromium coatings are electrodeposited from aqueous solution.

Trivalent Chromium Coated Steel (TCCT) is manufactured by electroplating chromium metal and chromium oxide onto the surface of blackplate substrate. Historically this process involved only one step whereby a mixed metal, carbide, oxide (M-C-O) layer was deposited. However, due to performance and aesthetic quality issues associated with the resultant coating, this method was phased out and hence replaced. Recently this process has developed into a dual electrolyte process whereby an initial layer of chromium, oxygen and carbon (Cr-O-C) is deposited, onto which a secondary oxygen rich layer comprising of chromium oxide (Cr-O) is placed. A method has previously been established for the laboratory scale production of TCCT by TATA Steel Europe, albeit not published.

Previous work in Chapters 4 and 5 of this thesis have examined the characteristics and performance of iterative substrates manufactured utilising this ‘two step’ process. However, the chemistries of the electrolytes as well as the method for successfully depositing this dual layer have been somewhat finalised. Therefore, becoming self-sufficient in the manufacture of TCCT on a laboratory scale meant that that samples could be made when required (without having to wait for a full-scale line trial). In addition, it presented the opportunity to study the electroplating process parametrically.

The reduction of Cr (III) to Cr (0), or metallic chromium, is difficult when water is used as a complexing agent forming the very stable $[\text{Cr}(\text{H}_2\text{O})_6]^{3+}$ complex.

Inherently the reduction mechanisms of Cr (III) will vary compared to those of Cr (VI) and have been investigated to some extent by Song et.al (26). Indeed the reduction mechanism of $[\text{Cr}(\text{H}_2\text{O})_6]^{3+}$ has also been investigated by *Del Pinanta et.al* who have demonstrated that the inactivity of this complex is due to cathodic electrons not being able to penetrate the H_2O molecules inner d-orbital as there are no vacancies. Thus, discharge can only take place at a potential more negative than required for the reduction of water. This results in hydrogen evolution and therefore an increase in pH.

In addition, an increase in pH also promotes oxidation, which is a reaction that leads to a thin film of polyoxides being formed on the substrates surface, in this case chromium hydroxide precipitation ($\text{Cr}(\text{OH})_3$). A complexing agent must be used in order to deposit metallic chromium on the substrates surface.

Complexing agents (L^-) for Cr (III) solutions have previously been investigated (154). These additions to electroplating chemistries destabilise the $[\text{Cr}(\text{H}_2\text{O})_6]^{3+}$ complex leading to the formation of a $[\text{Cr}(\text{H}_2\text{O})(\text{L})_x]^{(3-x)+}$ mixed complex.

This section of work will focus on replicating the TCCT manufacturing process on a laboratory scale and investigate the key mechanisms of both chromium metal and oxide deposition. This is done by investigating the effect of the applied current density, pulsing, bath pH and bath temperature and evaluating the chromium layers deposited for chemical composition and homogeneity.

6.2 Strategy Employed

Before the electroplating processes can be studied parametrically (in the interest of process optimisation) the initial set-up and procedure must be validated.

6.3 Electrolyte Chemistry

TCCT production involves a two-step electroplating process and therefore two different electrolytes. The first deposits mainly chromium metal (Cr-O-C) while the second deposits chromium oxide (Cr-O).

Over a period of years, the exact chemistry of these electrolytes has been adapted to ensure the final substrate manufactured performs adequately in industrial settings. The chemistries of the two electrolytes are correct as of August 2021 and have not changed since. Table 6.1 shows the electrolyte compositions used as well as the solution pH and temperature at each stage.

Table 6.1 - Electrolyte chemistries used to electroplate the chromium metal and oxide TCCT layers.

TCCT	Chemistry	pH	Temperature (°C)
STEP 1 Cr-Metal	(CrOHSO ₄) ₂ ×Na ₂ SO ₄ Na ₂ SO ₄ HCOONa	2.3	37
STEP 2 Cr-Oxide	(CrOHSO ₄) ₂ ×Na ₂ SO ₄ Na ₂ SO ₄	3.2	55

The chromium in solution comes from basic chromium (III) sulphate hydrate with the sodium sulphate being added separately. Sodium formate acts to destabilise the Cr(H₂O)₆³⁺ complex to allow for the deposition of chromium metal onto the cathodic substrate, and so is only required in electrolyte 1. The respective pH values of both electrolytes are managed using sulphuric acid and sodium hydroxide as necessary. The exact method for making the electrolytes was defined from colleagues in TATA Steel IJmuiden.

6.3.1 Electroplating Process and Equipment Set Up

In all of the following experiments, the TCCT coatings (whether it be chromium metal or chromium oxide) were independently electroplated onto blackplate substrate. Sample preparation involved cutting the blackplate samples to size, scrubbing the surface with an acetone soaked cloth (removing the majority of any DOS oil that may be present or fingerprints), alkaline cleaning with at a current density of 1.5 A/dm² and pickling in sulphuric acid to activate the surface, Table 6.2. The equipment used to clean substrates and to electroplate is shown in Figure 6.1 and Figure 6.2.

Table 6.2 - Pre-treatment steps for substrate material prior to electroplating processes.

Pre-Treatment	Cleaning	Rinsing	Activation	Rinsing
Solution Composition	50 ml l ⁻¹ Unisurfa KB35	DI Water	50 g l ⁻¹ H ₂ SO ₄	DI Water
Temperature (°C)	60	25	25	25
Current Density (A/dm²)	+1.5 (anodic)	n/a	0 (dip)	n/a
Time (s)	60	10	10	10

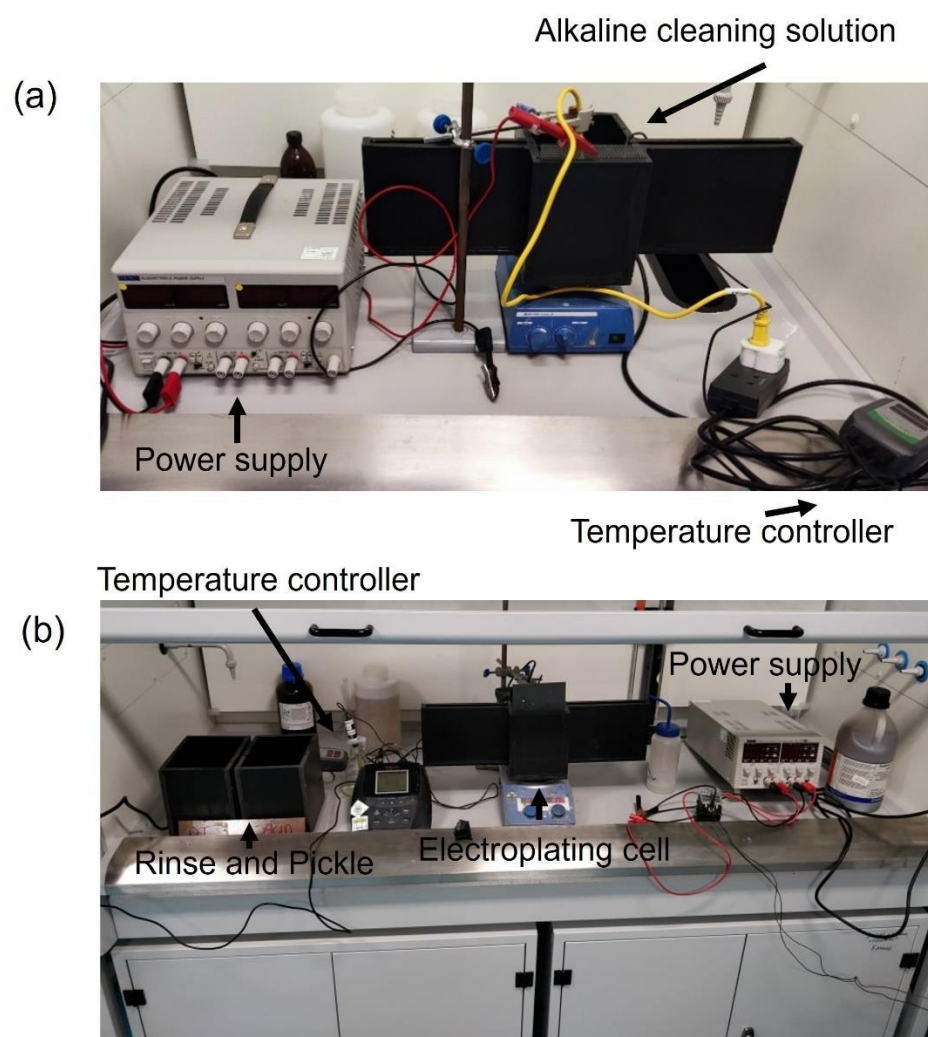


Figure 6.1 – Images of the laboratory scale electroplating set up used in Swansea University detailing (a) the alkaline cleaning station and (b) the rinse, pickle and electroplating cell.

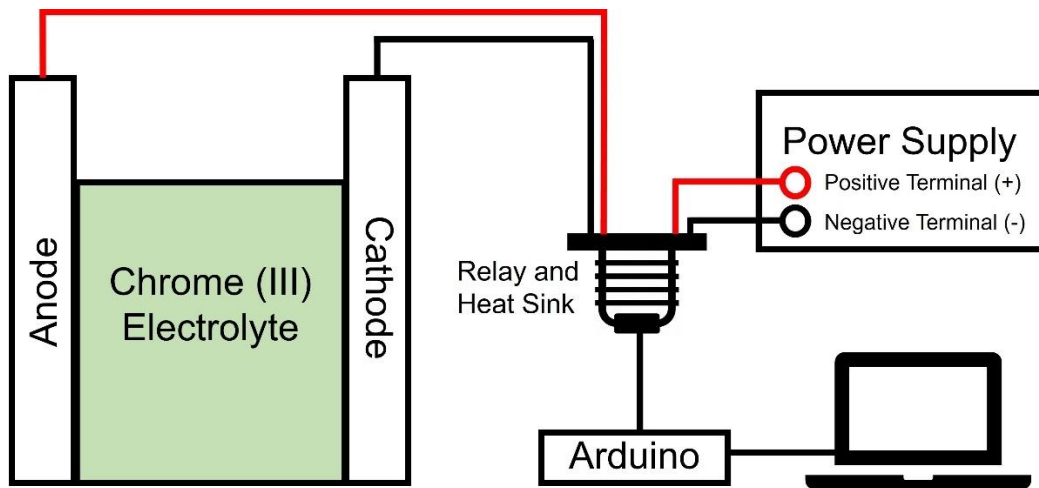
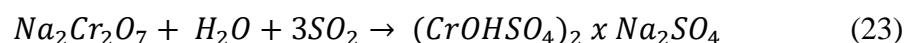


Figure 6.2 - Simplified schematic detailing the TCCT electroplating set up highlighting the electrical connections and equipment used.

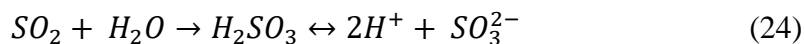
A titanium plate electrode with iridium / tantalum mixed metal oxide (MMO) coating acted as the anode and was sourced from MAGNETO special anodes (32). This was placed in a custom-made electroplating bath constructed from a chemical resistant polymer. The anode was placed parallel to the cathode with a gap of 4 cm. This distance was fixed due to the bath geometry. The electrolytes were heated with an external element controlled by an Inkbird digital temperature controller accurate to ± 1 °C. The current was controlled using an AIM-TTI CPX400DP DC power supply connected to an Arduino relay system with which time pulses of between 0.8 s and 5 s could easily be controlled and modified. The currents required to deposit both chromium metal and chromium oxide were calculated by multiplying the area of submerged cathode by the current density required. A magnetic flea was used to agitate the solutions throughout the whole process.

6.3.2 Sulphite Removal Process

In industrial settings, the basic chromium salt used in the TCCT electroplating process is produced by the reduction of Cr (VI) in the form of sodium dichromate to Cr (III) with SO_2 (155). Ensuring the chromium is fully reduced to the 3+ oxidation state requires an excess of sulphur dioxide, *Equation 23*.



Chemical suppliers often use a second process to remove the residual sulphur dioxide. However, if present, excess SO_2 will result in the formation of sulphurous acid (H_2SO_3), which may in turn form sulphite anions, *Equation 24*.



The presence of sulphite anions has been shown to inhibit the efficiency of the electroplating process and therefore prove detrimental to the industrial procedure as a whole (31). By limiting or removing any sulphite anions present, the laboratory scale deposition of the TCCT coatings may well be made easier and more practical.

Using cyclic voltammetry, the presence of sulphite anions can be inferred if it is assumed that if present, they strongly adsorb onto the platinum electrode. If this were to be true, then the oxidation of formic acid to CO_2 would be inhibited and the $\text{CO}_{2(\text{g})}$ ‘explosive’ peak at approximately 0.1-0.2 V vs SCE (in the negatively directed scan) would be suppressed. And indeed, this is what would be expected if a fresh electrolyte were to be tested. In contrast, however, if an electrolyte were to be free of sulphite anions, then the formic acid in solution would be free to oxidise therefore causing a characteristic peak at 0.1-0.2 V vs SCE. Experimentally this process has already been validated by de Vooy et. Al. (31) and so it was replicated in order to check the purity of the chemicals bought for the university laboratories. It is noted from this work that a feasible way of removing any sulphite ions from a contaminated electrolyte is by applying a prolonged reductive current consequently forming sulphide ions.

6.3.3 Cyclic Voltammetry

Cyclic voltammetry was conducted on the first, chromium metal depositing electrolyte prior to any experimental procedure to ensure that there was no contamination from sulphite ions which often pollute industrially manufactured Cr (III) sulphate hydrate. The consequence of this being that, as formate is used as a complexing agent, oxidation may be suppressed inhibiting deposition, Figure 6.3.

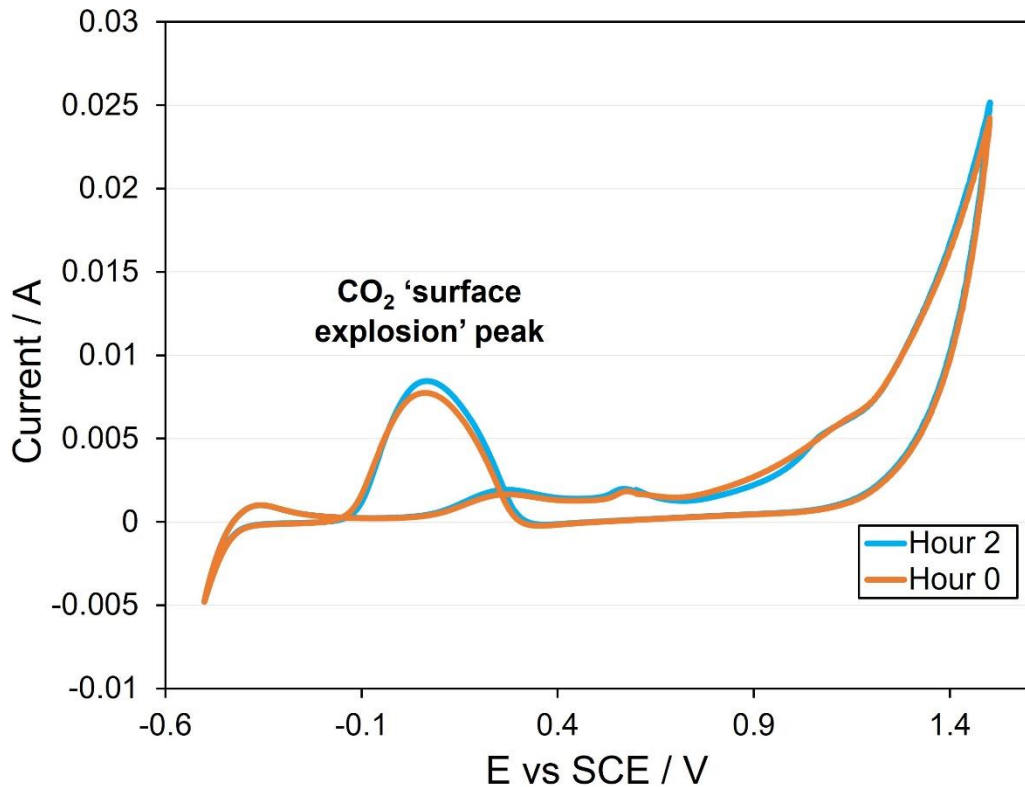


Figure 6.3 - Cyclic voltammograms of fresh and pre-plated electrolyte used for chromium metal deposition illustrating the characteristic CO_2 surface explosion peak of formic acid oxidation indicating that the electrolyte is sufficiently uncontaminated from sulphite ions.

Hydrogen and oxygen evolution can be observed to the far left and right peaks on the cyclic voltammogram respectively. The characteristic CO_2 'surface explosion' peak is observed at approximately -0.2 V vs SCE for both a fresh electrolyte and an electrolyte which has been subjected to a reductive current for 2 hours indicating the relative purity of the Cr (III) sulphate hydrate source.

6.4 Validation of the Electroplating Process

The first step taken towards validating the TCCT electroplating process was attempting to electroplate each of the two electrolytes separately onto blackplate at varying current densities, electrolysis time, temperatures and pH values in order to ascertain the optimal parameters for sample production and to confirm the efficacy of the process. These samples were measured with an XRF (measuring total chromium) in parts per million and converted to mg/m^2 . In doing this the so-called 'regimes' of the electroplating process, as defined by Wijenberg et. Al (28). At low current densities, no chromium deposit is formed on the electrode and graphically, this is visualised as regime 1, Figure 6.5 (b). As current density then increases, a threshold is

surpassed and chromium is successfully deposited on the electrode within regime 2 as part of the Cr (III) deposit is reduced to chromium metal and formate is broken down leading to the formation of carbide. Regime (III) is where chromium oxide is deposited.

Once cleaned and electroplated, the samples were dried and four XRF measurements were taken of the surface. Chromium PPM values were noted with standard errors being calculated. The applied current density was limited to 40 A/dm².

6.4.1 Calibration of the XRF

The total quantity of chromium deposited was measured using an Oxford Instruments X-7500 XRF. This instrument elementally quantifies chemical constituents ranging from Mg – U in atomic mass, yielding a parts per million (ppm) measurement. Chromium is measured irrespective of oxidation state with measurements being converted to mg/m² after calibration against XPS depth profiles. As the PPM / mg/m² relationship was initially unknown, samples with a known Cr-Total mg/m² were measured and plotted against each other to ascertain a conversion factor, Figure 6.4. The chromium total measurements were undertaken by TATA Steel IJmuiden via XPS depth profiling and published via internal literature (99). Readings were corrected for the contribution of the base substrate to the chromium signal.

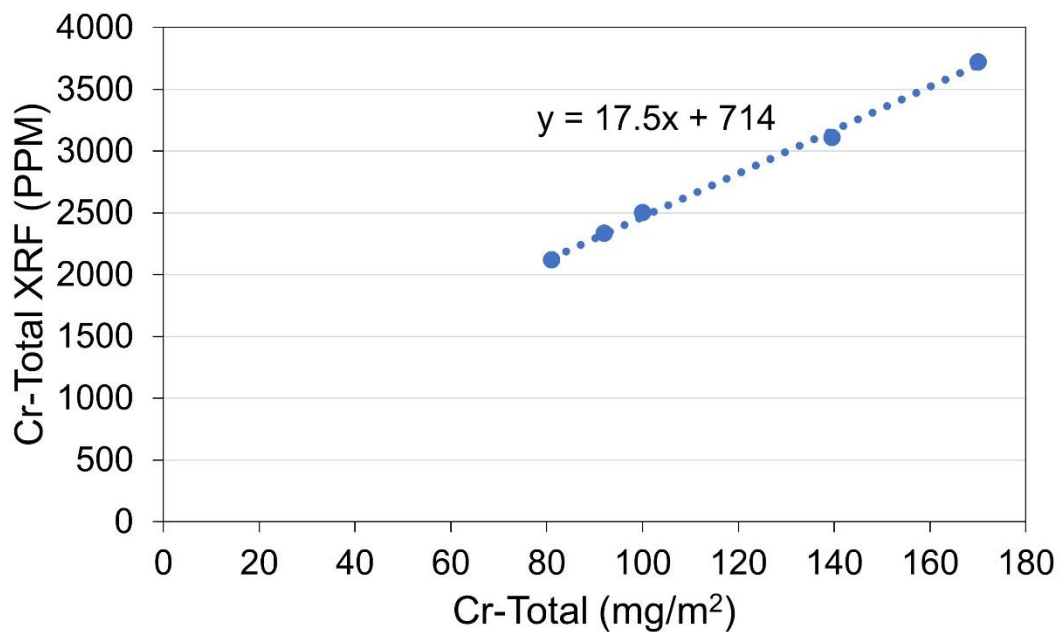


Figure 6.4 - XRF calibration: Conversion from PPM to mg/m².

It is clear that there is a linear relationship between chromium total and PPM as measured by XRF, Figure 6.4. This provides a conversion factor of 0.038 which is used for the forthcoming data sets. One caveat must be made with regard to characterising the chromium oxide layer. Due to the fact that XRF measures chromium irrespective of oxidation state, it does not account for the difference in molar weight of Cr and Cr₂O₃. Therefore, a conversion factor of 1.46 must be employed when converting this PPM measurement to a mg/m² chromium oxide measurement as per *Equation 25 (29)*

$$\frac{(2 * 52) + (3 * 16)}{(2 * 53)} = 1.46 \quad (25)$$

In a one-bath process where the chromium metal and chromium oxides are deposited at different current densities, but without removing from the bath, the chromium oxide quantity is calculated differently due to the XRF being unable to differentiate between the metallic and oxidic contributions. In this case samples are submerged in 7.5 M sodium hydroxide at 90 °C for 10 minutes as defined in EN 10202:2001, E 2.5.2 (10). Chromium that is present as chromium oxide or hydroxide dissolves as a result, leaving behind chromium carbide and chromium metal. The total amount of chromium is calculated using XRF after another thorough rinse. Chromium oxide content is the difference between the two readings.

6.4.2 Chromium Metal Depositing Electrolyte

The effect of electroplating current density, electrolysis time, temperature, pH, and current pulsing have been investigated for a chromium metal depositing electrolyte.

6.4.2.1 The Effect of Current Density and Electrolysis Time on Chromium Metal Deposit

During electroplating, metal ions in solution accept electrons to become a solid deposit. Therefore, the amount of solid that can be electroplated is limited by the number of electrons available and hence the applied current density. It has been shown in previous literature for the one step TCCT process that when electroplating using a similar chemistry, three clear regimes of deposition are realised, Figure 6.5 (b). Regime two defines where chromium metal is deposited once a threshold current

density is reached. To investigate the effect of current density on chromium metal deposition for this process, samples were electroplated for 0.8 s in solution at intervals of 5 A/dm² starting at 25 A/dm². This time pulse was advised from industrial partners; however, the current interval was decided as a logical step due to a limitation of 40 A/dm² capacity.

The electrolysis time was varied to understand its impact on the process, Figure 6.5.

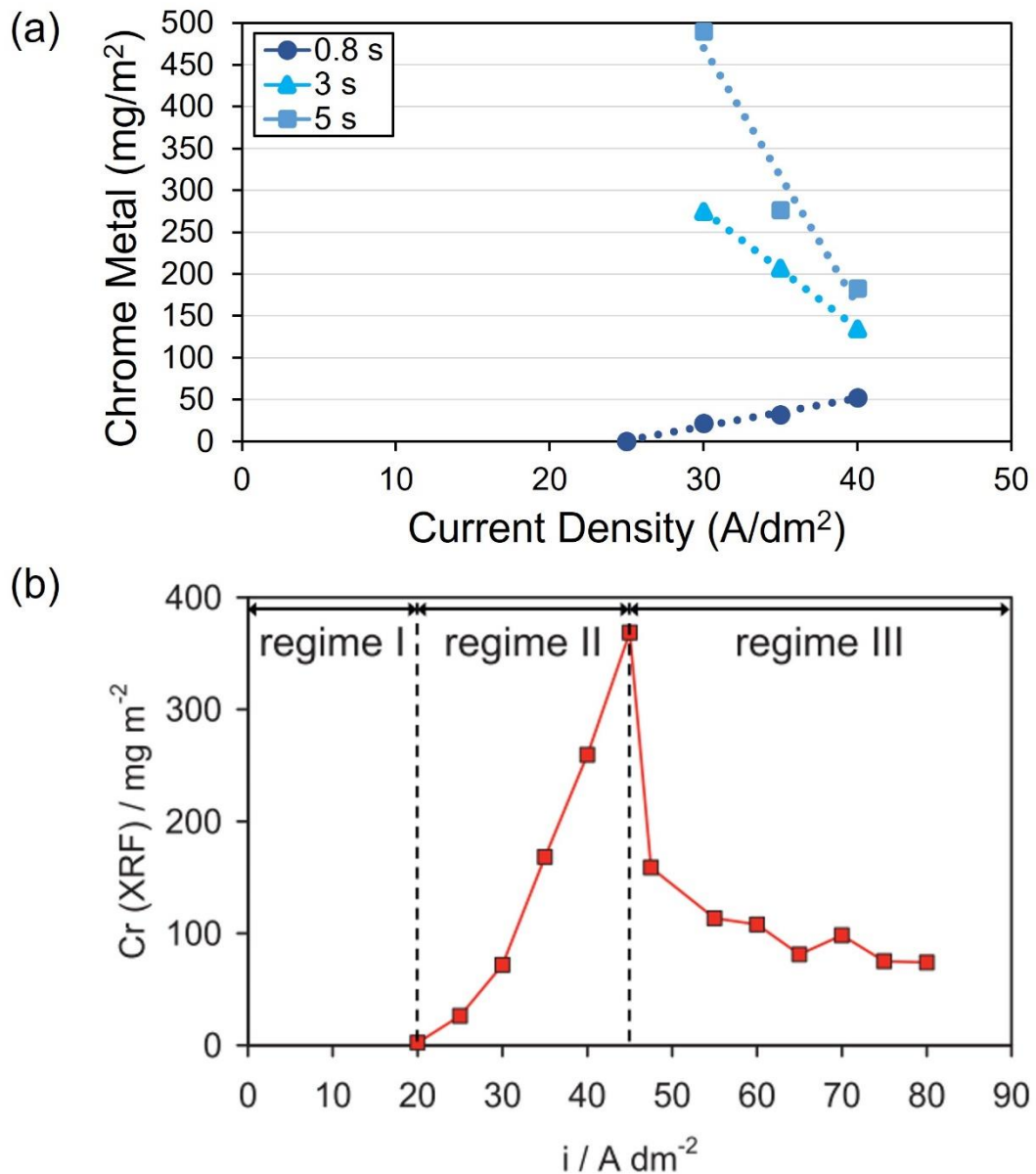


Figure 6.5 - (a) Relationship between applied current density, electrolysis time and quantity of chromium metal deposit and (b) regimes of TCCT layer deposition as proposed by TATA Steel Europe.

Irrespective of electrolysis time, no chromium metal was deposited on blackplate until a threshold current density of 30 A/dm^2 was applied. For the samples subjected to an electrolysis time of 0.8 s, the amount of chromium metal deposited increased with increasing current density. An increase in current density of 10 A/dm^2 caused an increase in chromium metal deposit of approximately 30 mg/m^2 . Although increasing the electrolysis time to 3 seconds caused an increase in Cr metal deposit in comparison to an electrolysis time of 0.8 s, it also caused the amount of Cr metal deposited to decrease with increasing current density. The same trend was seen when the electrolysis time was increased again to 5 s. At every interval of current density, the quantity of chromium metal deposit increases. It is proposed that the limiting factor which restricts the deposition at higher current densities and prolonged electrolysis times is cathodic hydrogen evolution. This has been witnessed in the laboratory, Figure 6.6.

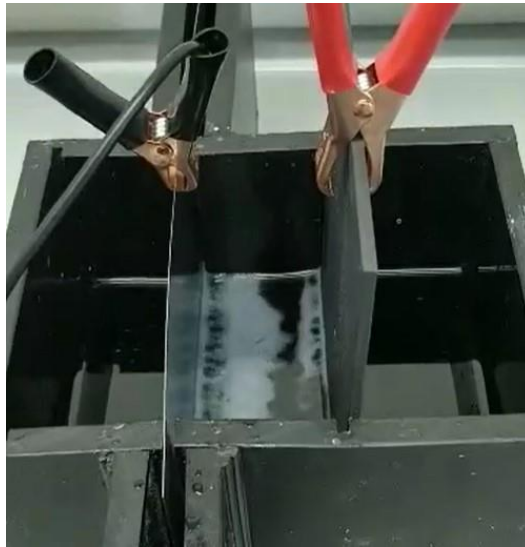


Figure 6.6 - Image showing cathodic hydrogen evolution in the TCCT manufacturing process.

This is compared to published literature by the IJmuiden research group in TATA Steel who proposed three regions of chromium deposition from a single electrolyte, with regime 2 depositing chromium metal, Figure 6.5 (b). It is noted that the linear trend for the 0.8 s deposition time in Figure 6.5 (a) is very similar to that on the right hand graph in regime 2. However, in this case the quantities of chromium do not compare. This may be for a number of reasons such as a difference in equipment used but also the fact that chemistries are not consistent.

In order to manufacture samples that have a chromium metal coating weight of 60-130 mg/m² (resembling TCCT samples manufactured industrially, Table 3.1) it is clear that further investigation is necessary as this deposition is not achieved in Figure 6.5 (a). A current density of 30 A/dm² was selected as this value represented the lowest current density at which deposition was a certainty, thus mitigating as much as possible the evolution of hydrogen. Time pulses of 0.8, 1, 1.2, 1.6, 3 and 5 s were used, Figure 6.7. Intervals of 0.8, 3 and 5 s were initially chosen as a logical stepwise increases in time pulse in order to evaluate the effect of prolonged electrolysis times on the deposit. However, this was later revised, and smaller increments of 0.2 s were investigated at smaller pulse times in order to attempt to achieve a deposit of 100 mg/m² of chromium metal which is industrially accurate.

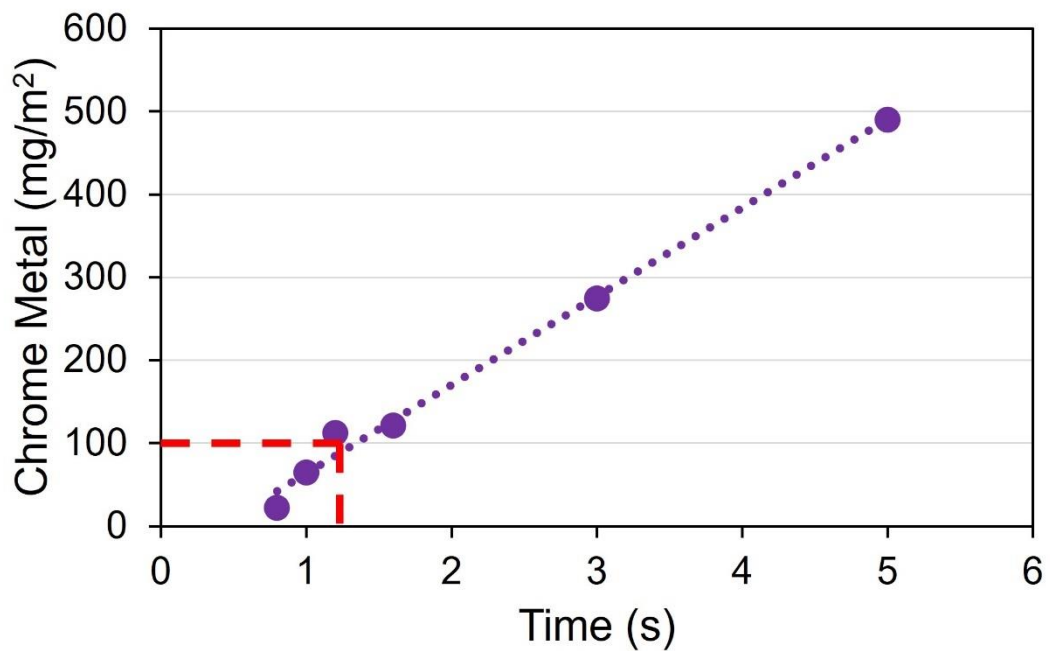


Figure 6.7 - The effect of the length of current pulse on the quantity of chromium metal deposit at a 30 A/dm² current density.

There is a clear linear trend in the relationship between increasing time pulse of current and quantity of chromium metal deposited. It is noted that to achieve a deposition of 100 mg/m², a time pulse of 1.2 s at a current density of 30 A/dm² is required.

6.4.2.2 The Effect of Pulsing Current on Chromium Metal Deposit

Packaging steel substrates are often subjected to multiple current pulses when manufactured industrially due to passing multiple sets of anodes. This process, otherwise known as continuous electroplating, provides a means to accurately control the coating weight of electrodeposited materials as well as ensuring uniformity of the coating (156) A total of three 0.8 s pulses were used at a range of current densities with pulses being applied within 20 s of each other. This 20 s gap represents the time it takes to reset the laboratory equipment. The current densities used for the chromium metal electrolyte were between 30 and 40 A/dm² at 5A intervals. These values were chosen as they represented certainties of deposition as per Figure 6.5 (a) as well as industrially attainable currents. It is shown that when pulsing this electrolyte, the quantities of metal increases with both pulse and current density, Figure 6.8.

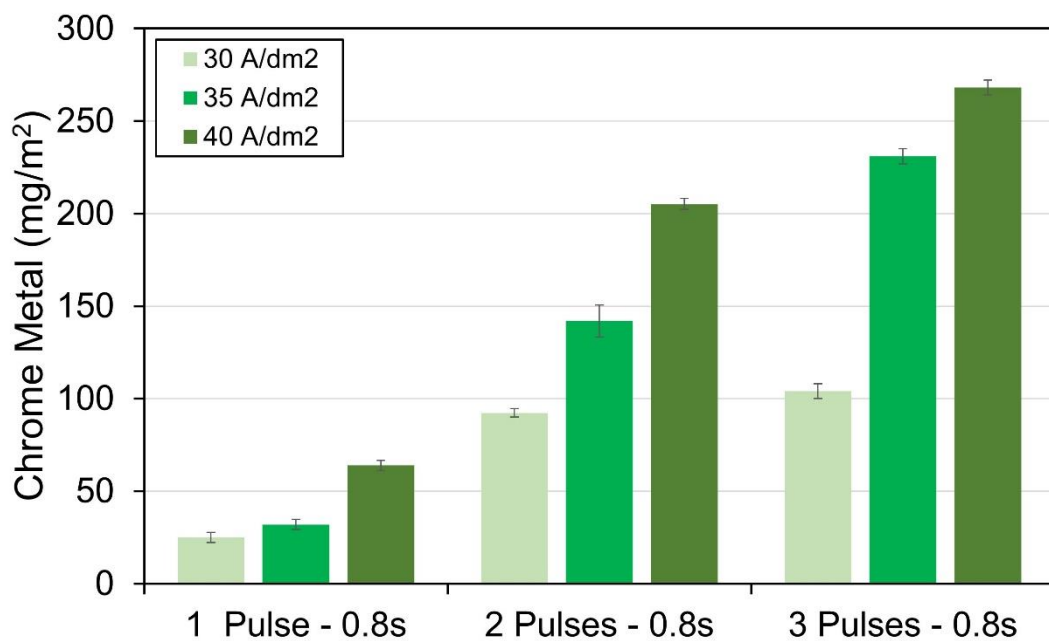


Figure 6.8 - The effect on the quantity of chromium metal deposition when pulsing the current for 0.8s.

The increase in metallic deposition is most dramatic at higher current densities, however, the increase in deposition quantity in all cases is not equal for each sequential pulse. This leads to the hypothesis that the chromium metal is more readily deposited on the iron-based substrate rather than a pre-existing chromium coating. Theoretically this makes sense as chromium has already been deposited, the chromium surface is already in the metallic state, which means that it has a lower electrochemical

potential (-0.41 V vs SHE) than the iron-based substrate (+0.77 V vs SHE); therefore, the deposit should preferentially occur on the iron-based substrate rather than the previously deposited chromium. Evidently, the first pulse at all current densities seems insufficient to cover all of the iron based substrates, as evidenced by more chromium being deposited after each pulse. This effect is exacerbated at higher current densities.

6.4.2.3 The Effect of Electrolyte Temperature on Chromium Metal Deposit

During electroplating processes, the temperature of the electrolyte can make a big difference in the quantity of deposition. Increasing the temperature can affect the kinetics of chemical reactions at both the anodic and cathodic interfaces. This may increase the quantities of deposition; however, it may also affect the stability of the Cr (III) ions causing them to precipitate into solution leading to a decrease in solution concentration and therefore lower quantities of deposit (157). Typical temperatures for electroplating Cr (III) thin metallic coatings are between 20 – 40 °C.

In the case of this chromium metal depositing electrolyte, the temperature was changed from 37 °C to 40°C, 45°C and 50°C with current densities being varied between 10 and 40 A/dm² at 10 A intervals; pulse time was kept consistent at 0.8 s, Figure 6.9.

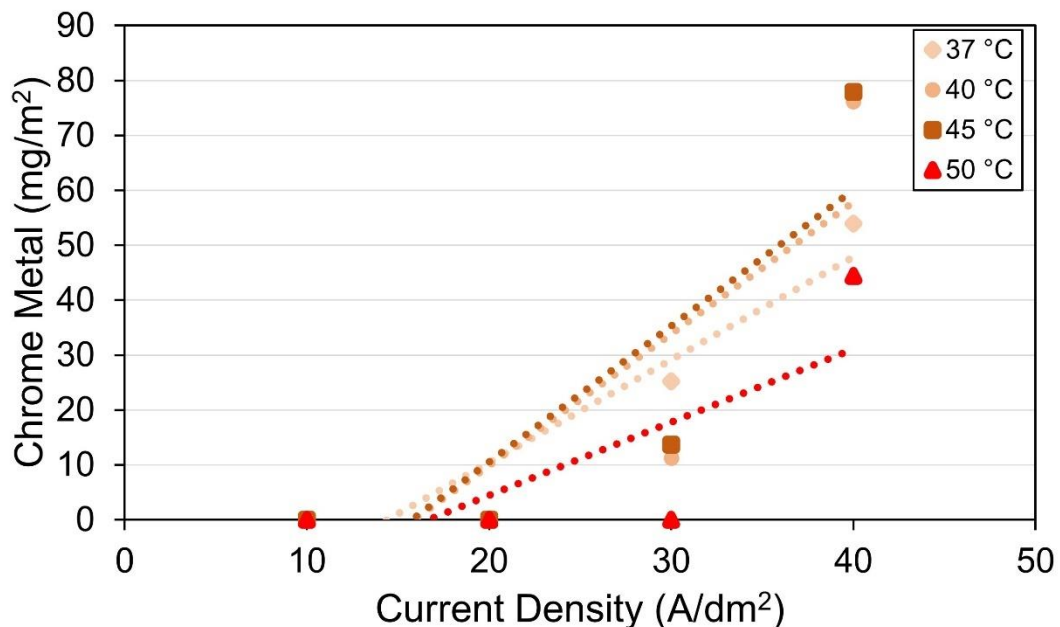


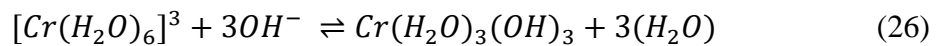
Figure 6.9 - The effect of electrolyte temperature changes on the quantity of chromium metal deposition at various current densities.

At all temperatures there is a critical current density which needs to be overcome before deposition is realised: 30 A/dm². The quantity of chromium metal deposition increases with temperature up until 50 °C where the total deposition, even at high current densities, is significantly reduced. This trend can be linked to a decrease in the cathodic film's viscosity, which encourages a more even distribution and a greater speed of dissolution (158).

6.4.2.4 The Effect of Electrolyte pH on Chromium Metal Deposit

The effect of pH on the deposition of Cr (III) from solution can be significant. In general, the pH of the electrolyte affects the solubility and stability of the Cr (III) ions in solution (157)

At higher pH values (alkaline conditions), hydroxide ions (OH⁻) can interact with Cr (III) ions, leading to the formation of hydroxide complexes, such as Cr (OH)₃, *Equation 26*. Any hydroxide ions in solution are also more likely to be oxidized, which can lead to the formation of a passivating layer on the surface of the substrate (made up of H₂O and O₂) impeding the current flow. This can also interfere with the electroplating reaction and slow down the rate of the deposit.



At a low pH the Cr (III) ions will be more stable due to increased solubility and enhanced charge density making deposition more likely, however, any hydrogen ions in solution are more likely to be reduced. The formation of hydrogen bubbles on the surface of the substrate may potentially interfere with the electroplating reaction, slowing down the rate of the deposit.

The pH of the chromium metal depositing electrolyte was increased to 2.8 from 2.3 and investigated for its influence on quantity of deposition at the same temperature intervals shown in section 6.4.2.3, Figure 6.10.

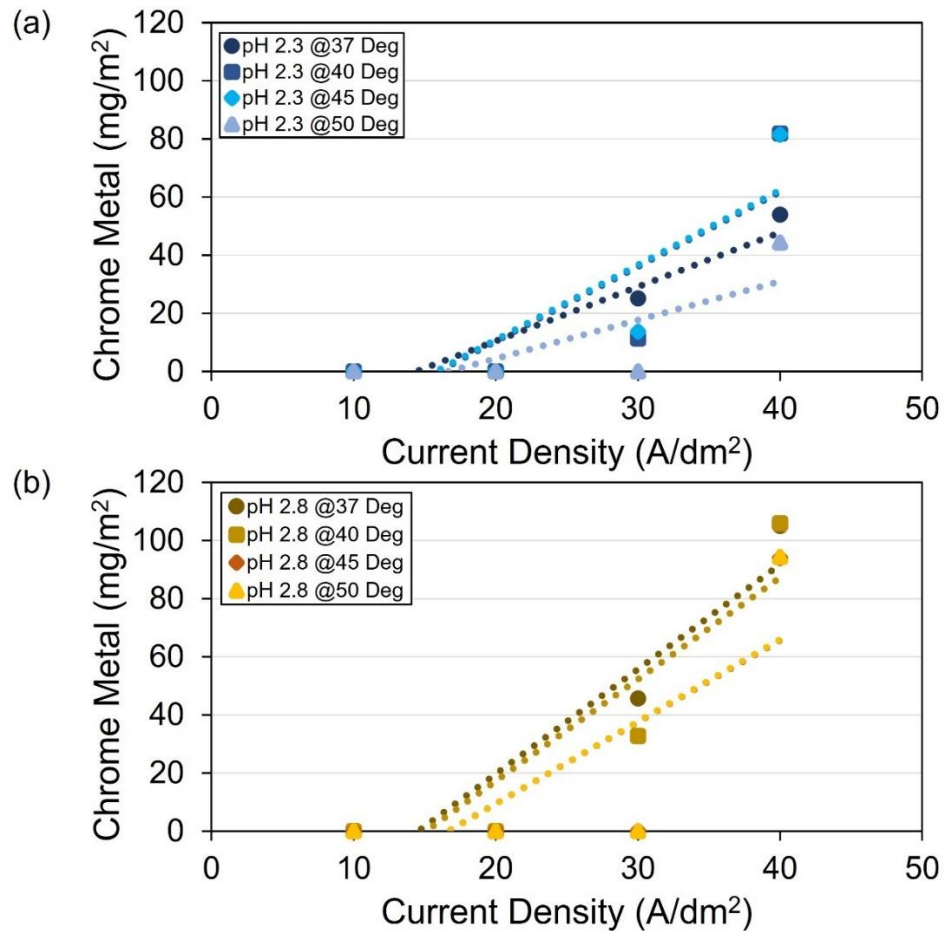


Figure 6.10 - The effect of electrolyte (a) at pH 2.3 and (b) at pH 2.8 on quantity of chromium metal deposition at varying electrolyte temperatures.

It can be seen that an increase in pH from 2.3 to 2.8 paired with an increase in temperature, in all conditions, increased the deposit of chromium metal. It is clear that the temperature increase along with pH increase is acting to increase the rate of electrodeposition up until a temperature of 50 °C where the deposit is reduced. It is thought that the increase in pH leads to increased deposition due to a decrease in the rate of reduction of hydrogen ions in solution which is exacerbated by the deprotonation of the water ligands within the $[\text{Cr}(\text{H}_2\text{O})_6]^{3+}$ complex along with the splitting of water in solution.

6.4.3 Chromium Oxide Depositing Electrolyte

Just as the first electrolyte was investigated, the second chromium oxide depositing electrolyte must also be in order to examine the effects of various electroplating parameters. The same experiments as per section 6.4.2 have been repeated and results plotted in the interest of continuity. Chromium oxide was electroplated onto blackplate substrate.

6.4.3.1 The Effect of Current Density and Electrolysis Time on Chromium Oxide Deposit

The effect of increasing current density on the quantity of chromium metal deposit using one electrolyte is profound. The following data examines whether this relationship holds true for step two of the dual electrolyte process.

A fresh, formate-free, electrolyte was prepared as per the method outlined in section 6.3 and heated to 55°C. Sample cleaning was kept consistent, as per section 6.3.1, and time pulses of 0.8, 3 and 5 s were used with current densities ranging between 10 A/dm² and 40 A/dm² at intervals of 2.5 A/dm². The resulting data showed an inversely proportional relationship between the total chromium measured and the current density used, Figure 6.11.

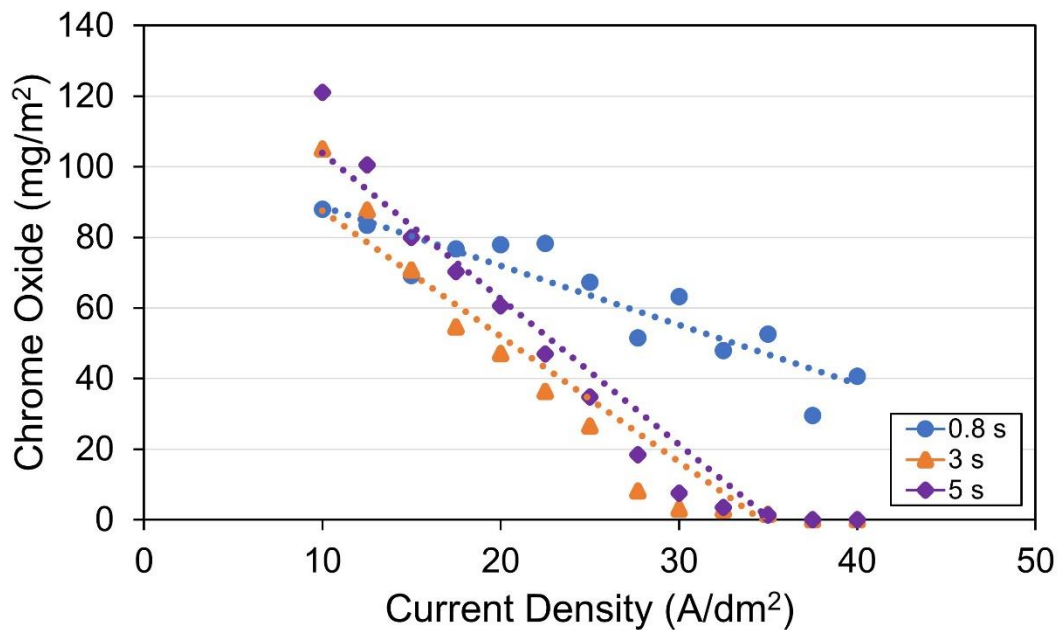


Figure 6.11 - Relationship between applied current density, electrolysis time and quantity of chromium oxide deposit.

An increase in applied current density caused a decrease in chromium oxide deposition irrespective of electrolysis time. However, a longer electrolysis time caused this decrease in chromium oxide deposition to be greater as the current density was increased. At an electrolysis time of 0.8 s and an applied current density of 10 A/dm² approximately 90 mg/m² was deposited. This decreased to approximately 40 mg/m² at 40 A/dm². At an electrolysis time of 5 s and a current density of 10 A/dm² approximately 120 mg/m² was deposited. At 40 A/dm², however, no chromium oxide was deposited. Furthermore, at low current densities a longer electroplating time increased chromium oxide deposition. However, this changes at higher current densities where a longer electrolysis time caused a decrease in chromium oxide deposition. When a current density of 30 A/dm² and above was applied, a significant amount of chromium oxide was only deposited when the electroplating time was 0.8 s. At 3 s and 5 s little to no chromium oxide was deposited at these higher current densities.

The relationship witnessed in Figure 6.11 is in line with the existing understanding that at higher current densities, hydrogen evolution increases significantly therefore hindering the deposition of the chromium coating.

In order to recreate the chromium oxide coating weights used industrially on packaging steel substrates (2-23 mg/m²), smaller electrolysis time increments were investigated. Chromium oxide deposition was evaluated at 0.1 s intervals from 0.3 s to 0.8 s at a current density of 30 A/dm² as this value represented surety of deposition and also provides continuity with the chromium metal electrolyte methodology.

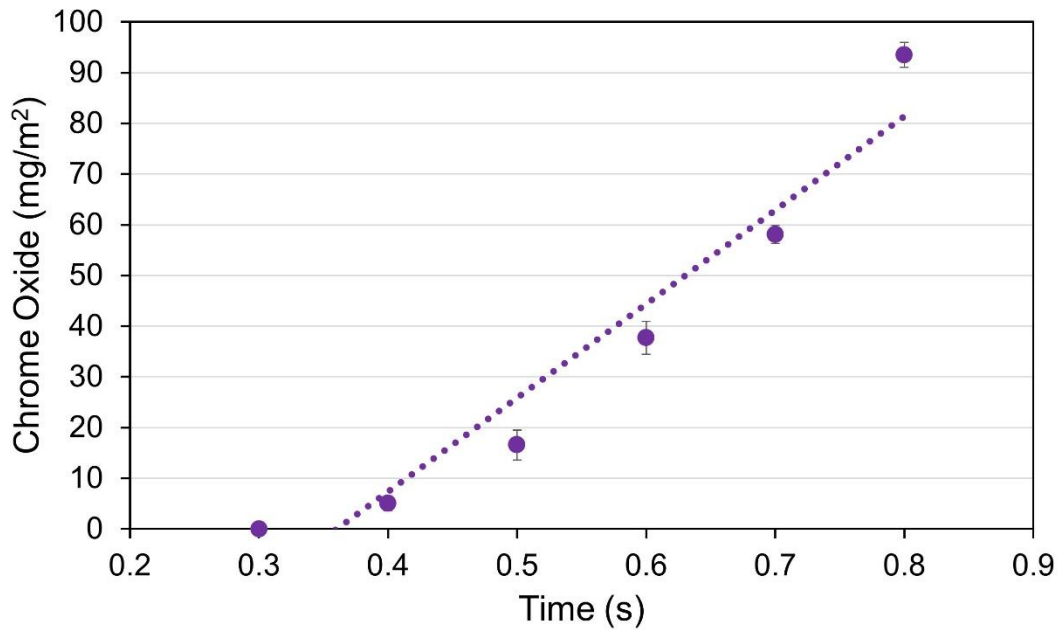


Figure 6.12 - The effect of the length of current pulse on the quantity of chromium metal deposit at a 30 A/dm² current density.

It was found that there is a linear trend between time pulse quantity of chromium oxide deposition. Electrolysis times of between 0.4 s and 0.5 s are required for the chromium oxide deposition to be between 5 and 20 mg/m².

6.4.3.2 The Effect of Pulsing Current on the Quantity of the Chromium Oxide Deposit

It has been established that hydrogen evolution is significant within this electrodeposition process. If this is the rate limiting step then theoretically if the current was pulsed in 0.8 s bursts, with enough time being given to allow refreshment of the electrolyte at the cathodes surface, then an increase in deposit over time may be observed. In this case ‘refreshment’ of the surface would mean the dissipation of the charge induced boundary layer.

To investigate this 1, 2 and 3 pulses were used to test this theory at a 0.8 s pulse time, Figure 6.13. A time of 20 seconds between each pulses was allowed for the electrolyte at the surface of the cathode to refresh; once again this time being dictated by the time taken to reset the laboratory equipment. The current densities used for this were between 10 and 40 A/dm² at 5 A intervals.

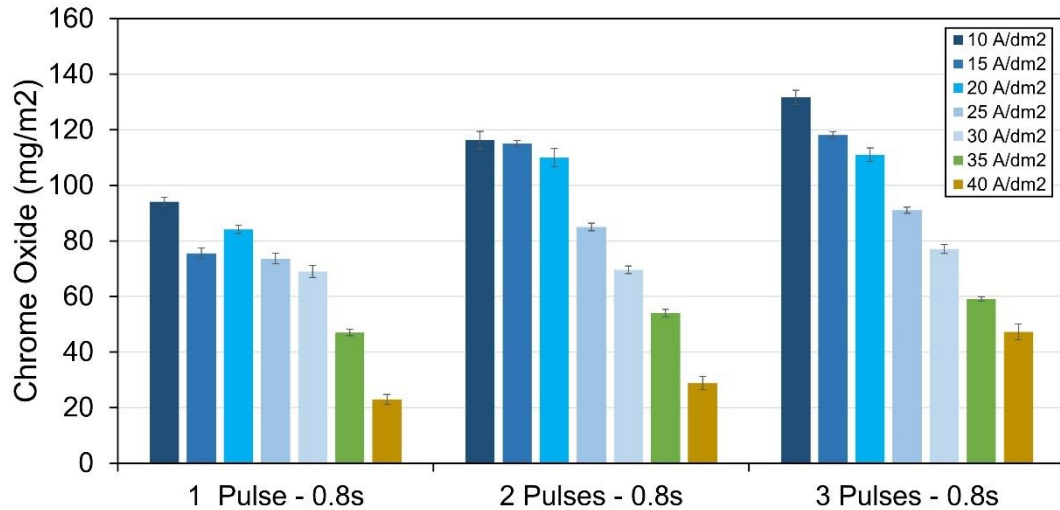


Figure 6.13 - The effect of pulsing current for 0.8 s on the quantity of chromium oxide deposit.

The quantity of chromium oxide deposition increases with each pulse but not significantly. This can be explained by the chromium oxide depositing preferentially onto the iron based substrate, just as the chromium metal did; section 6.4.2.2. This suggests that pulsing current may be a good technique with which to fully cover the iron in the base substrate.

6.4.3.3 The Effect of Temperature on the Quantity of the Chromium Oxide Deposit

As established, the temperature of electrolytes used for the electrodeposition of metallic coating is an important parameter in ensuring both quality and quantity of deposition. The industrially used temperature of the chromium metal depositing electrolyte is 55 °C, notably higher than that of the chromium metal electrolyte. A range of temperatures have been investigated for this electrolyte, electroplated at varying current densities, Figure 6.14.

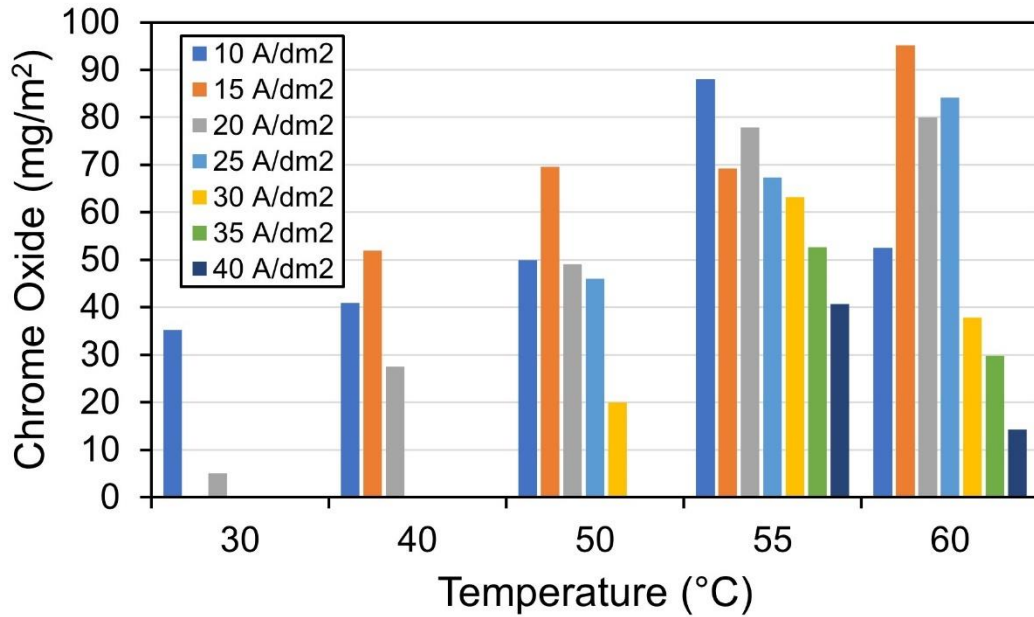


Figure 6.14 - The effect of electrolyte temperature changes on the quantity of chromium oxide deposition at various current densities.

At low temperatures of 30 and 40 °C, deposition is favoured at lower current densities of 10 – 20 A/dm² compared to higher current densities where there is no deposit (25-40 A/dm²). An increase in temperature is seen to widen the electroplating plating window across the full range of current densities, up to 40 A/dm². Total quantity of deposit across the range of current densities peaks at a temperature of 55 °C. This illustrates that using a chromium oxide depositing electrolyte at 55 °C establishes the biggest potential for deposition across the range of current densities using this chemistry.

6.4.3.4 The Effect of pH on the Quantity of the Chromium Oxide Deposit

It is important to maintain the pH of a Cr (III) oxide electroplating bath within a specific range to ensure a good quality of the coating and also to avoid any issues in the electroplating process. The main implications of pH changes in a Cr (III) electroplating have already been discussed, section 6.4.2.4. The pH of the chromium oxide depositing electrolyte was changed using values of 2, 2.4, 2.8, 3.2, 3.6 and 4 with the quantity of deposition being measured at various current densities.

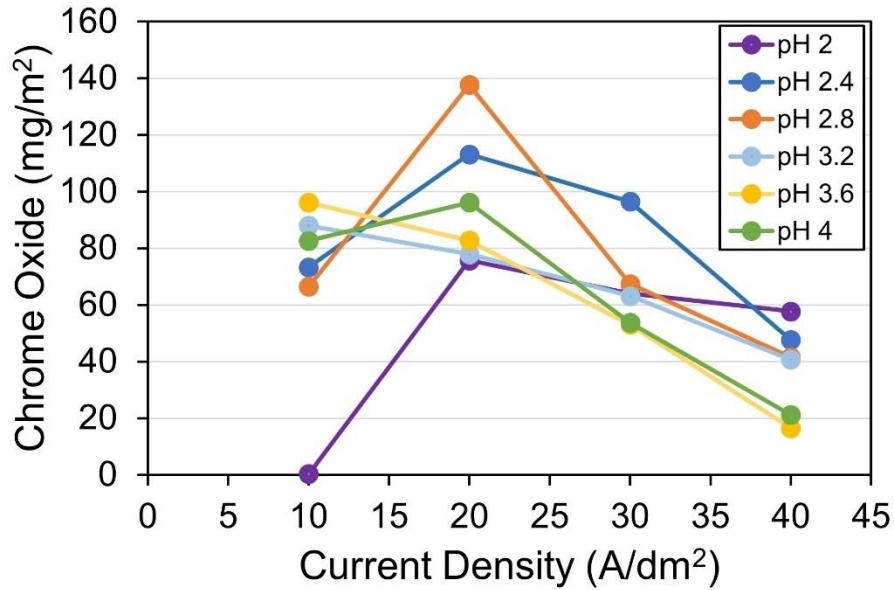


Figure 6.15 - The effect of electrolyte pH changes on the quantity of chromium oxide deposition at various current densities.

At all but the lowest value of pH 2, similar quantities of chromium oxide deposition are realised at a current density of 10 A/dm². Increasing current density to 20 A/dm² in most cases increases the quantity of deposition, however, this then decreases for all pH values as current density is increased further. Industrial partners had specified that the pH of this electrolyte is to be kept at 3.2; the data for this pH value has the least steep gradient implying that the deposition quantities vary the least at varying current densities. This value gives the process more stability.

At a lower pH, the conductivity of the electrolyte is relatively higher than when the pH is elevated due to an increase in quantity of H⁺ ions. This is good for charge transfer through the electrolyte however this also means that there is lots of H₂ potentially increasing the chances of hydrogen evolution at the cathode. At higher current densities (40A/dm² and to a certain extent 30 A/dm², Figure 6.15) there looks to be an almost linear relationship between pH and the chromium oxide level adding weight to this theory. At 20 A/dm², the pattern is less clear so H₂ production is likely limited by charge arrival rate and not H⁺ availability. This becomes less evident at low current densities.

6.5 The Two-step Electroplating Process

As TCCT is manufactured using a two-step electroplating process, two different layers must be characterised chemically to understand the deposition quantities. Measuring the chromium metal is a simple enough procedure, however, once a second, oxide rich layer is deposited on top, an XRF will measure the total chromium in both layers. As presented in section 4.4.2, GDOES has proved a valid method to assess the two distinct chromium layers deposited onto TCCT. To ensure that the electroplating process employed in the laboratory is accurate, depth profiles were repeated and compared as per the methodology outlined in section 3.3.11, Figure 6.16. Samples were prepared with approximately 60 mg/m^2 chromium metal (using a time pulse of 1 s, Figure 6.7) and a very low quantity of chromium oxide which was measured to be 5 mg/m^2 (using a time pulse of 0.4 s, Figure 6.12). These parameters were chosen in order to recreate a TCCT pilot line sample already possessed and measured.

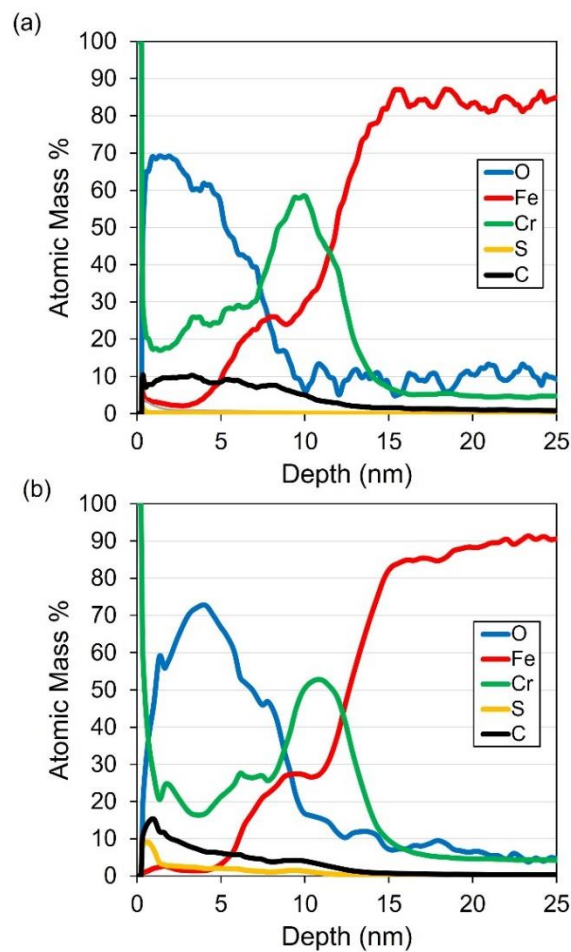


Figure 6.16 - GDOES profiles of (a) industrially made TCCT with 3 mg/m^2 of chromium oxide and (b) TCCT made in Swansea University attempting to replicate industrial quantities of 60 mg/m^2 chromium metal and $2-5 \text{ mg/m}^2$ of chromium oxide.

As can be seen in Figure 6.16, the Swansea University made TCCT GDOES profile closely resembles that of the GDOES profile of TCCT made industrially. Notably, the oxygen signal peaks in both cases at approximately 70 % atomic mass illustrating a total oxide thickness of approximately 10 nm. The chromium signal peaks in both cases between 50 and 60 % atomic mass with a total layer thickness of 15 nm. Iron is present in both scans all of the way through the duplex chromium coating with the profiles of both signals being extremely similar.

This comparison of chemical characterisation data illustrates the appropriate manufacturing of TCCT on a laboratory scale in a University setting and validates the sample manufacturing process.

6.6 Chromium Oxide Homogeneity - CuSO₄ Test

The chemical make-up of laboratory made TCCT has been established and compared to industrially made samples. It is now relevant to investigate the homogeneity of the chromium oxide layer deposited on the laboratory made TCCT samples. This is important given the relationship between the electrodeposited coating continuity and the adhesion of protective coatings.

Samples tested were all electrocoated with approximately 60 mg/m² of chromium metal and varying levels of chromium oxide respectively, these samples coating weights measured at 5, 16 and 25 mg/m² respectively. This was achieved by altering the length of time pulse in each case. The copper sulphate dip test was repeated on these samples as per the methodology outlined in section 5.5.2 with standard errors for all values stated in parentheses, Table 6.3 and Figure 6.17.

Table 6.3 - Area ration of copper on the surface of TCCT and ECCCS substrate materials highlighting differences in site density and therefore chromium oxide layer homogeneity.

Sample and Corresponding Chromium Oxide Coating Weight	Area Ratio Cu %	Site Density
TCCT (5 mg/m ²)	6.5 (0.2)	4800 (180)
TCCT (16 mg/m ²)	4.3 (0.2)	3300 (160)
TCCT (25 mg/m ²)	3.0 (0.1)	2500 (140)

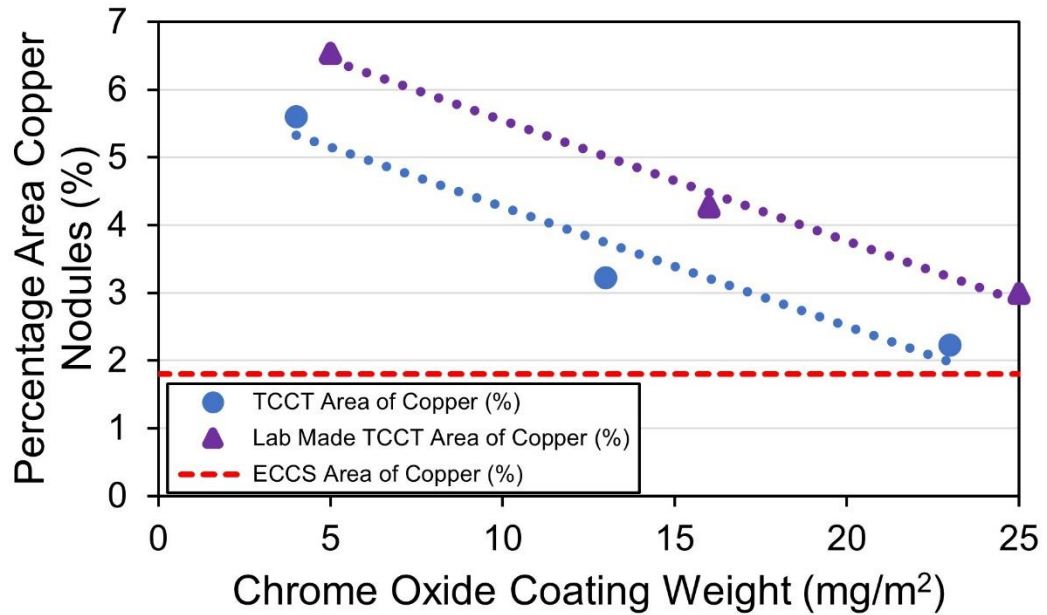


Figure 6.17 - Area ratio of copper on the surface of industrially made TCCT samples compared with lab made TCCT samples.

Compared to industrially made TCCT, lab made samples of the same chromium metal and oxide coating weights exhibit approximately 1 % more surface area of copper after exposure to the CuSO_4 test, Figure 6.17. In both cases, as chromium oxide coating weights increase the percentage area of copper measured on the surface decreases linearly. The chromium oxide values which industrially and lab made TCCT samples require to rival ECCS in chromium oxide layer homogeneity are approximately 24 and 31 mg/m^2 respectively. This increase in copper area is also accompanied by increase in number of sites.

6.7 Rate Limiting Step of Chromium Metal and Chromium Oxide Deposition

From the evaluation of the data relating to the electrodeposition of the chromium metal and chromium oxide layers, there is evidently a rate limiting step present within the process. It has been previously established that during electroplating metal ions in solution accept electrons to become a solid deposit. Therefore, the amount of solid that can be electroplated is limited by the number of electrons available and hence the applied current density.

The plating efficiency therefore can be estimated by comparing the quantity of solid that is deposited with the quantity of electrons that go through the circuit. The

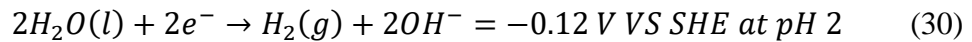
charge Q , defined as the total current passed in a given time. The charge can therefore be related to the moles of electrons n_e using Faraday's constant (96485 C/mol), F . These relationships are shown in *Equations 27, 28 and 29*.

$$Q = It \quad (27)$$

$$Q = n_e F \quad (28)$$

$$n_e = \frac{It}{F} \quad (29)$$

From observing the processes and consulting the literature this rate limiting step is almost certainly the evolution of hydrogen at the strip, which is the cathodic half reaction of water splitting. This hydrogen evolution reaction (HER) involves the reduction of protons or water molecules followed by the evolution of gaseous hydrogen, *Equation 30*. This can cause metallic depositions to vary in morphology effecting mechanical properties such as hardness as well as passing porosity into the cathode (157)



An increase in current thus results in an increase in hydrogen evolution at the cathode therefore inhibiting the deposit – and in this case may be exacerbated by the lack of hydrodynamics in the bath providing a means of refreshing the cathode surface with ions. The issue with this being that there is no easy way to measure or quantify the amount of hydrogen being evolved in this reaction but doing so would give a good approximation of the efficiency of the process. It might also help explain the counter intuitive negative correlation between chromium oxide deposition and current density.

From a theoretical point of view if we assume that the deposition of chromium oxide (Cr_2O_3) and the evolution of hydrogen (H_2) are the two reactions taking place in the second chromium oxide depositing step, we can use the charge density, calculate the number of electrons available for each process and calculate the chromium deposition efficiency at the various current densities, Figure 6.18.

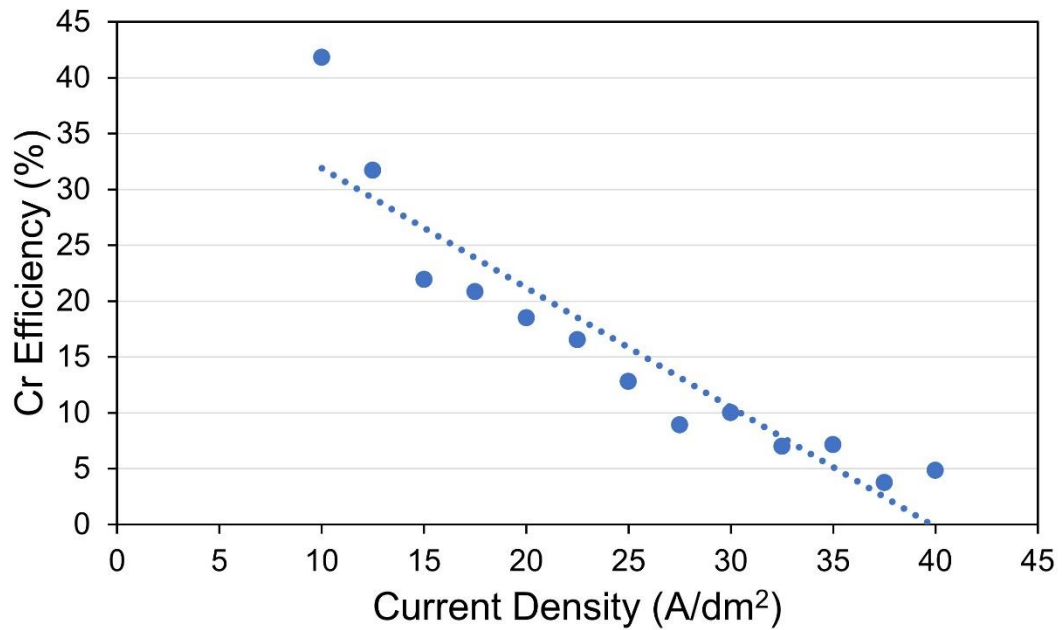


Figure 6.18 - The efficiency of the chromium oxide deposition process plotted against varying current densities, highlighting the effect of the hydrogen evolution cathodic reaction as a rate limiting step.

At lower current densities, the chromium oxide deposition efficiency is as high as 42%, but when the current densities are increased there is a dramatic decrease in the efficiency of the chromium oxide and the hydrogen evolution process dominates. This is quite obviously significant and may well lend insight into the operational process parameters for sample production.

The work conducted on both TCCT electrolytes suggests that in order to ensure a suitable quantity and quality of deposition, the current density, time pulse used, temperature and pH of electrolyte must be chosen.

For the deposition of a chromium metal coating of approximately 100 mg/m², using a time pulse of 1.2 s and current density of 30 A/dm² it would be preferable to ensure a low temperature of 37 °C and pH value of 2.3. A low temperature is able to be used in this case as a low pH value is used. Using a low temperature industrially is economically favourable.

For the deposition of a homogenous chromium oxide layer between 5-25 mg/m² on top of a chromium metal layer, electroplating parameters must also be optimised. Using a time pulse of 0.4 – 0.5 s at a current density of 30 A/dm² at 55 °C is ideal to deposit this chromium oxide layer. The pH value of 3.2 ensures that deposition is maximised across a range of current densities.

In the case of both electrolytes, it has been shown that the pulsing of current may help in mitigating any free iron on the surface of the substrate as the electrodeposition in these areas is electrochemically favourable.

6.8 Additional Work to Assess the Impact of Hydrogen Evolution on the Electroplating Process

It has already been postulated that the increase in number of defects on lab made TCCT samples compared to industrially made samples is a product of hydrogen evolution. Further work was undertaken with view to assessing this effect in the form of the design of a rotating cylinder electrode electroplating rig. This design is still in development within the University, however, the initial design is presented below as a rendered CAD image, Figure 6.19.



Figure 6.19 - Rendered CAD image of the initial design of a rotating cylinder electrode set-up to investigate the effect of hydrogen evolution on the deposition of chromium metal and oxide coatings.

In this design, a Perspex cylindrical vessel houses a cylindrical anode mounted on PTFE feet, allowing for adequate electrolyte flow beneath the rotating cylinder. This anode is of the same specification as the rectangular material used in previous experiments sourced from the same supplier. A solid PTFE cylinder was machined and attached to 3D printed sample holders which were secured with nylon hardware. The PTFE cylinder was bored holding a solid copper shaft with a press fit. Eventually the main rotating cylinder was to be fitted with clips on the top face attached to the copper shaft. It was planned that the current would be supplied to the cylinder through a slip ring system where-by the rotating of the cylinder was enabled by a motor, at first this was envisioned as a pillar drill. With this set up the rotation in RPM could be accurately controlled and changed as necessary. Samples for electroplating are to be placed in between the 3D printed components ensuring consistent anode-cathode gap and conforming to the radius of the anode. A top view of this design is shown in Figure 6.20.

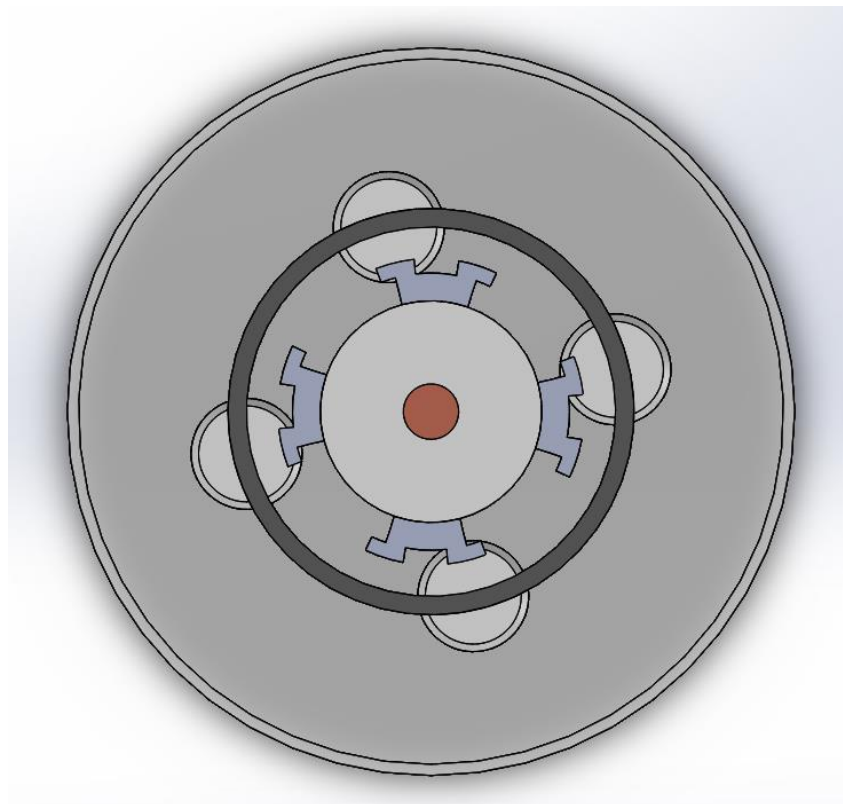


Figure 6.20 - Top view of CAD drawing of the rotating cylinder electrode design.

6.9 Conclusions

This section of work has highlighted the importance of electroplating parameters when depositing TCCT coatings and has also emphasised the sensitivity of the process. Within the wealth of data presented, the main conclusions are as follows:

- Cyclic voltammetry has confirmed the purity of the Cr (III) sulphate hydrate by illustrating that the oxidation of formic acid within the first, chromium metal depositing electrolyte, is not inhibited by the contamination of sulphite ions.
- The quantity of both chromium metal and chromium oxide deposited using this electroplating procedure is strongly dependant on the current density and electrolysis time applied (and thus charge). In the case of chromium metal, deposition increases with current density at low electrolysis times (0.8 s) but this trend is reversed at electrolysis times of 3 and 5 s. In the case of chromium oxide, increasing current density leads to reduced deposits. Threshold current densities of 30 A/dm^2 and 10 A/dm^2 were noted respectively for each electrolyte, below which there was no deposit.
- Metallic and oxidic chromium coating weights of $\sim 60 \text{ mg/m}^2$ and $5\text{-}25 \text{ mg/m}^2$ have been achieved by investigating the impact of electrolysis time using small variations in the range of 0.1 s. The electrolysis times required for these quantities of deposition are 1 s and 0.4 - 0.7 s respectively. There is a strong positive correlation between these small variations of electrolysis times at low total times.
- Pulsing the electrolyte resulted in incremental but not significant increases in both chromium metal and chromium oxide coating weights. This suggests that chromium metal and oxide deposit preferentially onto the iron based substrate material.
- The amount of chromium metal / oxide deposit strongly depends on temperature. Generally speaking, an increase in temperature results in an increase in the rate of deposition up to a point, 45 and 55 °C in both chromium metal and chromium oxide depositing electrolytes respectively. At higher temperatures, the solubility of chromium (III) ions in the electrolyte solution increases, leading to higher ion concentrations in solution (159). This results in a higher rate of migration of ions to the cathode, leading to faster deposition

onto the cathode. Lower temperatures can cause the electrolyte to become more viscous, slowing down the migration of chromium (III) ions to the cathode decreasing the rate of deposition along with the ion concentration (158). It is proposed the ideal temperatures at which to deposit chromium metal and chromium oxide are 37 and 55 °C respectively.

- The pH of both electrolytes has a significant effect on the deposition of chromium metal and oxide from chromium (III) based electrolytes. Lower pH values can result in higher deposition rates. It is generally recommended to maintain the pH within a specific range, typically between 2 and 4, to achieve optimal results in terms of both quality and quantity in chromium plating. In the case of these two electrolytes, it is recommended that the chromium metal and oxide depositing electrolytes are held at 2.3 and 3.2 respectively.
- Repeating the CuSO₄ dip methodology on lab made TCCT samples illustrated a more inhomogeneous covering of chromium oxide compared to industrially pilot line manufactured samples. This is attributed to the hydrogen evolved in the static bath inhibiting deposition compared to industrial electroplating baths where the substrate is moving continually and so hydrogen is continually ‘flushed’ off the surface.
- Theoretically, the efficiency of the chromium oxide depositing electrolyte has been shown to be hindered significantly by the evolution of hydrogen, the evolution of which is proportional to the applied current density.

7 Conclusions

Throughout the course of this work, Cr (III) based packaging steel substrate materials, TCCT, have shown their potential as replacement material to the Cr (IV) based ECCS. This has been investigated using a range of physical and chemical characterisation methods. Their lacquered performance pre and post-retort has been shown to be comparable to that of the incumbent ECCS substrate. The manufacturing of TCCT has also been investigated in-depth illustrating the sensitivities of the process to current density, temperature, pH, and electroplating time.

The scientific impact of this work is considerable, having contributed to the industrial optimisation of manufacturing parameters for TCCT and providing a continuous assessment of their performance in a range of simulated industrial conditions using both established and novel methodologies.

At the beginning of this work three main objectives were listed. The work completed to address each objective is detailed below:

1. To characterise the novel TCCT substrate and coating materials physically and chemically.

A plethora of physical and chemical characterisation techniques were used to characterise a range of TCCT samples which varied in chromium oxide coating weight. From these methods it can be concluded that:

- Chromium oxide coating weights in the range of 3-23 mg/m² do not have a measurable impact on the surface roughness of the materials, within the accuracy of the methods used. This suggests that the mechanical interlocking mechanism of lacquer adhesion contributes a constant value across the sample set.
- Lacquers used were shown to have similar surface tension values and contact angle values on TCCT substrates alluding to their similar wetting characteristics and solvent contents.
- SEM imagery highlighted surface porosity on substrate materials in the form of 1-5 um defects and nano-scale pinholes. It was subsequently shown, using XPS and GDOES, that the surface of TCCT samples contained low levels of iron.

- Aesthetic characterisation using spherical spectrophotometry showed that TCCT becomes more yellow and red simultaneously whilst darkening with increasing levels of chromium oxide on its surface.
- 2. To understand how the adhesion interface between a novel substrate and applied organic coatings react to the processing environment in the context of a food packaging can, investigating their interaction both before and after a retort process.**

A large range of TCCT substrate materials were lacquered with two different coatings and assessed for their adhesion characteristics both pre and post retort process:

- The studies pertaining to the adhesion of lacquers to these substrates have highlighted the importance of optimal chromium oxide coating weight on the substrates surface. Changing just the lacquer alone makes a severe difference in the adhesion performance of the substrate. This is validated by the similar drop in adhesion characteristic between the ECCS / epoxy and ECCS / BPANI system. In all cases it seems that increasing the level of chromium oxide increases the failure force of the coating / substrate system.
- Water uptake in BPANI lacquered substrates is exacerbated by the retort process and the presence of increasing concentrations of salt. This is as a result of physical diffusion of water molecules as opposed to a chemical reaction. The loss of adhesion of the BPANI lacquers due to the retort process is attributed to surface substrate corrosion as it was postulated NaCl does not interact chemically with the lacquers; this has been subsequently proven. The impact of NaCl in solution is profound for both the TCCT and ECCS materials. The addition of citric acid to the NaCl solution showed that further passivation of the substrates surface is achieved therefore limiting the corrosion of the surface.
- Chemically comparing the surfaces of TCCT and ECCS, it is plausible that the primary mechanism which lowers the adhesion performance of TCCT substrates is the presence of small (1-3 micron) defects in the substrate which provides access to the iron in the underlying steel substrate. Whether these defects are a result of the fundamental Cr (III) deposition process chemistry or

whether they are associated with pilot manufacture which, by its nature is less consistent compared to a commercial production line, is yet unknown.

- A CuSO_4 dip test has illustrated the presence of iron on the surface of all TCCT samples and ECCS. Area averaging has proven that in the case of TCCT, chromium oxide coating weight is directly proportional to the quantity of copper and therefore iron on the substrates surface.
- Using the SVET, it has been shown that TCCT samples with low chromium oxide coating weights exhibit a scarring mechanism of corrosion which is characterised by significant quantities of insulating corrosion product (Fe_2O_3). This makes the process self-limiting and therefore not destructive to the metallic coating. TCCT samples with medium and high chromium oxide coating weights exhibit an unstable pitting mechanism of corrosion whereby the metallic coating is destroyed through the continual diffusion of oxygen to surface defects as evidenced by their positive gradients within the anodic activity data.

3. Replicate TCCT on a lab-scale to understand the effect of a range of electroplating parameters and to optimise the deposition process so as to create samples which could be proven to be chemically comparable thus enabling manufacturing process recommendations to industry.

The TCCT manufacturing process was replicated on a laboratory scale and validated. The effect of various electroplating parameters were investigated however no optimisation experiments were undertaken due to time constraints:

- Cyclic voltammetry has confirmed the purity of the Cr (III) sulphate hydrate source by illustrating that the oxidation of formic acid within the first, chromium metal depositing electrolyte, is not inhibited by the contamination of sulphite ions.
- The quantity of both chromium metal and chromium oxide deposited using this electroplating procedure is strongly dependant on the current density and electrolysis time applied. In the case of chromium oxide, increasing current density leads to reduced deposits. Threshold current densities of 30 A/dm^2 and

10 A/dm² were noted respectively for each electrolyte, below which there was no deposit.

- Metallic and oxidic chromium coating weights of ~ 60 mg/m² and 5-25 mg/m² have been achieved by investigating the impact of electrolysis time using small variations in the range of 0.1 s. There is a strong positive correlation between these small variations of electrolysis times at low total times.
- Pulsing the electrolyte resulted in incremental but not significant increases in both chromium metal and chromium oxide coating weights. This suggests that chromium deposits preferentially onto the iron based substrate material.
- The amount of chromium metal / oxide deposit strongly depended on temperature. At higher temperatures, the solubility of chromium (III) ions in the electrolyte solution increases, leading to higher ion concentrations in solution. This results in a higher rate of migration of ions to the cathode, leading to faster deposition onto the cathode. Lower temperatures can cause the electrolyte to become more viscous, slowing down the migration of chromium (III) ions to the cathode decreasing the rate of deposition along with the ion concentration. It is proposed the ideal temperatures at which to deposit chromium metal and chromium oxide are 37 and 55 °C respectively.
- The pH of both electrolytes has a significant effect on the deposition of chromium metal and oxide from chromium (III) based electrolytes. Lower pH values can result in higher deposition rates (and improved adhesion of the deposited chromium to the substrate). In the case of these two electrolytes, it is recommended that the chromium metal and oxide depositing electrolytes are held at 2.3 and 3.2 respectively.
- Repeating the CuSO₄ dip methodology on lab made TCCT samples illustrated a more inhomogeneous covering of chromium oxide. This is attributed to the hydrogen evolved in the static bath inhibiting deposition.
- Theoretically, the efficiency of the chromium oxide depositing electrolyte has been shown to be hindered significantly by the evolution of hydrogen; the evolution of which is proportional to the applied current density.

TCCT sample materials manufactured industrially show promise in becoming the substrate material to take over from ECCS in light of REACH legislation. Their

lacquer adhesion characteristics, when electrocoated with 10-12 mg/m² of chromium oxide show comparable results.

8 Recommendations for Future Work

The work undertaken in this thesis has highlighted several areas in which further investigation could progress the work already completed:

- The adhesion of protective lacquers to recently developed ultra-low tin coating weight products could help diversify substrate materials used for REACH compliancy withing the packaging steel industry.
- Further characterising these lacquers to investigate the rate at which they wet out onto substrate materials could help with materials and process optimisation within the coating process by highlighting the ideal solvent content for these coatings, potentially reducing curing times.
- Use the spherical spectrophotometry method outlined in this work to characterise the copper deposited on the surface of substrate materials to aid in a quicker analysis of the chromium oxide coatings homogeneity.
- Investigate the corrosion of TCCT substrates further in order to fine the chromium oxide coating weight which illustrates the change in corrosion mechanism from scarring to pitting. In addition, measuring the mass loss of TCCT samples accurately using gravimetric analysis (ISO 8407) or a hydrogen capture set up would provide accurate quantification of mass lost due to corrosion as opposed to the semi-quantitative data output from the SVET.
- Manufacture samples of TCCT in a laboratory setting with chromium metal chromium oxide coating weight of 60-100 mg/m² and 5-25 mg/m² and subject them to a simulated retort process to assess their lacquer adhesion characteristics, comparing them to industrially made samples.
- Further analyse the duplex chromium coating homogeneity utilising electrochemical impedance spectroscopy (EIS). The impedance spectrum of a homogeneous coating will typically exhibit a single, well-defined peak, while the impedance spectrum of a non-homogeneous coating will typically exhibit multiple peaks or a broad peak. Additionally, the value of the impedance at different frequencies can be used to infer information about the thickness and uniformity of the coating.

- Conduct additional experiments to assess the impact of hydrogen evolution at the cathode within the Cr (III) electroplating process, potentially through use of a rotating cylinder electrode. This should confirm that it is hydrogen evolution limiting the chromium layers deposition as opposed to ion diffusion to the surface.
- Stimulate the electrolytes used for Cr (III) deposition using ultrasound. This has been shown to increase the efficiency of deposition through increasing the movement of ions, increasing the replenishment rate at the cathode boundary layer, decreasing the thickness of the diffusion layer thereby minimising the diffusion time (160).

9 Appendix I – SVET Repeats

Below are a collection of images detailing repeated SVET scans for TCCT samples with low can high chromium oxide coatings (3 and 23 mg/m²) respectively, as well as ECCS (9 mg/m²). It is noted that samples with a low chromium oxide coating weight exhibit scarring mechanism of corrosion, Figure 9.1. In this case the anodic activity grows over the whole length of the scan with Fe₂O₃ visible on the sample. This scan agrees with a scarring mechanism of corrosion for samples with a low chromium oxide coating weight shown in section 5.5.3. The high chromium oxide coating weight of TCCT appears to pit dramatically with high current values of up to 3 A/m² witnessed, Figure 9.2. This signifies the destruction of the metallic coating; a picture of the sample post-scan was not taken. A repeat scan of ECCS illustrated a more generic corrosion mechanism consisting of small pits across a large surface area of the sample resulting in a comparably low anodic activity peak of 0.95 A/m², Figure 9.3.

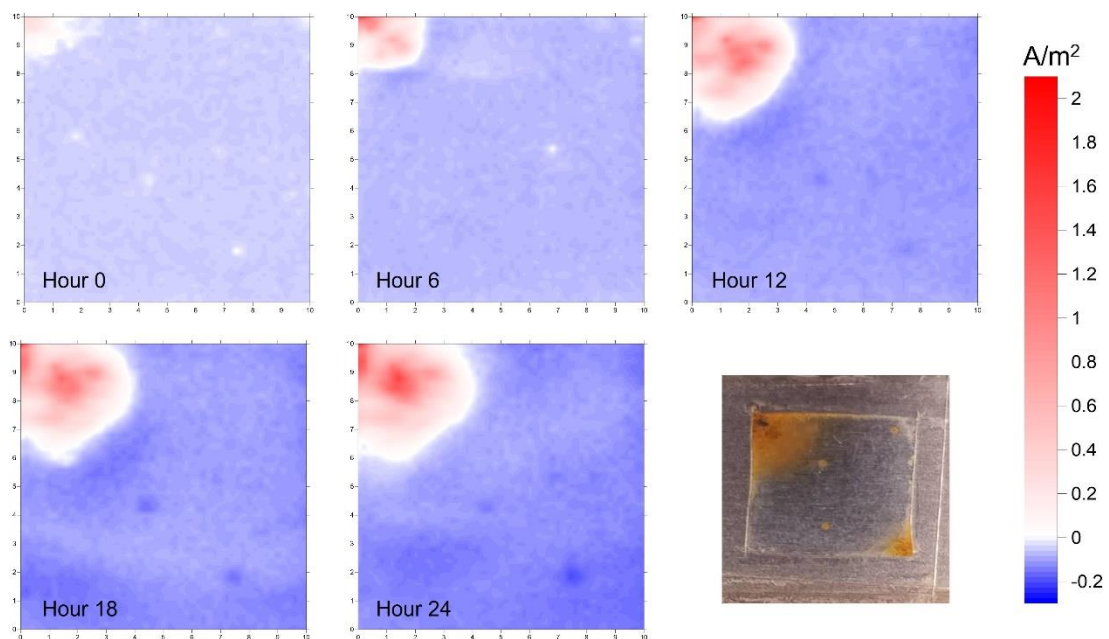


Figure 9.1 - SVET colour charts representing a repeat scan of TCCT coated with 3 mg/m² of chromium oxide and image of sample post-process.

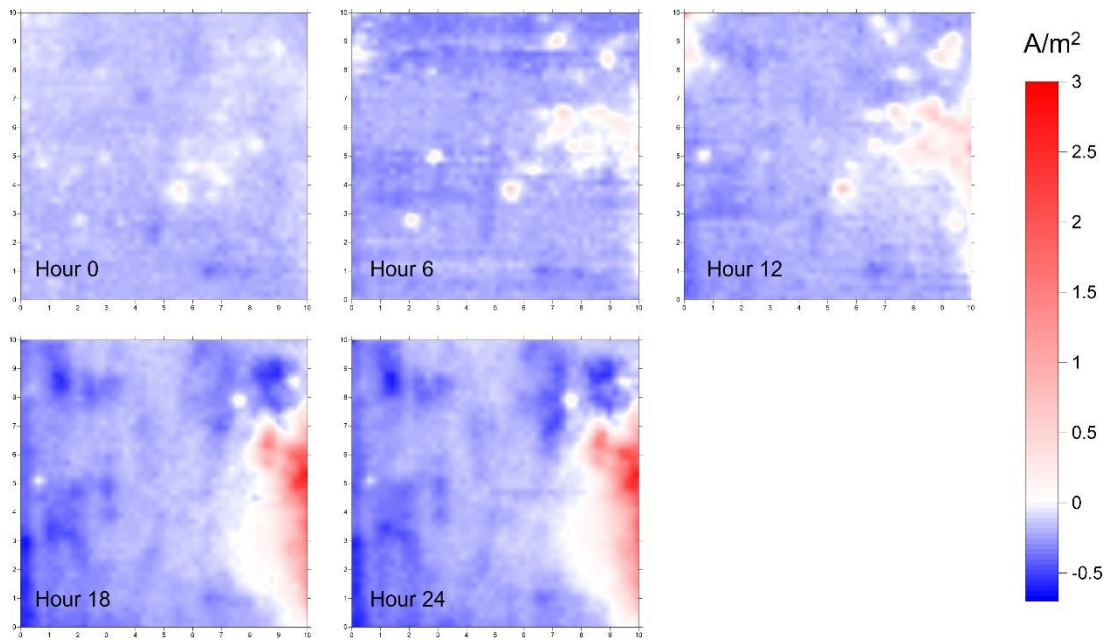


Figure 9.2 - SVET colour charts representing a repeat scan of TCCT coated with 23 mg/m^2 of chromium oxide.

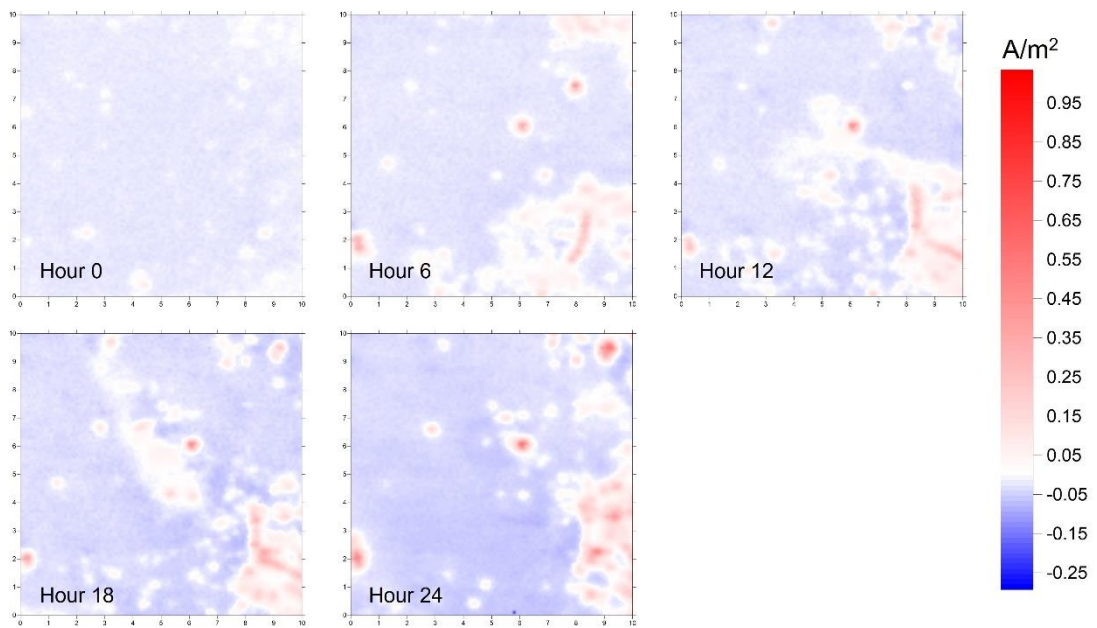


Figure 9.3 - SVET colour charts representing a repeat scan of ECCS coated with 9 mg/m^2 of chromium oxide.

10 Appendix II – List of Publications

Below is a list of publications that have been produced as a direct result of the work conducted and presented within this thesis.

1. The Adhesion of Protective Coatings to Novel Trivalent Cr Metal / Cr Oxide Coatings Used for Packaging Applications

M. Dodd, E. Jewell, N. Wint, A. deVoos

ECS Meeting, Volume MA2022-02

DOI: 10.1149/MA2022-0210684

2. Performance Assessment of Chromium Coated Packaging Steel Manufactured via a Cr (III) Processing Route

M. Dodd, E. Holding, C. Griffiths, E. Bluett, A. Mescall, K. Lammers, A. deVoos, N. Wint, E. Jewell

International Journal of Adhesion and Adhesives

(Submitted – In Review)

3. The Influence of Chromium Oxide Coating Weight on Filiform Corrosion of Trivalent Chromium Coatings for Packaging Steel

E. Bluett, M. Dodd, A. Mescall, A. deVoos, N. Wint, E. Jewell, H. N. McMurray

Corrosion Science

(Yet to be Submitted)

11 Bibliography

1. Metal Packaging Market by Type Trends and Forecast to 2020. 2015.
2. Bell JD, Sharp MK, Havice E, Batty M, Charlton KE, Russell J, et al. Realising the food security benefits of canned fish for Pacific Island countries. *Mar Policy*. 2019 Feb 1;100:183–91.
3. Metal Packaging Market Share, Size, Analysis, Forecast (2018-23). 2018.
4. Kadoya T. Food Packaging. Food Packaging. Academic Press; 2012. 1–424 p.
5. Castillo VE, Mollenkopf DA, Bell JE, Bozdogan H. Supply Chain Integrity: A Key to Sustainable Supply Chain Management. *Journal of Business Logistics*. 2018 Mar;39(1):38–56.
6. Petry T, Knowles R, Meads R. An analysis of the proposed REACH regulation. *Regulatory Toxicology and Pharmacology*. 2006;44(1):24–32.
7. European Chemicals Agency. Substances restricted under REACH - ECHA [Internet]. 2019 [cited 2019 May 6]. Available from: <https://echa.europa.eu/substances-restricted-under-reach>
8. Morgan E. Tinplate and modern can making technology [Internet]. Pergamon Press; 1985 Available from: https://openlibrary.org/books/OL2841207M/Tinplate_and_modern_canmaking_technology
9. Huang XQ, Li N, Jiang LM, Li DY. Effect of Black Plate on Corrosion Resistance of T5 Tinplate. *Journal of Iron and Steel Research International* 2006 13:2. 2006 Feb 1;13(2):59–64.
10. EN 10202:2001 - Cold reduced tinmill products - Electrolytic tinplate and electrolytic [Internet]. [cited 2022 Feb 28]. Available from: <https://standards.iteh.ai/catalog/standards/cen/eb353920-e059-4b31-a83c-2b0deb0069d0/en-10202-2001>
11. World Intellectual Property Organization. Analysis of Alternatives and Socio-economic Analysis: Thyssenkrupp Rasselstein [Internet]. 2014 [cited 2020

May 15]. Available from:

<https://patents.google.com/patent/WO2014079909A1>

12. Boelen B. The influence of deformation on the product performance of pre-coated packaging steels. Technische Universiteit Delft; 2009.
13. Mora N, Cano E, Bastidas JM, Almeida E, Puente JM. Characterization of passivated tinplate for food can applications. *Journal of Coatings Technology*. 2002 Dec;74(12):53–8.
14. Coles R, Kirwan M. *Food and Beverage Packaging Technology: Second Edition*. Food and Beverage Packaging Technology: Second Edition. Wiley; 2011. 746 p.
15. Boelen B, den Hartog H, van der Weijde H. Product performance of polymer coated packaging steel, study of the mechanism of defect growth in cans. *Prog Org Coat* [Internet]. 2004 Jun 1 [cited 2018 Dec 1];50(1):40–6. Available from: <https://www.sciencedirect.com/science/article/pii/S0300944003002200>
16. Allman A. *Understanding and Improving the Post Retort Adhesion of BPANI Lacquers on Cr (III) Electroplated Steel*. Swansea University; 2020.
17. Edy JE. *Corrosion of Organic Coated trivalent Chromium Coated Technology Steel (TCCT)*. Swansea University; 2019.
18. Kudryavtsev VN, Vinokurov EG, Schachameyer SR, Azarko OE. Electroplating of Thick, Hard Chromium Coatings from Cr (III) Baths. In: AESF annual technical conference [Internet]. 1995 [cited 2022 Jun 9]. p. 503–12. Available from: <https://www.researchgate.net/publication/285409928>
19. Zhao H, Liu W, Li Q, Zhang B, Liu J, Yan C, et al. Mechanism of chromium electrodeposition from Cr(III) baths on nickel and chromium electrode surfaces. *Int J Electrochem Sci* [Internet]. 2020 [cited 2022 Jun 16];15(9):8979–89. Available from: www.electrochemsci.org
20. Ogle K, Wolpers M. *Phosphate Conversion Coatings*. *Metal Finishing* [Internet]. 2003 Aug [cited 2023 Sep 12];83(8):15–8. Available from: <https://dl.asminternational.org/handbooks/edited-volume/46/chapter/541344/Phosphate-Conversion-Coatings>

21. Słowik M, Cępa P, CZAPLA K, Zabiński P. Steel packaging production process and a review of new trends. *Archives of Metallurgy and Materials*. 2021;66(1):135–43.
22. Protsenko V, Danilov F. Kinetics and mechanism of chromium electrodeposition from formate and oxalate solutions of Cr (III) compounds. *Electrochim Acta*. 2009 Oct 1;54(24):5666–72.
23. Haque M, Hoque M, Islam M, Islam M, Mustafa C. Effect of Various Operating Parameters on Trivalent Chromium Electroplating. *J Sci Res Rep*. 2017 Jan 10;13(3):1–9.
24. Helm L, Merbach AE. Inorganic and bioinorganic solvent exchange mechanisms. *Chem Rev [Internet]*. 2005 Jun [cited 2023 Jan 26];105(6):1923–59. Available from: <https://pubs.acs.org/doi/abs/10.1021/cr030726o>
25. Zeng Z, Sun Y, Zhang J. The electrochemical reduction mechanism of trivalent chromium in the presence of formic acid. *Electrochem commun*. 2009 Feb;11(2):331–4.
26. Song YB, Chin DT. Current efficiency and polarization behavior of trivalent chromium electrodeposition process. *Electrochim Acta*. 2002 Dec 20;48(4):349–56.
27. Giovanardi R, Orlando G. Chromium electrodeposition from Cr(III) aqueous solutions. *Surf Coat Technol*. 2011 Apr 25;205(15):3947–55.
28. Wijenberg JHOJ, Steegh M, Aarnts MP, Lammers KR, Mol JMC. Electrodeposition of mixed chromium metal-carbide-oxide coatings from a trivalent chromium-formate electrolyte without a buffering agent. *Electrochim Acta*. 2015 Jun 3;173:819–26.
29. Wijenberg JHOJ, Wittebrood AJ, Litz MW. Method For Manufacturing Chromium-Chromium Oxide Coated Blackplate. 2019.
30. Protsenko VS, Danilov FI, Gordiienko VO, Kwon SC, Kim M, Lee JY. Electrodeposition of hard nanocrystalline chrome from aqueous sulfate trivalent chromium bath. *Thin Solid Films*. 2011 Oct 31;520(1):380–3.

31. de Vooy's ACA, Wijenberg JHOJ, Koper MTM. Cyclic voltammetry study of trivalent basic chromium sulphate electrolytes contaminated with sulphite. *Electrochim Acta*. 2018 Apr 10;269:700–5.
32. Wijenberg JHOJ, de Vooy's ACA, Kortlever R, Koper MTM. Oxidation reactions in chromium(III) formate electrolytes at platinum and at a catalytic mixed metal oxide coating of iridium oxide and tantalum oxide. *Electrochim Acta*. 2016 Sep 20;213:194–200.
33. Melvin C, Jewell E, de Vooy's A, Lammers K, Murray NM. Surface and Adhesion Characteristics of Current and Next Generation Steel Packaging Materials. *J Packag Technol Res* [Internet]. 2018 Jul 17 [cited 2019 Feb 18];2(2):93–103. Available from: <http://link.springer.com/10.1007/s41783-018-0031-8>
34. Wint N, de Vooy's ACA, McMurray HN. The corrosion of chromium based coatings for packaging steel. *Electrochim Acta*. 2016;203:326–36.
35. Wint N, Geary S, McMurray HN, Williams G, de Vooy's ACA. The Kinetics and Mechanism of Atmospheric Corrosion Occurring on Tin and Iron-Tin Intermetallic Coated Steels. *J Electrochem Soc* [Internet]. 2015 [cited 2019 May 29];162(14):C775–84. Available from: <http://jes.ecsdl.org/lookup/doi/10.1149/2.0681514jes>
36. Bautista A. Filiform corrosion in polymer-coated metals. *Prog Org Coat*. 1996 May 1;28(1):49–58.
37. Grundmeier G, Schmidt W, Stratmann M. Corrosion protection by organic coatings: electrochemical mechanism and novel methods of investigation. *Electrochim Acta*. 2000 May 3;45(15–16):2515–33.
38. Allman A, Jewell E, de Vooy's A, Hayes R. Inter-layer Adhesion Performance of Steel Packaging Materials for Food Cans Under Retort Conditions. *J Packag Technol Res* [Internet]. 2018 Jul 17 [cited 2018 Dec 1];2(2):115–24. Available from: <http://link.springer.com/10.1007/s41783-018-0033-6>
39. Prabhakar JM, Varanasi RS, da Silva CC, Saba, de Vooy's A, Erbe A, et al. Chromium coatings from trivalent chromium plating baths: Characterization

- and cathodic delamination behaviour. *Corros Sci* [Internet]. 2021 Jul 15 [cited 2021 May 17];187:109525. Available from:
<https://linkinghub.elsevier.com/retrieve/pii/S0010938X21002912>
40. Food and Agriculture Organization of the United Nations. Guidelines for can manufacturers and food canners. Prevention of metal contamination of canned foods. *FAO Food Nutr Pap* [Internet]. 1986 [cited 2019 May 21];36:82. Available from:
https://books.google.co.uk/books?id=rcopDa4Ky08C&printsec=frontcover&source=gbg_ge_summary_r&cad=0#v=onepage&q&f=false
41. Page B, Edwards M, May N. Metal cans. *J Food Sci* [Internet]. 2006 [cited 2023 Jan 10];(38593283). Available from:
<https://www.semanticscholar.org/paper/5-Metal-cans>
42. Robertson GL. Packaging and Food and Beverage Shelf Life. In: Reference Module in Food Science. Elsevier; 2019.
43. Awuah GB, Ramaswamy HS, Economides A. Thermal processing and quality: Principles and overview. *Chemical Engineering and Processing: Process Intensification*. 2007 Jun;46(6):584–602.
44. Ginés MJL, Benítez GJ, Egli W, Giuliani J, Zubimendi JL, Rissone H. Tinplate wettability by organic coatings. 15th IAS Rolling Conference, 2004 [Internet]. 2004 [cited 2021 Jun 23];(November 2004). Available from:
https://www.researchgate.net/publication/299340595_Tinplate_wettability_by_organic_coatings
45. Peter K.T Oldring & Ulrich Nehring. Metal Packaging for foodstuffs: Europe Report Series Packaging Materials Task Force. 2007.
46. Barilli F, Fragni R, Gelati S, Montanari A. Study on the adhesion of different types of lacquers used in food packaging. In: *Progress in Organic Coatings* [Internet]. Elsevier; 2003 [cited 2019 Mar 13]. p. 91–6. Available from:
<https://www.sciencedirect.com/science/article/pii/S0300944002002151>

47. Manfred LB, Ginés MJL, Benftez GJ, Egli WA, Rissone H, Vázquez A. Use of epoxy-phenolic lacquers in food can coatings: Characterization of lacquers and cured films. *J Appl Polym Sci*. 2005 Mar 15;95(6):1448–58.
48. Biedermann M, Grob K. Phenolic resins for can coatings: I. Phenol-based resole analysed by GC–MS, GC×GC, NPLC–GC and SEC. *LWT - Food Science and Technology*. 2006 Aug 1;39(6):633–46.
49. Manfred LB, Ginés MJL, Benftez GJ, Egli WA, Rissone H, Vázquez A. Use of epoxy-phenolic lacquers in food can coatings: Characterization of lacquers and cured films. *J Appl Polym Sci*. 2005 Mar 15;95(6):1448–58.
50. Ashcroft WR. Curing agents for epoxy resins. In: *Chemistry and Technology of Epoxy Resins* [Internet]. Springer, Dordrecht; 1993 [cited 2022 Sep 1]. p. 37–71. Available from: https://link.springer.com/chapter/10.1007/978-94-011-2932-9_2
51. Kawamura Y, Inoue K, Nakazawa H, Yamada T, Maitani T. Cause of bisphenol A migration from cans for drinks and assessment of improved cans. *Journal of the Food Hygienic Society of Japan* [Internet]. 2001 [cited 2022 Sep 1];42(1):13–7. Available from: <https://pubmed.ncbi.nlm.nih.gov/11383151/>
52. de Vooy A, Boelen B, Penning JP, van der Weijde H. Improving coating resistance to acetic acid sterilisation: An EIS approach. *Prog Org Coat*. 2009 Apr 1;65(1):30–6.
53. Food and Agriculture Organization of the United Nations. Guidelines for can manufacturers and food canners. Prevention of metal contamination of canned foods. *FAO Food Nutr Pap* [Internet]. 1986 [cited 2022 Sep 1];36:82. Available from: <https://agris.fao.org/agris-search/search.do?recordID=XF8661929>
54. Ebnesajjad S. Characteristics of Adhesive Materials. *Handbook of Adhesives and Surface Preparation*. 2011 Jan 1;137–83.
55. Lestido-Cardama A, Sendón R, Bustos J, Nieto MT, Paseiro-Losada P, Rodríguez-Bernaldo de Quirós A. Food and beverage can coatings: A review

- on chemical analysis, migration, and risk assessment. *Compr Rev Food Sci Food Saf.* 2022 Jul 1;21(4):3558–611.
56. Simal-Gándara J. Selection of can coatings for different applications. <http://dx.doi.org/101080/87559129909541180>. 2009;15(1):121–37.
 57. NACE International. International Measures of Prevention, Application, and Economics of Corrosion Technologies Study. 2012.
 58. Zumelzu E, Cabezas C. Observations on the influence of microstructure on electrolytic tinsplate corrosion. *Mater Charact* [Internet]. 1995 Mar 1 [cited 2019 Mar 4];34(2):143–8. Available from: <https://www.sciencedirect.com/science/article/pii/104458039400060X>
 59. Edy JE, McMurray HN, Lammers KR, deVooy ACA. Kinetics of corrosion-driven cathodic disbondment on organic coated trivalent chromium metal-oxide-carbide coatings on steel. *Corros Sci.* 2019;
 60. Marcus P. Corrosion mechanisms in theory and practice. Third. *Corrosion Mechanisms in Theory and Practice: Third Edition*. Taylor and Francis Group; 2011. 349–391 p.
 61. Soltis J. Passivity breakdown, pit initiation and propagation of pits in metallic materials – Review. *Corros Sci.* 2015 Jan 1;90:5–22.
 62. Williams G, McMurray HN. Pitting corrosion of steam turbine blading steels: The influence of chromium content, temperature, and chloride ion concentration. *Corrosion.* 2006;62(3):231–42.
 63. SCHWENK W. Theory Of Stainless Steel Pitting. *Corrosion* [Internet]. 1964 Apr 1 [cited 2023 May 13];20(4):129t–37t. Available from: <https://meridian.allenpress.com/corrosion/article/20/4/129t/157561/Theory-Of-Stainless-Steel-Pitting>
 64. GALVELE JR. Pitting Corrosion. 1983 Jan 1;23:1–57.
 65. Roy D, Simon GP, Forsyth M, Mardel J. Modification of thermoplastic coatings for improved cathodic disbondment performance on a steel substrate: a study on failure mechanisms. *Int J Adhes Adhes.* 2002 Jan 1;22(5):395–403.

66. Roy D, Simon GP, Forsyth M, Mardel J. Towards a better understanding of the cathodic disbondment performance of polyethylene coatings on steel. *Advances in Polymer Technology* [Internet]. 2002 Mar 1 [cited 2023 May 13];21(1):44–58. Available from: <https://onlinelibrary.wiley.com/doi/full/10.1002/adv.10010>
67. Vogt LO, Villeveille -Chemical C, Properties of FeSn E, Covert RA, Uhlig - HH, Lu H, et al. The Kinetics and Mechanism of Atmospheric Corrosion Occurring on Tin and Iron-Tin Intermetallic Coated Steels. *J Electrochem Soc* [Internet]. 2015 Oct 20 [cited 2023 May 13];162(14):C775. Available from: <https://iopscience.iop.org/article/10.1149/2.0681514jes>
68. Doherty M, Sykes JM. A quantitative study of blister growth on lacquered food cans by scanning acoustic microscopy. 2008;
69. Lin YC, Chen X. Investigation of moisture diffusion in epoxy system: Experiments and molecular dynamics simulations. *Chem Phys Lett*. 2005 Sep 5;412(4–6):322–6.
70. Marais S, Metayer M, Nguyen TQ, Labbe M, Saiter JM. Diffusion and permeation of water through unsaturated polyester resins—influence of resin curing. *Eur Polym J*. 2000 Mar 1;36(3):453–62.
71. Kregl L, Wallner GM, Lang RW, Mayrhofer G. Effect of resin modifiers on the structural properties of epoxy resins. *J Appl Polym Sci*. 2017 Nov 20;134(44).
72. Wint N. The atmospheric corrosion of novel coatings for packaging steel . Swansea University; 2016.
73. Allman A, Whiteside J, Jewell E, Griffiths C, McMurray N, de Vooy A. Surface modification of Cr(III) packaging substrates for enhanced adhesion via citric acid processing. *Surfaces and Interfaces*. 2020 Sep 1;20:100545.
74. Mittal KL. Adhesion Measurement of Thin Films. *Active and Passive Electronic Components* [Internet]. 1976 [cited 2023 Jan 27];3(1):21–42. Available from: <https://www.hindawi.com/journals/apec/1976/936912/>

75. Jokar M, Aliofkhazraei M. 3.20 Surface Preparation and Adhesion Tests of Coatings. *Comprehensive Materials Finishing*. 2017 Jan 1;306–35.
76. Wei H, Xia J, Zhou W, Zhou L, Hussain G, Li Q, et al. Adhesion and cohesion of epoxy-based industrial composite coatings. *Compos B Eng*. 2020 Jul 15;193.
77. Ingo GM, Giorgi L, Zacchetti N, Azzerri N. Electrochemical and XPS studies on lacquer—low tinplated steel adhesion. *Corros Sci*. 1992 Mar 1;33(3):361–77.
78. Ghanem A, Lang Y. *Introduction to polymer adhesion*. 2017;
79. Osouli-Bostanabad K, Tutunchi A, Eskandarzade M. The influence of pre-bond surface treatment over the reliability of steel epoxy/glass composites bonded joints. *Int J Adhes Adhes*. 2017 Jun 1;75:145–54.
80. Juhász G, Berczeli M, Weltsch Z. Surface activation of High Impact Polystyrene substrate using dynamic atmospheric pressure plasma. *International Journal of Engineering and Management Sciences [Internet]*. 2019 Mar 3 [cited 2023 Jan 10];4(1):80–7. Available from: <https://ojs.lib.unideb.hu/IJEMS/article/view/5193>
81. Wypych G. *Handbook_of_Neu.pdf*. Vol. 1, ChemTec Publishing. ChemTec Publishing; 2018. 5–44 p.
82. Mittal KL. *Physiochemical Aspects of Polymer Surfaces [Internet]*. Boston, MA: Springer US; 1983 [cited 2019 May 27]. Available from: <http://link.springer.com/10.1007/978-1-4615-7584-9>
83. Petrie EM. Silanes as Primers and Adhesion Promoters for Metal Substrates. *Metal Finishing*. 2007 Jul 1;105(7–8):85–93.
84. Randow CL, Williams CA, Ward TC, Dillard DA, Dillard JG, Wightman JP. An investigation of the cling of thin polymeric films. *Journal of Adhesion*. 1997;63(4):285–307.
85. Mittal KL. Adhesion Measurement of Thin Films. *ElectroComponent Science and Technology*. 1976;3(1):21–42.

86. Laugier M. The development of the scratch test technique for the determination of the adhesion of coatings. *Thin Solid Films*. 1981 Feb 13;76(3):289–94.
87. ISO - ISO 1518-1:2019 - Paints and varnishes — Determination of scratch resistance — Part 1: Constant-loading method [Internet]. [cited 2020 Mar 30]. Available from: <https://www.iso.org/standard/73853.html>
88. Deflorian F, Rossi S. The role of ions diffusion in the cathodic delamination rate of polyester coated phosphatized steel. <http://dx.doi.org/10.1163/156856103762302050> [Internet]. 2012 [cited 2022 Oct 21];17(2):291–306. Available from: <https://www.tandfonline.com/doi/abs/10.1163/156856103762302050>
89. Leidheiser H, Wang W, Igetoft L. The mechanism for the cathodic delamination of organic coatings from a metal surface. *Prog Org Coat*. 1983 Jan 17;11(1):19–40.
90. Aubrey DW, Welding GN, Wong T. Failure mechanisms in peeling of pressure-sensitive adhesive tape. *J Appl Polym Sci*. 1969 Oct 1;13(10):2193–207.
91. Chen Z, Zhou K, Lu X, Lam YC. A review on the mechanical methods for evaluating coating adhesion. Vol. 225, *Acta Mechanica*. Springer; 2014. p. 431–52.
92. ASTM D7093 - 19 Standard Test Method for Formability of Thin Film Organic Coatings on Steel Over a Biaxially Stretched Dome [Internet]. [cited 2020 May 26]. Available from: <https://www.astm.org/Standards/D7093.htm>
93. ISO - ISO 4624:2016 - Paints and varnishes — Pull-off test for adhesion [Internet]. [cited 2020 May 26]. Available from: <https://www.iso.org/standard/62351.html>
94. ASTM D4541-17. Standard Test Method for Pull-Off Strength of Coatings Using Portable Adhesion. *ASTM Int*. 2017;1–16.

95. Montanari A, Pezzani A, Cassarà A, Quaranta A, Lupi R. Quality of organic coatings for food cans: evaluation techniques and prospects of improvement. *Prog Org Coat.* 1996 Sep 1;29(1–4):159–65.
96. Ahn S, Kim EK, Jang S. Study of UV Degradation of Lacquer and Natural Adhesives Using Lacquer Mixed with Animal Glue. *Journal of Conservation Science [Internet].* 2016 Dec 31 [cited 2023 Sep 14];32(4):501–10. Available from: <http://dx.doi.org/10.12654/JCS.2016.32.4.05>
97. Benítez JJ, Ramírez-Pozo MC, Durán-Barrantes MM, Heredia A, Tedeschi G, Ceseracciu L, et al. Bio-based lacquers from industrially processed tomato pomace for sustainable metal food packaging. *J Clean Prod.* 2023 Feb 1;386:135836.
98. Kršulja M, Rožkanin P, Kudláček J, Pomenić L, Car Z. Investigation of Coatings Friction Coefficient Used In Production of Deep Drawn Packaging Cans. 2012;26.
99. de Vooy A. Chromium Oxide from Second Step TCCT, *Testrun* 33. 2019.
100. Metlac. Technical Data Sheet EP Lacquer For Int/Ext. 2020.
101. Melvin C, Jewell E, Miedema J, Lammers K, Vooy A, Allman A, et al. Identifying interlayer surface adhesion failure mechanisms in tinplate packaging steels. *Packaging Technology and Science [Internet].* 2019 Jul 20 [cited 2020 Mar 19];32(7):345–55. Available from: <https://onlinelibrary.wiley.com/doi/abs/10.1002/pts.2443>
102. Jones S. *Surface Texture and Visual Appearance of Packaging Steel.* Swansea; 2020.
103. Lindseth I, Bardal A. Quantitative topography measurements of rolled aluminium surfaces by atomic force microscopy and optical methods. *Surf Coat Technol.* 1999 Jan 29;111(2–3):276–86.
104. Smith JR, Breakspear S, Campbell SA. AFM in surface finishing: Part II. Surface roughness. *Transactions of the Institute of Metal Finishing.* 2003;81(3).

105. Zosel A. Adhesion and tack of polymers: Influence of mechanical properties and surface tensions. *Colloid Polym Sci* [Internet]. 1985 Jul [cited 2022 Dec 23];263(7):541–53. Available from:
<https://link.springer.com/article/10.1007/BF01421887>
106. Kash L. Mittal. *Contact Angle, Wettability and Adhesion, Volume 3. Contact Angle, Wettability and Adhesion, Volume 3* [Internet]. 2003 Dec 1 [cited 2022 Dec 23];117–61. Available from:
<https://www.taylorfrancis.com/books/mono/10.1201/9789047403326/contact-angle-wettability-adhesion-volume-3-kash-mittal>
107. X-Rite. The Difference Between a 0:45 and a Sphere Measurement | X-Rite Blog [Internet]. [cited 2022 Dec 21]. Available from:
<https://www.xrite.com/blog/difference-between-0-45-and-sphere-measurement>
108. Palus H. Representations of colour images in different colour spaces. In: *The Colour Image Processing Handbook* [Internet]. Springer, Boston, MA; 1998 [cited 2022 Dec 21]. p. 67–90. Available from:
https://link.springer.com/chapter/10.1007/978-1-4615-5779-1_4
109. X-rite. LAB Colour Space and Values | X-Rite Color Blog [Internet]. [cited 2022 Dec 21]. Available from: <https://www.xrite.com/blog/lab-color-space>
110. ASTM D523 - 14(2018) Standard Test Method for Specular Gloss [Internet]. [cited 2021 Sep 9]. Available from: <https://www.astm.org/Standards/D523>
111. Inc P. Pyris 1 TGA Thermogravimetric Analyzer Technical Specifications. 2003;
112. ThermoNicolet. *Introduction to Fourier Transform Infrared Spectrometry*. 2001;
113. Allman A, Jewell E, Vooy's A, Hayes R, McMurray HN, Jewell E, et al. Food packaging simulant failure mechanisms in next generation steel packaging. *Packaging Technology and Science*. 2019 Sep;32(April):1–15.

114. Brouwer P. Theory of XRF Getting acquainted with the principles [Internet]. Almelo: PANalytical BV. 2010 [cited 2022 Dec 23]. 20–59 p. Available from: www.panalytical.com
115. Lachance GR, Claisse F. Quantitative X-Ray Fluorescence Analysis: Theory and Application. John Wiley & Sons, Inc. 1995;391.
116. Briggs D. Handbook of X-ray and ultraviolet photoelectron spectroscopy. Physik in unserer Zeit [Internet]. 1979 Jan 1 [cited 2022 Sep 16];10(1):30–30. Available from: <https://onlinelibrary.wiley.com/doi/full/10.1002/piuz.19790100107>
117. Kawai J, Adachi H, Kitajima Y, Maeda K, Hayakawa S, Gohshi Y. Inelastic Mean Free Path of Photoelectrons in Ag Determined by Total Reflection X-Ray Photoelectron Spectroscopy. Analytical Sciences. 1997 Oct 10;13(5):797–801.
118. Thomas Nelis RP. Glow Discharge Optical Emission Spectroscopy: A Practical Guide. 2003.
119. Vontorová J, Mohyla P. Use of GDOES method for evaluation of the quality and thickness of hot dip galvanised coating. <https://doi.org/101080/0020296720181520531>. 2018 Nov 2;96(6):313–8.
120. Whiteside J, de Vooy ACA, Sackett E, McMurray HN. Influence of uniaxial deformation on surface morphology and corrosion performance of chromium-based coatings for packaging steel. Corros Sci. 2021 Sep 1;190.
121. Williams G, Neil McMurray H. Localized Corrosion of Magnesium in Chloride-Containing Electrolyte Studied by a Scanning Vibrating Electrode Technique. J Electrochem Soc. 2008 May 16;155(7):C340.
122. Worsley DA, McMurray HN, Sullivan JH, Williams IP. CORROSION SCIENCE SECTION Quantitative Assessment of Localized Corrosion Occurring on Galvanized Steel Samples Using the Scanning Vibrating Electrode Technique. 2004 [cited 2022 Nov 10]; Available from: http://meridian.allenpress.com/corrosion/article-pdf/60/5/437/1535680/1_3299239.pdf

123. McMurray HN, Worsley DA. Scanning electrochemical techniques for the study of localised metallic corrosion. *Research in chemical kinetics*. 1997;4:149–202.
124. Isaacs H. *Electrochemical Corrosion Testing*. Electrochemical Corrosion Testing. 1981. 3–33 p.
125. Rossi S, Fedel M, Deflorian F, del Carmen Vadillo M. Localized electrochemical techniques: Theory and practical examples in corrosion studies. *Comptes Rendus Chimie*. 2008 Sep 1;11(9):984–94.
126. Isaacs HS. The Effect of Height on the Current Distribution Measured with a Vibrating Electrode Probe. *J Electrochem Soc* [Internet]. 1991 Mar 1 [cited 2023 May 13];138(3):722–8. Available from: <https://iopscience.iop.org/article/10.1149/1.2085665>
127. Yezhovskiy YK, Dubrovenskii SD. Preparation and Adhesive Properties of Chromium Oxide Nanolayers. *Inorganic Materials: Applied Research* [Internet]. 2018 Jan 1 [cited 2023 May 13];9(1):9–13. Available from: <https://link.springer.com/article/10.1134/S2075113318010124>
128. Watson T. *Corrosion mechanisms and inhibition on organic coated packaging steel*. Swansea University; 2006.
129. Shimizu Y, Chen LC, Wook Kim D, - al, Niehues J, Lehmann P, et al. Fundamental aspects of resolution and precision in vertical scanning white-light interferometry. *Surf Topogr* [Internet]. 2016 Mar 4 [cited 2023 May 13];4(2):024004. Available from: <https://iopscience.iop.org/article/10.1088/2051-672X/4/2/024004>
130. Lucas S, vanden Brande P, Weymeersch A. Plasma treatment of cold-rolled steel: Actual state, problems to overcome and future. *Surf Coat Technol*. 1998;100–101(1–3):251–9.
131. Saborowski E, Dittes A, Steinert P, Lindner T, Scharf I, Schubert A, et al. Effect of Metal Surface Topography on the Interlaminar Shear and Tensile Strength of Aluminum/Polyamide 6 Polymer-Metal-Hybrids. *Materials*

- [Internet]. 2019 Sep 1 [cited 2023 May 13];12(18). Available from:
[/pmc/articles/PMC6766192/](#)
132. Weidner DE, Schwartz LW, Eley RR. Role of surface tension gradients in correcting coating defects in corners. *J Colloid Interface Sci.* 1996 Apr 15;179(1):66–75.
 133. Sina Ebnesajjad. *Handbook of Adhesives and Surface Preparation: Technology, Applications and ...* - Sina Ebnesajjad - Google Books. 2011.
 134. Han K, Woghiren OE, Priefer R. Surface tension examination of various liquid oral, nasal, and ophthalmic dosage forms. *Chem Cent J.* 2016 May 9;10(1):31.
 135. Van De Grampel RD, Ming W, Van Gennip WJH, Van Der Velden F, Laven J, Niemantsverdriet JW, et al. Thermally cured low surface-tension epoxy films. *Polymer (Guildf).* 2005 Nov 14;46(23):10531–7.
 136. Joanny JF, De Gennes PG. A model for contact angle hysteresis. *J Chem Phys* [Internet]. 1984 Jul 1 [cited 2023 May 13];81(1):552–62. Available from: <https://pubs.aip.org/aip/jcp/article/81/1/552/607274/A-model-for-contact-angle-hysteresis>Model-for
 137. Manfred LB, Ginés MJL, Benftez GJ, Egli WA, Rissone H, Vázquez A. Use of epoxy–phenolic lacquers in food can coatings: Characterization of lacquers and cured films. *J Appl Polym Sci* [Internet]. 2005 Mar 15 [cited 2023 Jan 5];95(6):1448–58. Available from: <https://onlinelibrary.wiley.com/doi/full/10.1002/app.21389>
 138. Rieger J. The glass transition temperature T_g of polymers—Comparison of the values from differential thermal analysis (DTA, DSC) and dynamic mechanical measurements (torsion pendulum). *Polym Test.* 2001 Oct 1;20(2):199–204.
 139. Yli-Pentti A. Electroplating and Electroless Plating. *Comprehensive Materials Processing.* 2014 Jan 1;4:277–306.
 140. Gabe DR. Mixed oxide films on tin. *Surface Technology.* 1977 Sep 1;5(6):463–78.

141. Pérez MM, Carrillo-Perez F, Tejada-Casado M, Ruiz-López J, Benavides-Reyes C, Herrera LJ. CIEDE2000 lightness, chroma and hue human gingiva thresholds. *J Dent*. 2022 Sep 1;124.
142. Gómez-Polo C, Gómez-Polo M, Celemin-Viñuela A, Martínez Vázquez De Parga JA. Differences between the human eye and the spectrophotometer in the shade matching of tooth colour. *J Dent*. 2014 Jun 1;42(6):742–5.
143. Parsons P, Christie C, DiRamio D, Drummond R, Foxton J, Freeman K, et al. Inorganic Pigments-Other. In: *Surface Coatings* [Internet]. Springer, Dordrecht; 1993 [cited 2023 Jan 27]. p. 449–72. Available from: https://link.springer.com/chapter/10.1007/978-94-011-1220-8_27
144. Dodd M, Jewell E, Wint N, Vooy's A de. The Adhesion of Protective Coatings to Novel Trivalent Cr Metal / Cr Oxide Coatings Used for Packaging Applications. *ECS Meeting Abstracts* [Internet]. 2022 Oct 9 [cited 2023 Jan 6];MA2022-02(10):684. Available from: <https://iopscience.iop.org/article/10.1149/MA2022-0210684mtgabs>
145. Sammon C, Yarwood J, Everall N. FT-IR study of the effect of hydrolytic degradation on the structure of thin PET films. *Polym Degrad Stab*. 2000;67(1):149–58.
146. Jung JH, Ree M, Kim H. Acid- and base-catalyzed hydrolyses of aliphatic polycarbonates and polyesters. *Catal Today*. 2006 Jun 30;115(1–4):283–7.
147. Brubach JB, Mermet A, Filabozzi A, Gerschel A, Roy P. Signatures of the hydrogen bonding in the infrared bands of water. *J Chem Phys*. 2005 May 8;122(18).
148. Choi JH, Cho M. Computational IR spectroscopy of water: OH stretch frequencies, transition dipoles, and intermolecular vibrational coupling constants. *J Chem Phys*. 2013 May 3;138(17):174108.
149. Lin-Vien D, Colthup NB, Fateley WG, Grasselli JG (Professor). Compounds Containing the Carbonyl Group. In: *The Handbook of infrared and raman characteristic frequencies of organic molecules*. Academic Press; 1991. 117–54 p.

150. Monfre SL, Brown SD. Estimation of ester hydrolysis parameters by using fourier-transform infrared spectroscopy and the extended kalman filter. *Anal Chim Acta*. 1987 Jan 1;200(C):397–410.
151. Groesbeck EC, Walkup HH. PREECE TEST (COPPER-SULPHATE DIP) FOR ZINC COATINGS. Part of Bureau of Standards Journal of Research. 1934;12.
152. Montanari A, Pezzani A, Cassarà A, Quaranta A, Lupi R. Quality of organic coatings for food cans: Evaluation techniques and prospects of improvement. *Prog Org Coat*. 1996;29(1–4):159–65.
153. Bastos AC, Quevedo MC, Ferreira MGS. The influence of vibration and probe movement on SVET measurements. 2014 [cited 2023 Jan 13]; Available from: <http://dx.doi.org/10.1016/j.corsci.2014.10.038>
154. del Pianta D, Frayret J, Gleyzes C, Cugnet C, Dupin JC, le Hecho I. Determination of the chromium (III) reduction mechanism during chromium electroplating. *Electrochim Acta* [Internet]. 2018 Sep 10 [cited 2022 Feb 1];284:234–41. Available from: <https://doi.org/10.1016/j.electacta.2018.07.114>
155. Chandrasekaran B, Rao R, Sreeram J, Nair BU, Ramasami T. Chrome Tanning: State-of-Art on the Material Composition and Characterization. *J Sci Ind Res (India)*. 1999;58:1–10.
156. Arthur. Continuous electroplating method. 1966.
157. Messier R. Electrodeposition: The materials science of coatings and substrates. *Advanced Materials* [Internet]. 1994 Jan 1 [cited 2023 Jan 13];6(1):88–9. Available from: <https://onlinelibrary.wiley.com/doi/full/10.1002/adma.19940060127>
158. Barbato R S, Ponce F J, Jara V M, Cuevas S J, Egana A R. Study of the effect of temperature on the hardness, grain size, and yeild in electrodeposition of chromium on 1045 steel. *Journal of the Chilean Chemical Society*. 2008 Mar;53(1).

159. Ziemniak SE, Jones ME, Combs KES. Solubility and phase behavior of Cr(III) oxides in alkaline media at elevated temperatures. *J Solution Chem* [Internet]. 1998 [cited 2023 May 19];27(1):33–66. Available from: <https://link.springer.com/article/10.1023/A:1022688528380>
160. Lorimer P, Mason TJ. The Applications of Ultrasound in Electroplating. *Electrochemistry*. 1999 Sep 5;67(9):924–30.